UNIVERSIDAD DE CHILE

FACULTAD DE CIENCIAS FÍSICAS Y MATEMÁTICAS

DEPARTAMENTO DE GEOLOGÍA

INTERPLAY BETWEEN BRITTLE DEFORMATION, FLUID-ROCK INTERACTION AND MINERALIZATION IN HYDROTHERMAL SYSTEMS FROM THE SOUTHERN ANDES

TESIS PARA OPTAR AL GRADO DE DOCTOR EN CIENCIAS

MENCIÓN GEOLOGÍA

PABLO VICTOR MIGUEL SÁNCHEZ ALFARO

PROFESOR GUÍA:

MARTIN REICH MORALES

PROFESORA CO-GUÍA:

GLORIA ARANCIBIA HERNÁNDEZ

MIEMBROS DE LA COMISIÓN:

JOSÉ CEMBRANO PERASSO

DIEGO MORATA CÉSPEDES

SANTIAGO DE CHILE

2015

RESUMEN DE LA TESIS PARA OPTAR AL GRADO DE:
Doctor en Ciencias, Mención Geología
POR: Pablo Victor Miguel Sánchez Alfaro
FECHA: 01/07/2015
PROF. GUÍA: Martin Reich Morales
PROF. CO-GUÍA: Gloria Arancibia Hernández

INTERACCIÓN ENTRE DEFORMACIÓN FRÁGIL, INTERACCIÓN FLUIDO-ROCA Y MINERALIZACIÓN EN LOS SISTEMAS HIDROTERMALES DE LOS ANDES DEL SUR

Las interacciones entre la actividad sísmica, el flujo de fluidos y precipitación mineral ejercen un control de primer orden en la resistencia y permeabilidad de la corteza y juegan un rol fundamental en el desarrollo de los sistemas hidrotermales y la formación de depósitos de minerales. Sin embargo, el rol de estas interacciones en la evolución de los sistemas hidrotermales y sus efectos transientes en la mineralización es poco limitada. Esta tesis contribuye a establecer la naturaleza de la interacción dinámica entre la deformación frágil, la interacción calor-fluido-roca y la mineralización de los sistemas hidrotermales en arcos volcánicos. El laboratorio natural utilizado para estudiar dicha interacción es la Cordillera de los Andes en la zona centro-sur de Chile, donde los sistemas hidrotermales ocurren en estrecha relación espacial con el volcanismo activo y los principales sistemas de fallas sísmicamente activos.

La combinación del análisis estructural a escala regional de áreas geotérmicas activas con la modelación geoquímica de aguas termales en la zona de Villarrica-Chihuio en el sur de Chile revela el rol de la deformación cortical en facilitar e inhibir el desarrollo de los sistemas geotérmicos. Los resultados revelan la presencia de dos dominios magmático-tectónico-geotérmales e indican que la evolución química de los fluidos hidrotermales en el área es dependiente de los mecanismos de transferencia de calor controlados por los sistemas de falla. Esta contribución proporciona conduce hacia estrategias de exploración más eficientes de los recursos geotérmicos en el sur de los Andes.

El sistema geotermal Tolhuaca al norte de Villarrica es de alta entalpía y tiene un alto contenido de metales, lo que permitió su estudio detallado con el fin de: (1) abordar cómo la interacción entre la actividad sísmica, la interacción calor-fluido-roca, flujo de fluidos y precipitación mineral controla la evolución físico-química de los sistemas hidrotermales en la región y (2) analizar los efectos transientes en la solubilidad del metales y en la mineralización producidos por las fluctuaciones de presión gatilladas por terremotos. Para lograr esto, se combinaron los análisis estructurales y mineralógicos a escala de terreno y de sondaje, con datos geoquímicos, y medidas de la temperatura en el pozo y de inclusiones fluidas obtenidas con microtermometría. Esta información fue integrada con simulaciones numéricas de la evolución física y química de los fluidos y de las condiciones de fallamiento de la roca. Los resultados obtenidos para el sistema geotermal Tolhuaca revelan que la alteración hidrotermal modifica la respuesta de las rocas a la deformación, produce una compartimentación vertical del sistema y promueve el desarrollo de una zona de baja permeabilidad rica en arcilla. Además, indican que la duración de la vida y la estructura termal de este sistema fueron altamente afectadas por la zona de baja permeabilidad desarrollada en la parte superior. Además, los modelos termodinámicos de la solubilidad mineral (cuarzo) y de metales (oro) en Tolhuaca revelan que el ambiente óptimo para la precipitación de metales se alcanza en condiciones de líquido saturado con una temperatura menor a 310°C, bajo el cual pequeños cambios en la presión gatillados por terremotos disminuyen la solubilidad en varios órdenes de magnitud. Las observaciones resultantes de esta tesis no sólo proporcionan nuevos conocimientos sobre cómo los reservorios hidrotermales se desarrollan a través de una combinación de calor sostenido y condiciones de alta permeabilidad que están fuertemente condicionados por la actividad tectónica, sino que también revelan cómo los sistemas hidrotermales evolucionan para maximizar la eficiencia de la precipitación de metales gatilladas por terremotos.

INTERPLAY BETWEEN BRITTLE DEFORMATION, FLUID-ROCK INTERACTION AND MINERALIZATION IN HYDROTHERMAL SYSTEMS OF SOUTHERN ANDES

The interactions between seismic activity, fluid flow and mineral precipitation exerts a first-order control on the strength and permeability of the crust and plays a critical role in promoting the development of hydrothermal systems and the formation of giant ore deposits. However the role of such interactions on the evolution of hydrothermal systems and its transient effects on mineralization is poorly constrained. This thesis contributes to establish the nature of the dynamic interplay between brittle deformation, heat-fluid-rock interaction and mineralization of hydrothermal systems in volcanic arcs. An ideal natural laboratory used to study such interplay is the Andean Cordillera of Central-Southern Chile, where hydrothermal systems occur in close spatial relationship with active volcanism as well as major seismically-active fault systems.

The combination of regional-scale structural analysis of active geothermal areas with geochemical modeling of hot springs in the Villarrica–Chihuio area in southern Chile unravel the role of crustal deformation in facilitating and inhibiting the development of geothermal systems. Results reveal the presence of two magmatic-tectonic-geothermal domains and indicate that the chemical evolution of hydrothermal fluids in the area is strongly dependent on structurally controlled mechanisms of heat transfer. This contribution provides new insights towards efficient exploration strategies of geothermal resources in Southern Andes.

The high enthalpy, metal-rich active Tolhuaca geothermal system north of Villarica was studied in detail in order to (1) address how the interplay between seismic activity, heat-fluid rock interaction, fluid flow and mineral precipitation controls the physicochemical evolution of hydrothermal systems in the studied region and (2) analyze the transient effects of earthquake-triggered pressure perturbations on metal solubility and mineralization. To achieve this, a comprehensive structural and mineralogical analysis at field and drillhole scales was combined with geochemical and thermometric data of borehole fluids and fluid inclusions, and numerical simulations of fluid evolution and rock failure conditions. Results obtained from this study reveal that hydrothermal alteration modifies the response of rock to deformation at Tolhuaca, produces a vertical compartmentalization of the system and promotes the development of a clay-rich low permeability zone. Moreover, they indicate that the life span and thermal structure of this system were highly affected by the low-permeability zone developed on top. Furthermore, thermodynamic modeling of metal (gold) and mineral (silica) solubility at Tolhuaca reveals that the optimum physical and chemical conditions for metal precipitation are reached at liquid-saturated conditions with a saturated liquid temperature less than 310°C, under which small pressure changes triggered by transient fault-rupture can drop solubility several orders of magnitude. The observations resulting from the thesis not only provide new insights about how hydrothermal reservoirs develop through a combination of sustained heat and high permeability conditions that are strongly conditioned by active tectonics, but also unveil how hydrothermal systems evolve to maximize the efficiency earthquake-induced mineral precipitation.

Escribí, mi escritura fue como la maleza
de flores ácimas pero flores en fin
Enrique Lihn

Porque un puente, aunque se tenga el deseo de tenderlo
y toda obra sea un puente hacia y desde algo,
no es verdaderamente puente mientras los hombres no lo crucen.
Un puente es un hombre cruzando un puente.
Julio Cortazar

AGRADECIMIENTOS

Agradezco los miembros de mi comisión de tesis, Martin Reich, Gloria Arancibia, José Cembrano y Diego Morata quienes motivaron, guiaron y sustentaron la realización de este trabajo de tesis. A lo largo estos años cada uno me entregó cotidianamente valiosos momentos en las dimensiones humanas y científicas. Martin fue un excelente guía que mantuvo el artístico balance entre libertad y exigencia; Gloria me ayudó en aterrizar las ideas y proyectos a lo posible y realizable; José me regaló su sabiduría de la vida y Diego desde el comienzo del CEGA me apoyó en muchos proyectos, desde el seminario "Cahuín-Pehuén" hasta aquellos proyectos relacionados con política energética. I particularly acknowledge Christoph Heinrich and Thomas Driesner for having me their research group during my 6-month stay at ETH-Zürich. I'm thankful of the fruitful discussions with Thomas and Chris about both science and life.

Esta tesis fue financiada por los proyectos CONICYT FONDAP 15090013 "Centro de Excelencia en Geotermia de los Andes" (CEGA) y FONDECYT 1130030. Financiamiento adicional provino de la Iniciativa Científica Milenio "Trazadores de Metales en Zonas de Subducción" (NC130065). Agradezco, en particular, al proyecto MECESUP0708 por mi beca de doctorado. La pasantía a ETH-Zürich fue financiada por el "Programa de Pasantías en el Extranjero" CONICYT convocatoria año 2012.

Agradezco a Sergio Iriarte, Silke Lohmar, Anna Colvin, Jim Stimac, Glen Melosh y Andrea González de GGE MRP-Chile Ltd. (ex-GGE Ltd) por proveer información y acceso al sistema geotermal Tolhuaca.

Agradezco desde lo más entrañable a mis padres y hermana quienes me entregaron amor, confianza, curiosidad, crítica y todo el resto, desde el comienzo. A Gabi le agradezco ser la compañera de mis días, del aquí y el ahora; que me floreces la experiencia de vivir.

Agradezco a mis compañeros de investigación, Pame, Daniele, Gerd, Martin L., Vladi, Dieguitz con quienes compartimos (y seguiremos compartiendo) buenos momentos, buenos terrenos y algunas ideas buenas. A Tapia, Viole, Feñin y el resto de querid@s ñoñ@s del "Cómete un paper" y de la oficina del postgrado por la amigable cotidianidad que alegra el trabajo y la vida.

I also thank Gabriel, Sam, Matt, Pilar, Markus and the rest of the fluids group at ETH-Zürich for their support that made my stay at Zurich a really enjoyable and memorable experience.

Aunque estén más lejos ahora, agradezco a Martín, Pau, Tania, Miguel, Naty, Buki y el resto de compañeros ejemplares, que hicieron de mi paso por esta facultad una experiencia universitaria; en ese discutir y reír mientras pensamos construir una sociedad más justa y mejor.

Finalmente te agradezco a ti que estás frente a estas palabras, porque una tesis no es una tesis mientras alguien no la lea. Una tesis es una persona curiosa leyendo una tesis.

A tod@s ustedes, muchas gracias.

TABLE OF CONTENTS

Chapter 1. Introduction

Studies bridging geochemistry and structural geology have shown that the interplay between seismic activity, fluid flow and mineral precipitation exerts a first-order control on the strength and permeability of the crust (Barton et al., 1995; Sibson, 1985; Manga et al., 2012). Moreover, there is evidence that such interaction plays a critical role in promoting the development of geothermal systems and the formation of giant ore deposits (Sibson, 1987; Cox, 2010; Moore and Simmons, 2013; Richards, 2013).

Despite such relevant advances there is still a severe lack of information about the role of brittle deformation on the evolution of hydrothermal systems and the transient effect that earthquakes have on mineralization events (Fagereng and Toy, 2011; Richards, 2013; Couples, 2013). Such information is crucial considering that the mechanisms of interplay between common deformation and geochemical processes are key to reveal the optimal conditions leading to the development of high enthalpy geothermal resources and to the formation of hydrothermal ore deposits (Richards, 2013). Despite decades of research advances, the optimal pathways and external (tectonic or seismic) forcing leading to metal precipitation in hydrothermal systems are still poorly quantified. Therefore, it is necessary to close this gap of knowledge to improve the effectiveness of exploration strategies in a contemporary society with growing needs of renewable energy and mineral resources.

This thesis contributes to unravel the dynamic interplay between brittle deformation, heat-fluid-rock interaction and mineralization in hydrothermal systems associated with subduction-related volcanism. To achieve this goal, the guiding research questions addressed here are: (1) What is the role of active tectonics in facilitating or inhibiting the development of hydrothermal systems? (2) What is the effect of the interplay between heat-fluid-rock interaction and brittle deformation on the evolution of hydrothermal systems? and (3) What is the enhancing effect that earthquakes have on mineralization?

In this study, I hypotethize that: (1) The interplay between active tectonics and volcanism defines the nature and evolution of geothermal systems by controlling its heat source and permeability architecture, (2) The resulting hydrothermal alteration changes the mechanical properties of the rock affecting the permeability architecture of the system and (3) Fault rupture transiently modifies the physical and chemical conditions of hydrothermal fluid by pressure fluctuations that trigger precipitation of silica and ore minerals such as native gold.

An excelent natural laboratory to test these hypotheses is the Andean Cordillera of Central-Southern Chile, where hydrothermal systems occur in close spatial relationship with active volcanism and regional fault systems. The nature of the relationship between active tectonics and volcanism in this region is the result of interaction between the crustal structures of the basement and the ongoing regional stress field, which is primarily controlled by the oblique convergence of the Nazca and South America Plates. Between 39° and 46°S, the tectonic activity is represented by two regional scale fault systems: the arc-parallel Liquiñe–Ofqui fault system (LOFS) and the arc-oblique WNW-striking long-lived basement fault systems (ALFS) (Cembrano, 1996; Rosenau et al., 2006; Cembrano and Lara, 2009). Near 25% of geothermal features in the Chilean Andes are spatially related to the LOFS and ALFS, evidencing a tectonic context that promotes the migration and accumulation of significant volumes of fluid (Sibson, 1996; Cox, 2010).

In the following pages, I provide a summary of this thesis and present the results of two case studies in the Southern Volcanic Zone, namely the Villarrica–Chihuio area and the Tolhuaca geothermal field. Since the integration of geochemical and structural methods was key component to this study, I highlight the multidisciplinary approach aimed at unraveling the complex and dynamic interaction between brittle deformation, fluid flow and mineral precipitation. Such approach involved combining field observations with geochemical data of borehole fluids and fluid inclusions, thermodynamic modeling of mineral solubility, and numerical simulations aimed at quantifying the physics of fault-fracture processes. These methods provided the opportunity to investigate hydrothermal systems under physico-chemical conditions and timescales that are not accessible to direct observation or laboratory experiments.

In Chapter 2, the role of crustal deformation in facilitating or inhibiting the development of geothermal systems is studied in the Villarrica–Chihuio area of southern Chile. It combines a regional-scale structural analysis of active geothermal areas with geochemical modeling of hot spring chemistry. This approach allowed the identification of two magmatic-tectonic-geothermal domains and revealed that the chemical evolution of hydrothermal fluids in the area is strongly dependent on heat transfer mechanisms that are structurally controlled. Moreover, these results indicate that the volcanic activity related to inherited basement faults of the ALFS yields favorable conditions to form crustal magma reservoirs and, therefore, to sustain a heat source that fuels high enthalpy geothermal reservoirs. Such conclusions provide new insights towards efficient exploration strategies of geothermal resources in the Southern Andes.

The regional-scale study presented in Chapter 2 has the advantage of exhibiting the tectonic controls that define the occurrence of hydrothermal systems along the Liquiñe-Ofqui Fault System (LOFS). However, addressing the interplay between brittle

deformation, heat-fluid-rock interaction and mineralization requires a local-scale case study to gain knowledge about the physical, chemical and mineralogical constraints that impact the evolution hydrothermal systems. To some extent such information has to come from subsurface sources to capture a well-constrained picture of fault-fracture meshes, hydrothermal alteration and thermodynamic conditions of borehole fluids and paleofluids. An excellent location to undertake such study was the active Tolhuaca geothermal field in the northern termination of the LOFS that hosts a high enthalpy system that has been drilled down to ~3 km depth but is not affected by geothermal production or re-injection. Moreover, the high gold content (~1 ppb) of the fluids sampled from a deep borehole makes Tohuaca suitable as an epithermal system analogue. Therefore, Chapters 3 and 4 are focused on the study of the Tolhuaca geothermal system.

Chapter 3 investigates the effect of the interplay between heat-fluid-rock interaction and brittle deformation on the evolution of Tolhuaca. Detailed structural measurements and mineralogical analyses at the field and drillhole scales were combined with chemical characterization of borehole fluids and microthermometric and micro-analytical determinations in fluid inclusions, and numerical simulations of fluid evolution and rock failure conditions. This study revealed that hydrothermal alteration processes at Tolhuaca modified the response of rock to deformation and compartmentalized the system, promoting the development of a clay-rich low permeability layer on top. Numerical simulations indicate that this low-permeability zone has helped increase the duration of high-enthalpy conditions by a factor of three in the deep upflow zone at Tolhuaca, extending the lifespan of the hydrothermal system.

The results reported in Chapters 2 and 3 provide new insights regarding the long-term interplay between brittle deformation and evolution of hydrothermal systems, and suggest that seismic activity may significantly impact the sustainability of geothermal reservoirs. Chapter 4 explores how the interplay between seismic activity, fluid flow and mineral precipitation controls the physicochemical evolution of geothermal resevoirs, and evaluates the effects of earthquake-triggered pressure perturbations on mineral solubility. By using borehole data retrieved from Tolhuaca, a novel a model that integrates mechanical processes and changes in mineral solubility during a seismic event is developed. This model constrains the optimal pressure and enthalpy window for gold and silica precipitation in the epithermal environment, in which small pressure changes (~50 bar) triggered by transient fault-rupture can drop gold solubility by several orders of magnitude. These results are relevant not only to better understand the feedbacks between active tectonics and mineral precipitation at Tolhuaca, but also provide new insights on how hydrothermal systems evolve to maximize efficiency of earthquake-induced gold precipitation.

Publications and Abstracts resulting from this Dissertation

Publications

Sánchez, P., Pérez-Flores, P., Arancibia, G., Cembrano, J., Reich, M. (2013). Crustal deformation effects on the chemical evolution of geothermal systems: The intra-arc Liquiñe-Ofqui Fault System, Southern Andes. *International Geology Review*, 55(11), 1384–1400, **(Chapter 2)**

Sanchez-Alfaro, P., Reich, M., Arancibia, G., Pérez-Flores, P., Cembrano, J., Lizama, M., Morata, D., Rowland, J., Driesner, T., Campos, E. Interplay between hydrothermal alteration and brittle deformation: insights from the evolution of an Andean Geothermal System. (*in preparation*), **(Chapter 3)**

Sanchez-Alfaro, P., Reich, M., Arancibia, G., Driesner, T., Pérez-Flores, P., Cembrano, J., Heinrich, C., Tardani, D., Campos, E., Rowland, J. The optimal pathways to form giant gold deposits by earthquakes. (*in preparation*), **(Chapter 4)**

Conference Abstracts

Sánchez, P., Alam, M.A., Parada, M.A., 2011. Origen de las fuentes termales en la Zona de Falla Liquiñe-Ofqui (39-45°S), zona volcánica sur, Chile. XVIII Congreso Geológico Argentino, Neuquén Argentina, May 2-6, 2011.

Sánchez, P., Pérez-Flores, P., Arancibia, G., Cembrano, J., & Reich, M. 2012. Efectos de la deformación cortical en la evolución química de los fluidos geotermales: Caso estudio Villarrica-Chihuio, Sistema de Falla Liquiñe-Ofqui , XIII Congreso Geológico Chileno (Chilean Geological Congress), Antofagasta, August 6-10, 2012

Sánchez, P., Pérez-Flores, P., Arancibia, G., Reich, M., & Cembrano, J. 2013 The interplay between fault-fracture networks activity, fluid flow and mineralization in the Andes: A case study in the Tolhuaca geothermal system, southern Chile. AGU Fall, Cancún Mexico, May 14-17 2013

Sánchez, P., Pérez-Flores, P., Arancibia, G., Reich, M., Cembrano, J. Campos, E. & Lohmar, S. 2013 The influence of fault-fracture network activity on fluid geochemistry and mineral precipitation at the Tolhuaca geothermal system, southern Chile. Goldschmidt Conference, Florence Italy, August 25-30 2013. Mineralogical Magazine, 77(5) 2122

Sanchez-Alfaro P, Driesner T, Heinrich C, Reich M, Perez P, Arancibia G, Cembrano J. 2014 Fluid evolution in an Andean geothermal system: coupling fluid

inclusions thermometry, LA-ICP-MS and geochemical modeling. Goldschmidt Conference, Sacramento USA, June 8-13 2014

Sanchez-Alfaro, P, Driesner T, Heinrich C, Reich M, Perez P, Arancibia G, Cembrano J., Campos, E., Lohmar, S. 2014 Fluid evolution in an Andean geothermal system: coupling fluid inclusions thermometry, LA-ICP-MS and geochemical modeling. Pan-American Current Research on Fluid Inclusions (PACROFI-XII), Denver, USA, June 2–5, 2014

Sanchez-Alfaro, P., Pérez-Flores, P., Tardani, D., Reich, M., Arancibia, G., Cembrano, J. 2015 Crustal Deformation Effects on the Chemical Evolution of Geothermal Systems: Case Studies from Southern Andes. World Geothermal Congress, April 19-24 2015, Melbourne Australia.

Publications and Abstracts resulting from side-projects

Publications

Deditius, A.P., Utsunomiya, S., Sanchez-Alfaro, P., Reich, M., Ewing., R.C., Kesler, S.E. (2015) Constraints on Hf and Zr mobility in high-sulfidation epithermal systems: formation of kosnarite, $KZr_2(PO_4)_3$, in the Chaquicocha gold deposit, Yanacocha district, Peru. *Mineralium Deposita*, vol. 50, 429-436.

Sanchez-Alfaro, P., Sielfeld, G., Dobson, P., Van Campen, B., Fuentes, V., Reed, A., Palma-Behnke, R., Diego Morata. Geothermal Energy in the Andes: A Geoscience, Regulatory and Economic Review of the Chilean Case. *Renewable & Sustainable Energy Reviews* (under review).

Conference Abstracts

Sánchez, P., Morata, D., Lahsen, A., Parada, M.A., 2011. Current Status of Geothermal Exploration in Chile and the Role of the new Andean Geothermal Center of Excellence (CEGA). Geothermal Resources Council (GRC) Transactions v. 35, 1215-1218

Pérez-Flores, P., Sánchez, P., Sielfeld, G., Cembrano, J. 2013. Tectonics, magmatism and fluid flow in a transtensional strike-slip setting: The northern termination of the dextral strike-slip Liquiñe-Ofqui Fault System, Chile. AGU Fall, Cancún Mexico, May 14-17 2013. V53A-08

Tardani, D., Reich, M., Sano, Y., Takahata., Wen, H., Roulleau, E., Sanchez-Alfaro, P., *et al.*, Metal fluxing in a large-scale intra-arc fault: insights from the Liquiñe-Ofqui Fault System (LOFS) and associated geothermal fields in southern Chile AGU Fall Meeting, San Francisco, California, USA, December 15-19, 2014, V21A-4734

Reich, M., Deditius, A., Tardani, D., Sanchez-Alfaro, P., The coupled geochemistry of Au and As in pyrite from ore deposits and geothermal fields: monitoring fluid evolution and external forcing factors in hydrothermal systems. AGU Fall Meeting, San Francisco, California, USA, December 15-19, 2014, V13D-08

Perez-Flores, P., Cembrano, J., Sanchez-Alfaro, P., Local Stress fields and paleo-fluid distribution within a transtensional duplex: An example from the northern termination of the Liquiñe-Ofqui Fault System. AGU Fall Meeting, San Francisco, California, USA, December 15-19, 2014, T23C-4697

Held, S., Schill, E., Sanchez-Alfaro, P., Neumann, T., Emmerich, K., Morata, D., Geological and Tectonic Settings Preventing High-Temperature Geothermal Reservoir Development at Mt. Villarrica (Southern Volcanic Zone): Clay Mineralogy and Sulfate-Isotope Geothermometry. World Geothermal Congress, April 19-24 2015, Melbourne Australia.

Bibliography

Barton, C.A., Zoback, M.D., and Moos, D., 1995, Fluid flow along potentially active faults in crystalline rock: Geology, v. 23, no. 8, p. 683, doi: 10.1130/0091-7613(1995)023<0683:FFAPAF>2.3.CO;2.

Cembrano, J., 1996, The Liquiñe Ofqui fault zone: a long-lived intra-arc fault system in southern Chile: Tectonophysics, v. 259, no. 1-3, p. 55–66, doi: 10.1016/0040-1951(95)00066-6.

Cembrano, J., and Lara, L., 2009, The link between volcanism and tectonics in the southern volcanic zone of the Chilean Andes: A review: Tectonophysics, v. 471, no. 1-2, p. 96–113, doi: 10.1016/j.tecto.2009.02.038.

Couples, G.D., 2013, Geomechanical impacts on flow in fractured reservoirs: Geological Society, London, Special Publications, p. 1–22, doi: 10.1144/SP374.17.

Cox, S.F., 2010, The application of failure mode diagrams for exploring the roles of fluid pressure and stress states in controlling styles of fracture-controlled permeability enhancement in faults and shear zones: Geofluids, p. 217–233, doi: 10.1111/j.1468-8123.2010.00281.x.

Fagereng, a., and Toy, V.G., 2011, Geology of the earthquake source: an introduction: Geological Society, London, Special Publications, v. 359, no. 1, p. 1–16, doi: 10.1144/SP359.1.

Manga, M., Beresnev, I., Brodsky, E.E., Elkhoury, J.E., Elsworth, D., Ingebritsen, S.E., Mays, D.C., and Wang, C.-Y., 2012, Changes in permeability caused by transient stresses: Field observations, experiments, and mechanisms: Reviews of Geophysics, v. 50, no. 2, p. RG2004, doi: 10.1029/2011RG000382.

Moore, J.N., and Simmons, S.F., 2013, More power from below.: Science, v. 340, no. 6135, p. 933–4, doi: 10.1126/science.1235640.

Richards, J.P., 2013, Giant ore deposits formed by optimal alignments and combinations of geological processes: Nature Geoscience, v. 6, no. 11, p. 911–916, doi: 10.1038/ngeo1920.

Rosenau, M., Melnick, D., and Echtler, H., 2006, Kinematic constraints on intra-arc shear and strain partitioning in the southern Andes between 38°S and 42°S latitude: Tectonics, v. 25, no. 4, p. 1–16, doi: 10.1029/2005TC001943.

Sibson, R.H., 1987, Earthquake rupturing as a mineralizing agent in hydrothermal systems: Geology, v. 15, no. 8, p. 701, doi: 10.1130/0091-7613(1987)15<701:ERAAMA>2.0.CO;2.

Sibson, R.H., 1985, Stopping of earthquake ruptures at dilational fault jogs: Nature, v. 316, no. 6025, p. 248–251, doi: 10.1038/316248a0.

Sibson, R.H., 1996, Structural permeability of fluid-driven fault-fracture meshes: Journal of Structural Geology, v. 18, no. 8, p. 1031–1042, doi: 10.1016/0191-8141(96)00032-6.

Chapter 2. Crustal deformation effects on the chemical evolution of geothermal systems: the intra-arc Liquiñe–Ofqui fault system, Southern Andes

Abstract

A better understanding of the chemical evolution of fluids in geothermal and hydrothermal systems requires data-based knowledge regarding the interplay between active tectonics and fluid flow. The Southern Andes volcanic zone is one of the best natural laboratories to address this issue because of the occurrence of numerous geothermal areas, recent seismic activity generated by regional fault systems, and intense volcanic activity. Geothermal systems have been understudied in this area, and limited scientific information exists about the role of local kinematic conditions on fluid flow and mineralization during the development and evolution of geothermal reservoirs. In this study, we provide data for a 1:200,000 scale geological and structural map of the Villarrica–Chihuio area as a setting in which to perform a structural analysis of active geothermal areas. This structural analysis, combined with geochemical modelling of hot spring data, allows the identification of two magmatic-tectonic-geothermal domains based on fault systems, volcanic activity, and lithologies. The Liquiñe–Ofqui fault system (LOFS) domain encompasses geothermal areas located either along the master or subsidiary faults. These are favourably orientated for shear and extension, respectively. In the LOFS domain, the geochemistry of hot spring discharges is controlled by interaction with the crystalline basement, and is characterized by low B/Cl conservative element ratios and high pH. In marked contrast, the arc-oblique long-lived fault systems (ALFS) domain includes geothermal occurrences located on the flanks of volcanoes forming WNW-trending alignments; these systems are built over faults that promote the development of crustal magma reservoirs. Unlike the first domain, the fluid chemistry of these geothermal discharges is strongly controlled by volcanic host rocks, and is typified by lower pH and higher B/Cl ratios. Reaction path modelling supports our model: chemical evolution of geothermal fluids in the Villarrica–Chihuio area is strongly dependent on structurally controlled mechanisms of heat transfer. Within this framework, heat transfer by conduction is responsible for the LOFS domain, whereas magmatically enhanced advective transport dominates heat flow in the ALFS domain. Although more studies are needed to constrain the complex interplay between tectonics and fluid flow, results from this study provide new insights towards efficient exploration strategies of geothermal resources in Southern Chile.

Introduction

Geothermal activity is dependent upon the interaction between a heat source, circulating fluids, and permeable pathways. The conceptual models considering this interaction guide the exploration and exploitation of geothermal resources. The main inputs of the geothermal conceptual models are the permeability architecture and the fluid geochemistry (D'Amore 1991; Goff and Janik 2000). The permeability architecture in geothermal systems is defined by the geometry and kinematics of fault–fracture networks (e.g. Sibson 1996). Faults may act as impermeable barriers to cross-fault flow or as high permeability conduits, although their permeability relative to the host rock depends on fault displacement, host rock lithology, hydrothermal mineral precipitation, and the seismic cycle (Sibson 1994; Wibberley et al. 2008). Fault–fracture networks including their damage zone damage zones are likely to develop directional permeability in the medium stress direction (σ_2) (e.g. Sibson 1996; Wibberley et al. 2008).

Correspondingly, the chemical evolution of geothermal fluids (Giggenbach 1984, 1991, 1997; Arnórsson et al. 2007) is defined by (1) transport and absorption of magmatic components (e.g. SO_2, HCl, HF, H_3BO_3) producing acidic and reactive fluids; (2) heat–fluid–rock interaction processes which neutralize fluids and hydrothermally alter rocks; and (3) surface processes such as boiling, mixing, and dilution with meteoric fluids. The continuous hydrothermal mineral precipitation seals both intrinsic permeability related to rock porosity and open fracture networks (Cox 2010). Therefore, the processes defining the chemical evolution of fluids are facilitated or inhibited by the dynamical permeability architecture, which creates a highly anisotropic system (Rowland and Simmons 2012).

A key question arising is how crustal deformation affects the chemical evolution of geothermal systems. The few works addressing this question have only analysed veins in fossil geothermal systems, which allows the determination of deformation (stress, strain) and thermodynamical (P–T–X) conditions of vein formation (Bons et al. 2012). However, the chemical analysis of fluids trapped in minerals as fluid inclusions has some analytical limitations, which have been only recently overcome (Heinrich 2007). Yet, vein fluid inclusion analysis is not as precise and accurate as the routine analysis of geothermal waters. The few studies on active geothermal systems addressing the interplay between deformation and chemical evolution of fluids, emphasize the relevance of fault and fracture network geometry and kinematics (Nemčok et al. 2007; Rowland and Simmons 2012). However, the conceptual models proposed based on specific geodynamical context still need to be specified.

The Southern Andes volcanic zone (SVZ) provides one of the best natural laboratories to address the interplay of fault–fracture networks and chemical evolution on geothermal systems, because of the occurrence of numerous geothermal areas (25% of Chilean geothermal areas; Hauser 1997), recent seismic activity generated by regional fault systems (e.g. Lange et al. 2008), and highly active volcanism (e.g. Stern 2004). Tectonic activity is represented by two regional scale fault systems: the arc-parallel Liquiñe–Ofqui fault system (LOFS) and the arc-oblique WNW-striking long-lived basement fault systems (ALFS) (Cembrano et al.1996; Potent 2003; Rosenau et al. 2006). Furthermore, these fault systems are genetically and spatially related to the magmatic evolution in the SVZ, forming two categories of volcano–tectonic associations (Cembrano and Lara 2009). (1) The LOFS, with NNE-striking master faults favourably orientated for dextral shear with respect to the prevailing stress field and NE-striking tension fractures likely to form under relatively low differential stress. Volcanic activity comprises NE-striking volcanic alignments containing mainly basaltic to basaltic–andesitic lithologies in either stratovolcanoes or minor eruptive centres. (2) The ALFS with WNW-striking faults severely misorientated with respect to the prevailing stress field. The volcanic activity comprises WNW-striking alignments of stratovolcanoes and displays a more evolved magma series (basaltic to rhyolitic).

Our study case is located in the Villarrica–Chihuio area (39°S–40°S in Chile), where both categories of volcano–tectonic associations are present and there is a high density of geothermal areas (Fig. 2.1). Moreover, the geothermal areas are spatially associated with the two different volcano–tectonic associations, being located either (1) over the NNE-striking master fault of the LOFS volcano–tectonic associations or (2) in the flanks of the volcanoes of the ALFS volcano–tectonic associations (Fig. 2.1(B)). These two volcano–tectonic associations allow analysis of the role of regional faults and volcanism in defining the chemical evolution of geothermal fluids.

The objective of this research is to get insights into the role of different fault systems in the chemical evolution of the geothermal fluids of the Villarrica–Chihuio area. Our hypothesis is that the interplay of volcanism and tectonics defines the occurrence of the major processes (e.g. magmatic gas absorption, fluid–rock interaction, fluid mixture) in the chemical evolution of geothermal fluids. This article aims to (1) interpret the role of fault systems in geothermal fluid flow through a structural analysis of published and new field data (geometry and kinematics) and (2) establish the processes that define the chemical evolution of fluids through sampling of thermal and meteoric fluids and the geochemical modelling. Our results show the occurrence of two distinctive magmatic-tectonic-geothermal domains, which define the heating mechanism and chemical evolution of geothermal fluids in the SVZ. Although more studies are needed to constrain the often-complex interplays between tectonics and fluid flow, results from this study show that

exploration of geothermal resources should focus on the long-lived arc-oblique magmatic-tectonic-geothermal domain.

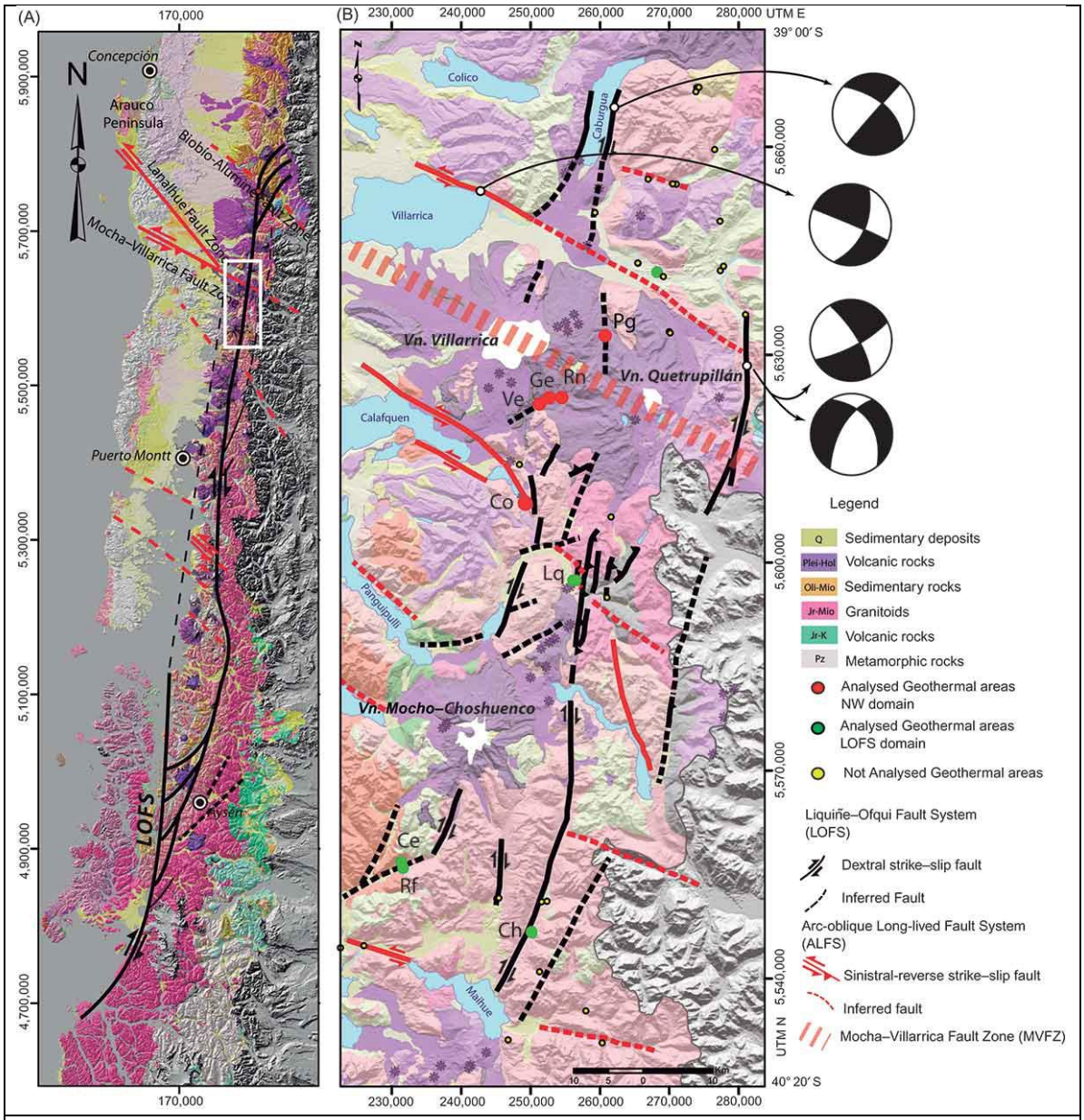

Figure 2.1 | (A) Regional geological map of the Southern Volcanic Zone showing the LOFS and the ALFS fault systems. (B) Geological map of the Villarrica–Chihuio area with the compilation and reinterpretation of fault systems based on Lara and Moreno (2004); Moreno and Lara (2008); Cembrano and Lara (2009); Rosenau et al. (2006); Rosenau (2004); and Potent (2003). Also shown are the chemically analysed geothermal areas of the two magmato-tectonic-geothermal domains: LOFS domain (green dots) and ALFS domain (orange dots). The rest of the geothermal areas are in yellow. The P/T dihedra related to faults are from Potent (2003), showing dextral strike–slip in the LOFS and sinistral strike–slip in the ALFS.

Geological setting

The Southern Andes shows a margin-parallel segmentation, consisting from west to east of (1) Palaeozoic metamorphic rocks on the Coastal Cordillera; (2) Oligocene to recent volcanic and sedimentary deposits in the Central Depression; and (3) Palaeozoic to Cenozoic plutonic and metamorphic rocks and Cenozoic volcano sedimentary rocks as basement for the present volcanic arc in the Principal Cordillera (Melnick and Echtler 2006). In Villarrica–Chihuio, the basement of the Pleistocene–Holocene volcanic arc is the Patagonian Batholith (e.g. Stern 2004; Cembrano and Lara 2009), which serves as impermeable host rock for the geothermal systems (Fig. 2.1). In turn, the sedimentary and volcanic rocks have intrinsic porosity and permeability enabling the development of a geothermal reservoir.

The main tectonic features in the Southern SVZ are the LOFS and the ALFS (Fig. 2.1) (e.g. Lavenu and Cembrano 1999; Rosenauet al. 2006; Cembrano and Lara 2009). The LOFS is a major intra-arc fault system that dominates the SVZ between 38°S and 47°S (Cembrano et al. 1996; Folguera et al. 2002; Adriasola et al. 2006; Rosenau et al. 2006). The LOFS accommodates strain along the intra-arc by dextral strike shearing along the NNE-striking master fault and normal and dextral strike–slip in subsidiary ENE-striking faults (Lavenu and Cembrano 1999; Rosenau et al. 2006). Fault–slip data and stress tensors for Pleistocene deformation along the northern portion of the LOFS consistently show a subhorizontal maximum principal compressive stress (σ_{Hmax}) trending N60°E (Lavenu and Cembrano 1999; Rosenau et al. 2006). NNE-striking master faults are favourably orientated for dextral shear with respect to the prevailing stress field and ENE-striking tension fractures likely form under relatively low differential stress (Lavenu and Cembrano 1999; Cembrano and Lara 2009). Ductile-to-brittle shear zones in the master fault document activity as a transpressional dextral strike–slip structure at least over the last 6 Ma, although geologic evidence suggests the LOFS was probably a leaky transform fault at about 25 Ma (e.g. Cembrano et al. 2002). The shortening component of Pliocene to recent intra-arc deformation increases to the south, as the LOFS approaches the Chile triple-Junction (e.g. Lavenu and Cembrano 1999; Cembrano et al. 2002; Thomson 2002; Rosenau et al. 2006). The margin-parallel intra-arc shear accommodates a mean rate of 13 mm per year corresponding to half of the margin-parallel component of the plate convergence vector (Rosenau et al. 2006) and forms a micro-plate (Moreno et al. 2010).

In the above-described tectonic setting, the WNW-striking faults of the ALFS are severely misorientated with respect to the prevailing stress field and have been interpreted as crustal weaknesses associated with pre-Andean faults reactivated as sinistral-reverse

strike–slip faults during arc development (Cembrano and Moreno 1994; López-Escobar et al. 1995; Lara et al. 2006; Melnick et al. 2006; Rosenau et al. 2006; Glodny et al. 2008; Lange et al. 2008). These fault systems are recognized as the contact of basement rocks with younger units and in some cases present mylonites as evidence of ductile deformation (Glodny et al. 2008). In the Villarrica–Chihuio area, the main feature of this system is the Mocha–Villarrica fault zone (MVFZ), (Hackney et al.2006) a regional lineament which comprises the Villarrica–Quetrupillán–Lanin volcanic chain. The nature and kinematics of the faults in this system are not well constrained; however, available field and seismic data indicate that some of them are active. Shallow seismicity indicates sinistral and normal–sinistral slip (Lange et al. 2008; Moreno et al. 2011).

The complex interaction between tectonic and magmatic processes is evidenced by both the architecture and geochemical signature of volcanic systems (López-Escobar et al. 1995; Lara et al. 2006; Cembrano and Lara 2009). The present-day kinematics of the volcanic arc is evidenced by several shallow crustal earthquakes and the morphology of volcanic systems. The subsidiary structures of the LOFS form NE-striking volcanic alignments of stratovolcanoes and/or monogenetic cones, which are directly related to the current dextral transpressional tectonic regime and exhibit mostly primitive magmas (Lara et al. 2006; Cembrano and Lara 2009). In the ALFS, the volcanic activity comprises WNW-striking alignments, where only stratovolcanoes occur and include a wide range of compositions with some centres that have erupted only rhyolitic products in historical times. Because of their misorientation with respect to the prevailing stress field, these faults require supralithostatic magmatic pressures to become active (Lara et al. 2004, 2006; Cembrano and Lara 2009).

The Villarrica Volcano is a large middle Pleistocene–Holocene stratovolcano, with most-recent eruptions in 1948–1949, 1963–1964, 1971–1972, and 1984 (e.g. Stern et al. 2007). Recent intense activity includes passive degassing from a summit lava lake (Witter et al. 2004). This volcano, although lying on top of a WNW-striking structure, exhibits NE-striking flank vents, suggesting that these are coupled with the present-day NE-striking maximum horizontal stress. The Quetrupillán Volcano, a Pleistocene to Holocene stratovolcano (Stern 2004) last erupting in 1872, has two nested calderas and a series of domes and pyroclastic cones (Stern et al. 2007). Minor eruptive centres are locally abundant in the study area and consist of basaltic scoria cones located along the LOFS master faults, parallel to the volcanic arc (e.g. López-Escobar et al. 1995; Lara et al. 2006). The Mocho–Choshuenco volcanic complex (Pleistocene–Holocene), last known to have erupted in 1937, consists of the remnants of an old edifice (Choshuenco peak) and an intra-caldera small stratocone (Mocho) (Moreno and Lara 2007).

In the Villarrica–Chihuio area, the geothermal fluids have been used for recreational purposes since early twentieth century (Hauser 1997), but the origin of these systems has only been recently studied. Risacher et al. (2011) performed a systematic sampling in Chile at regional scale and used conservative elements (Br–Cl) and reaction models to propose that the origin of components for thermal fluids is mixing with seawater and magmatic contribution. However, their model does not consider the spatial distribution of volcanoes nor the distance to the sea, which is as far away as 150 km. More local studies (Lahsen 1986; Hauser 1997; Pérez 1999) have proposed a tectonic origin for the geothermal areas located over the master fault of the LOFS based on the structural context and the crystalline host rock. However, these authors' ideas are not supported by geochemical data.

Methods

A 1:200,000 scale geological and structural map based on published data and satellite imagery was compiled for the structural analysis (Potent 2003; Lara and Moreno 2004; Rosenau 2004; Rosenau et al. 2006; Moreno and Lara 2008; Cembrano and Lara2009). Structural data consisted of establishing the geometry and kinematics of faults, volcanic chains, and lineaments. The nature, geometry, kinematics, and relative ages of faults were analysed to elaborate an internally consistent structural map. Fieldwork in key places was conducted to confirm the structural interpretation. The location of geothermal areas and alignments of hot springs in a specific geothermal area were obtained in the fieldwork using GPS and compass. The structural analysis of geothermal areas was performed using the geological and structural map and taking onto account fault–fracture network model (e.g. Sibson 1996).

To assess the hypothesis of heating mechanism effects on the chemical evolution of geothermal fluids, thermal water sampling, geochemical analysis, and geochemical modelling were performed. The sampling was conducted in thermal and meteoric fluids from eleven geothermal areas selected according to their distribution with respect to regional faults and volcanoes and their higher fluid flux and temperature. For the geochemical modelling, two conceptual models were run in the forward reaction modelling program, React (Bethke 1996): (1) magmatic gas absorption and fluid–rock interaction, emulating the heat and mass transfer from a magmatic reservoir, and (2) fluid–rock interaction emulating deep convection of meteoric waters in areas of high heat flow. These models allow analysis of the effect of heating mechanisms in the chemical evolution of fluids. At regional scale, chemical modelling can only be achieved on a semi-quantitative basis to identify trends on the chemical evolution of fluids (Mark et al.2005; Smith et al. 2010). Thus, the precise reconstruction of water composition is meaningless because of the complexity of actual processes. The geochemical modelling codes, Act2 and React

(Bethke 1996), were used to calculate the activity diagrams and the aqueous activities for the geothermal fluids at the subsurface (reservoir) condition.

In some geothermal areas, more than one hot spring was sampled. In total, 19 water samples were collected for geochemical analyses (major and minor elements) and nine for isotopic analysis (D, ^{18}O). Sampling procedures (sampling, filtering, acidification, etc.), in situ measurement techniques used in this study (temperature, pH and carbonate alkalinity), and the ionic balance computation follow reported methodologies by Giggenbach and Gouguel (1989) and Arnórsson (2000). Carbonate alkalinity ($HCO_3^- + CO_3^{2-}$) was measured directly in the field by acidimetric titration using an alkalinity test kit (Hanna, HI-3811). Inductively coupled plasma optical emission spectrometry (ICP-OES, Perkin Elmer Optima 7300V) and ion chromatography (IC, Metrohm 861 Advanced Compact) were used for measuring cation and anion concentrations, respectively. Carbonate species concentrations were measured in the laboratory by acidimetric titration with back titration, using the Giggenbach and Gouguel (1989) method to avoid the contributions of other acids. The analytical work was carried out in the Geochemistry Laboratory of the Department of Geology, University of Chile. Stable isotopes were analysed in the Nuclear Energy Chilean Commission (CCHEN) laboratory, with an IR MS Delta S mass spectrometer using the EQ measuring method with the V-SMOW standard.

Results

Fault systems

The geological and structural map of the Villarrica–Chihuio area (Fig. 2.1(B)) shows the location of the main stratovolcanoes (Villarrica, Quetrupillán, Mocho–Choshuenco), geothermal areas, and fault systems. Within this area, two contrasting lithology assemblages exist: a crystalline basement of low intrinsic permeability, overlain by relatively permeable Pliocene to Holocene volcanoclastic units. The geothermal areas are spatially correlated to fault systems, and some of them are in the flanks of the Villarrica volcano (Fig. 2.1(B); Table 1). To assess the interplay of volcano–tectonic associations and geothermal systems we define two magmatic-tectonic-geothermal domains: the LOFS domain and the ALFS domain.

The LOFS domain includes geothermal areas located along either master or subsidiary faults of the LOFS. There, thermal water emerges from fractures in granitoids or sediments overlying them (Table 1). Main structural features of this domain are the arc-parallel NNE-striking dextral strike–slip master faults and subsidiary NE-striking dextral and normal faults which are favourably oriented for shear and/or extension with respect to the prevailing stress field. The LOFS cuts and displaces the ALFS in the vicinities of Liquiñe (Lq) and Coñaripe (Co), but locally, the opposite cross-cutting relationship is

observed (Fig. 2.1(B)). Volcanic systems linked to these faults exhibit primitive magmas, which are transported through tension cracks with no magmatic chamber development (Lara et al. 2006; Cembrano and Lara 2009).

The ALFS domain hosts geothermal areas, which are located on the WNW-trending aligned volcano flanks where hot springs discharge from volcanic rocks or sedimentary deposits overlying them. The condition for reactivate faults of ALFS promotes long residence of magma in crustal reservoirs, which may serve as heat sources for geothermal systems.

Most of the studied geothermal areas consist of several hot springs, which in some cases form well-defined alignments. These alignments are mainly NE and coincide with the faults mapped in the vicinities of both magmatic-tectonic-geothermal domains (Table 1). In the Geométricas (Ge) and Vergara (Ve) geothermal areas from the ALFS domain (see Fig. 2.1), hot springs are aligned N55E and N62E, respectively, spatially associated with a NE inferred fault affecting Pleistocene–Holocene volcanic units. In the Liquiñe (Lq) geothermal area, which belongs to the LOFS domain, the hot springs trend N15E and lie within fractures in granites, close to one NNE master fault of the LOFS.

Table 1. Location and main characteristics of the geothermal areas of the Villarrica–Chihuio area.

Geothermal area	Latitude	Longitude	Elevation (m)	Nearest stratovolcano (km)	Upwelling rock	Hot springs alignment			Nearest fault system (strike)	Domain
						n°	Length (m)	Strike (°)		
San Luis	39°20.49′S	71°41.47′N	390	Q(18)	Piroclastic deposits overlying granitoids	1	N/A	N/A	ALFS (NW)	LOFS
Palguin	39°25.27′S	71°47.11′N	761	Q(11)	Fluvial deposits overlying Villarrica volcanic units	7	159	N36°E	LOFS (NNE)	ALFS
Geométricas	39°30.01′S	71°52.40′N	888	V(8)	Villarrica volcanic units	7	150	N48°E	LOFS (NE) & ALFS (NW)	ALFS
Rincón	39°30.47′S	71°51.26′N	878	V(8)	Fluvial deposits overlying Villarrica volcanic units	5	45	N34°W	ALFS (NW)	ALFS
Vergara	39°30.44′S	71°53.36′N	758	V(9)	Fluvial deposits overlying Villarrica volcanic units	4	22	N36°E	LOFS (NE) & ALFS (NW)	ALFS
Coñaripe	39°38.10′S	71°55.44′N	251	V(22)	Glacial deposits overlying granitoids	7	106	N64°W	ALFS (NW)	ALFS
Trifupán	39°44.17′S	71°51.64′N	300	MC(25)	Fluvial deposits overlying granitoids	1	N/A	N/A	LOFS (NNE) & ALFS (NW)	LOFS
Liquiñe	39°44.33′S	71°50.58′N	312	MC(26)	Fractured granitoids	7	110	N15°E	LOFS (NNE) & ALFS (NW)	LOFS
Rio Florín	40°05.95′S	72°08.96′N	277	MC(20)	Fractured granitoids	1	N/A	N/A	LOFS (NE)	LOFS
Cerrillos	40°06.12′S	72°08.90′N	314	MC(20)	Fractured granitoids	3	20	N52°E	LOFS (NE)	LOFS
Chihuio	40°11.64′S	71°56.07′N	339	MC(30)	Fluvial deposits overlying granitoids	5	13	N70°E	LOFS (NNE)	LOFS

Note: N/A, Alignment not available; Q, Quetrupillán; V, Villarrica; MC, Mocho–Choshuenco.

Table 2. Physicochemical characteristics of the thermal springs in the Villarrica–Chihuio area.

Geothermal area	Sample ID	T (°C)	pH	Li	Na	K	Mg	Ca	B	Br	Sr	Al	F	Fe	NO_3	HCO_3	CO_3	SiO_2	SO_4	Cl	Σcat	Σani	Balance
San Luis	SL	39.3	9.4	0.085	55.2	0.96	0.153	5.17	0.110	b.d.	0.069	0.013	1.755	0.009	1.4	29.3	12.0	49.2	76.8	8.0	2.7	2.8	−1.88%
Palguin	Pg-GS	35.4	8.7	0.079	42.0	1.87	1.330	4.19	0.434	1.269	0.015	0.058	1.037	0.016	1.4	66.8	0.0	46.6	31.6	10.0	2.2	2.1	1.92%
Palguin	Pg	35.5	8.7	0.058	52.6	2.51	1.500	4.17	0.690	1.269	0.015	0.075	1.476	0.029	1.5	80.5	0.0	52.2	37.9	12.2	2.7	2.6	2.44%
Geométricas	Ge	72.4	8.4	0.286	160.0	9.63	0.129	46.54	5.020	1.322	0.433	0.027	1.196	0.007	1.3	29.0	0.0	83.0	421.3	48.7	9.6	10.7	−5.55%
Rincón	Rn	35.7	8	0.143	62.0	4.02	1.950	10.21	1.420	1.268	0.031	0.026	0.860	0.021	1.5	52.0	0.0	69.1	103.3	17.3	3.5	3.6	−1.14%
Vergara	Ve-01	40.7	7.8	0.118	72.4	5.00	2.590	16.96	1.900	1.277	0.081	0.011	0.490	0.008	1.6	48.0	0.0	68.0	150.8	18.1	4.4	4.5	−1.64%
Coñaripe	Co-04	55	7.9	0.177	82.3	2.66	0.873	7.17	4.700	1.354	0.058	0.053	0.852	0.008	1.6	77.6	0.0	55.0	60.9	49.7	4.1	4.0	1.02%
Coñaripe	Co	68	8.6	0.255	136.0	3.64	0.335	5.61	7.340	1.408	0.049	0.121	1.503	0.010	1.4	93.5	0.6	78.3	102.5	81.4	6.4	6.1	2.07%
Coñaripe	Co-01	60	8.3	0.198	98.9	3.15	0.215	6.89	5.350	1.361	0.050	0.053	1.117	0.008	1.3	83.3	0.0	61.4	77.9	61.6	4.8	4.8	−0.44%
Trifupán	Tp	37.3	8.9	0.070	59.7	1.38	0.883	9.75	0.518	1.282	0.062	0.014	0.652	0.008	1.7	41.7	0.0	42.4	77.3	22.8	3.2	3.0	3.12%
Liquiñe	Lq-02	71.1	9.4	0.115	73.4	2.23	0.031	3.65	0.213	1.276	0.063	0.040	1.321	0.009	*b.d.*	24.0	21.6	82.6	78.4	15.6	3.5	3.3	2.73%
Liquiñe	Lq	71.4	9.5	0.134	71.1	2.21	0.014	3.75	0.197	1.278	0.063	0.041	1.474	0.008	1.3	66.9	0.9	87.1	80.5	16.0	3.4	3.4	−0.11%
Liquiñe	Lq-04	70	8.8	0.067	26.0	1.14	0.708	5.19	0.010	b.d.	0.034	0.015	0.340	0.007	1.4	35.1	0.0	40.9	29.5	7.1	1.5	1.4	2.19%
Liquiñe	Lq-01	70.4	9.4	0.133	69.3	2.16	0.072	3.78	0.164	1.266	0.061	0.076	1.387	0.008	1.3	39.7	1.2	84.1	80.2	15.6	3.3	2.9	6.13%
Rio Florín	Rf	54.4	9.7	0.066	59.8	0.99	0.025	7.66	0.509	1.286	0.036	0.025	0.543	0.008	1.3	26.1	0.0	56.9	78.1	25.7	3.0	2.8	3.10%
Cerrillos	Ce	41.2	9.4	0.061	55.2	0.81	0.092	8.29	0.435	1.280	0.044	0.020	0.414	0.011	1.5	29.3	8.0	53.7	75.1	21.4	2.9	3.0	−2.03%
Cerrillos	Ce-GS	32	8	0.077	42.1	0.66	0.690	11.83	0.232	1.261	0.041	0.019	0.259	0.011	1.4	46.6	0.0	42.1	57.5	14.9	2.5	2.4	1.65%
Chihuio	Ch	82	9.4	0.114	107.0	4.15	0.055	9.93	0.008	1.263	0.294	0.073	0.920	0.026	1.5	23.5	1.1	95.8	212.6	13.5	5.3	5.3	−0.27%
Chihuio	Ch-01	82.4	9.4	0.108	106.0	4.00	0.017	9.87	0.005	1.263	0.302	0.043	0.882	0.013	1.5	24.4	2.1	96.9	212.2	12.6	5.2	5.3	−0.91%

Note: Concentrations of cations and anions are shown in mg/l; the sum of cations (Σcat) and anions (Σani) for the ionic balance is expressed in meq/l; b.d. = below detection limit.

Chemistry of thermal fluids

Physicochemical characteristics of the thermal springs and surface waters of the study area are summarized in Table 2. In geothermal areas with more than one sample, the sample least diluted with cold meteoric water is selected as representative by considering the highest discharge temperature, Cl and SiO_2 concentrations (Table 2). Only these representative samples were used for the geochemical modelling and interpretation diagrams. The chemical analysis for all the geothermal fluid samples has good ionic balance (<±6%) and accuracy.

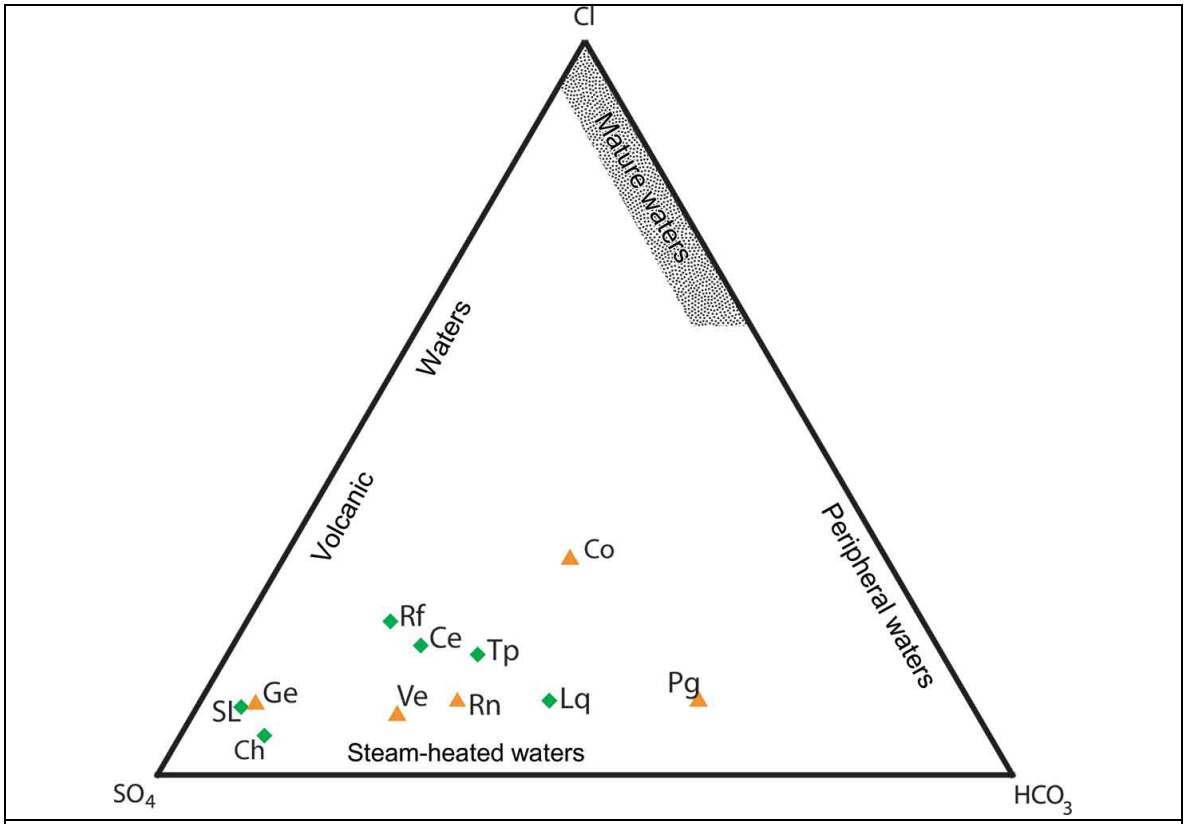

Figure 2.2 | Anion ternary diagram for thermal waters in mg/Kg. Fields defined by Giggenbach (1988). LOFS domain samples in green diamonds and ALFS domain in orange triangles. Note: SL = San Luis; Pg = Palguín; Geométricas = Ge; Rincón = Rn; Vergara = Ve; Coñaripe = Co; Trifupán = Tp; Liquiñe = Lq; Río Florín = Rf; Cerrillos = Ce; Chihuio = Ch.

The thermal waters have low content of dissolved solids (TDS <550 mg/l) and are classified as Na–SO_4 type based on major ion concentration (Table 2). The thermal waters of the LOFS domain are alkaline (pH 8.9–9.7) with surface temperatures between 37 and 82°C, whereas those of the ALFS domain are sub-alkaline (pH 7.8–8.7) and have temperatures from 36°C to 70°C. The Cl–SO_4–HCO_3 diagram is commonly used to classify

geothermal fluids and interpret the main geochemical processes occurring (Giggenbach 1988, 1991). In this diagram, the low chloride and relatively high sulphate concentrations place thermal waters of Villarrica–Chihuio close to the steam-heated water field (Fig. 2.2).

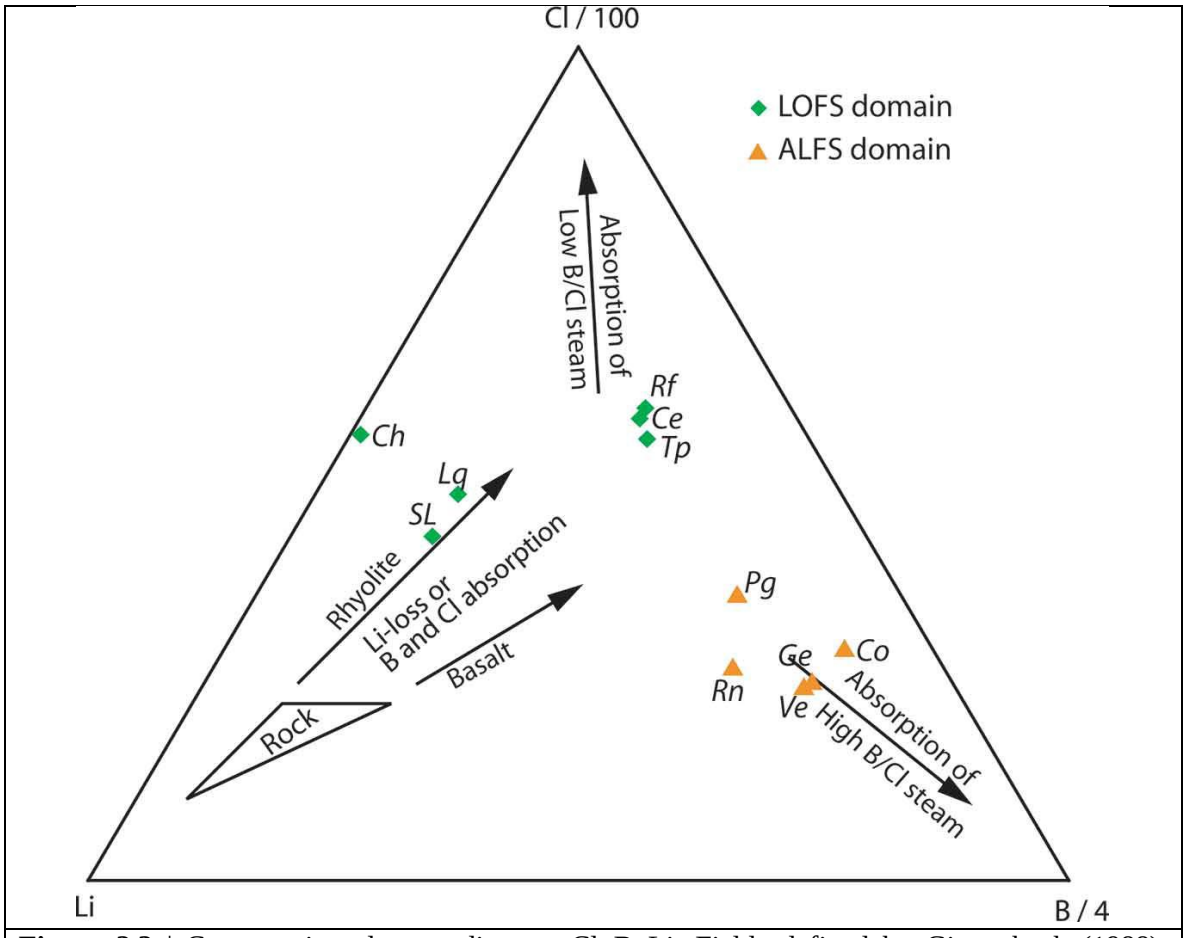

Figure 2.3 | Conservative element diagram Cl–B–Li. Fields defined by Giggenbach (1988). Sample legend as in Fig. 2.2.

The ratios between conservative elements such as chorine (Cl), boron (B), and lithium (Li) normally do not get modified and remain unchanged even with dilution, which allows them to be used as tracers of the geothermal fluid sources (Giggenbach 1991). In the B–Cl–Li triangular plot the two domains are plotted as different clusters (Fig. 2.3). Also, the absolute B concentrations in the ALFS domain (0.4–7 mg/l) are higher than the background levels detected in rivers and cold springs nearby (B < 0.03 mg/l; e.g. Aihue river, San Luis cold spring; Pérez 1999).

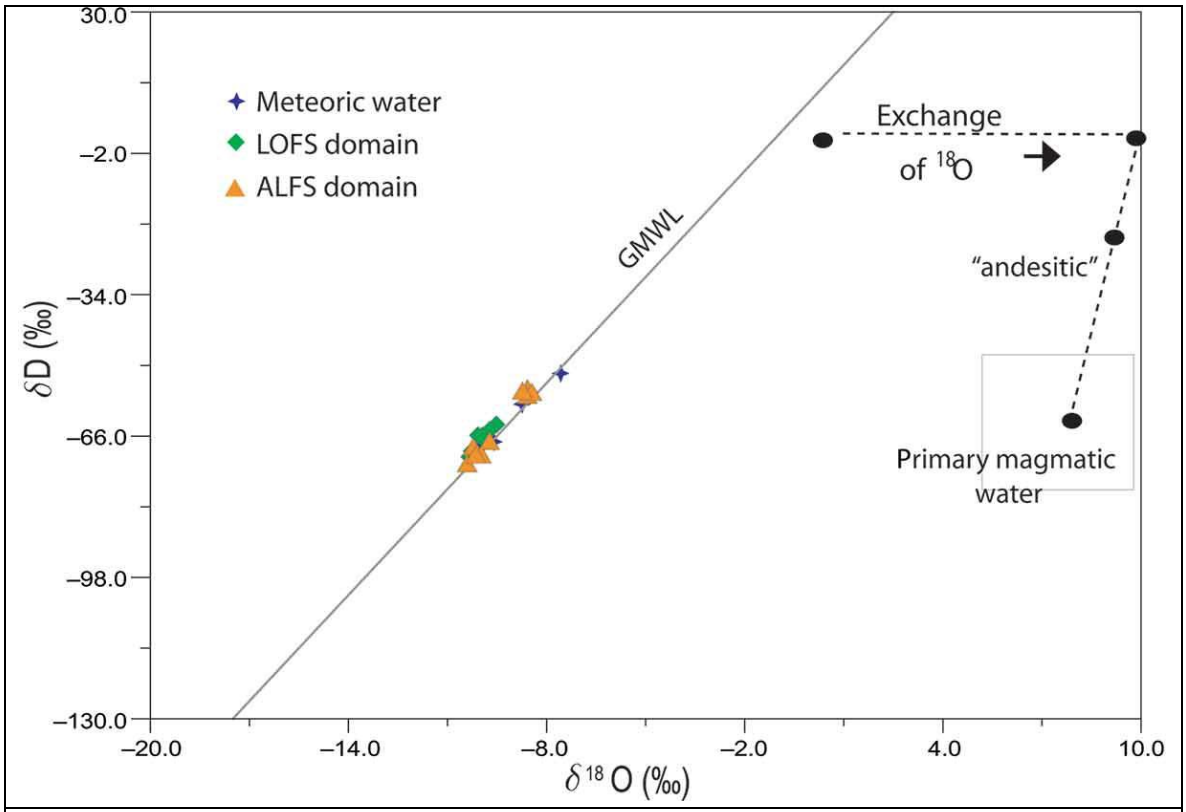

Figure 2.4 | Isotopic composition of geothermal fluids of the Villarrica–Chihuio area. Global meteoric water line (GMWL) and the field of magmatic fluids are shown (Giggenbach and Glover 1992). Sample legend as in Fig. 2.2.

Stable isotopes in water (D, ^{18}O) are tracers to identify the origin of the geothermal fluids, secondary processes (e.g. boiling, mixing), and the extent of water–rock interaction in geothermal systems (D'Amore 1991; Arnórsson 2000). In the δD versus $\delta^{18}O$ diagram (Fig. 2.4), the meteoric water samples of Villarrica–Chihuio lie on the global meteoric water line (GMWL; Craig 1963). Thermal fluids also lie close to the GMWL without significant shift of $\delta^{18}O$ (<0.13) with respect to the GMWL (Fig. 2.4; Table 3).

The ratio-based geothermometers (Na–K, K–Mg) are considered to be less affected by dilution than single constituent-based geothermometers. The Na–K–Mg ternary diagram allows the estimation of temperatures in subsurface and approach to equilibrium state (Giggenbach 1984, 1988). Fully equilibrated samples have all the phases saturated and both geothermometers whereas partially equilibrated waters suffer re-equilibration during fluid ascent, but both are suited for temperature estimations. In the study area, Ch, Lq, Ge, Rf, and Co samples are in the partially equilibrated field (Fig. 2.5). Considering the geothermal areas least affected by dissolution, as indicated by higher temperature, and Silica and Cl concentrations of the geothermal discharges, we obtained estimations for reservoir

temperatures of 100–150°C (Lq, Ch) for the LOFS domain and 140–180°C (Ge) for the ALFS domain.

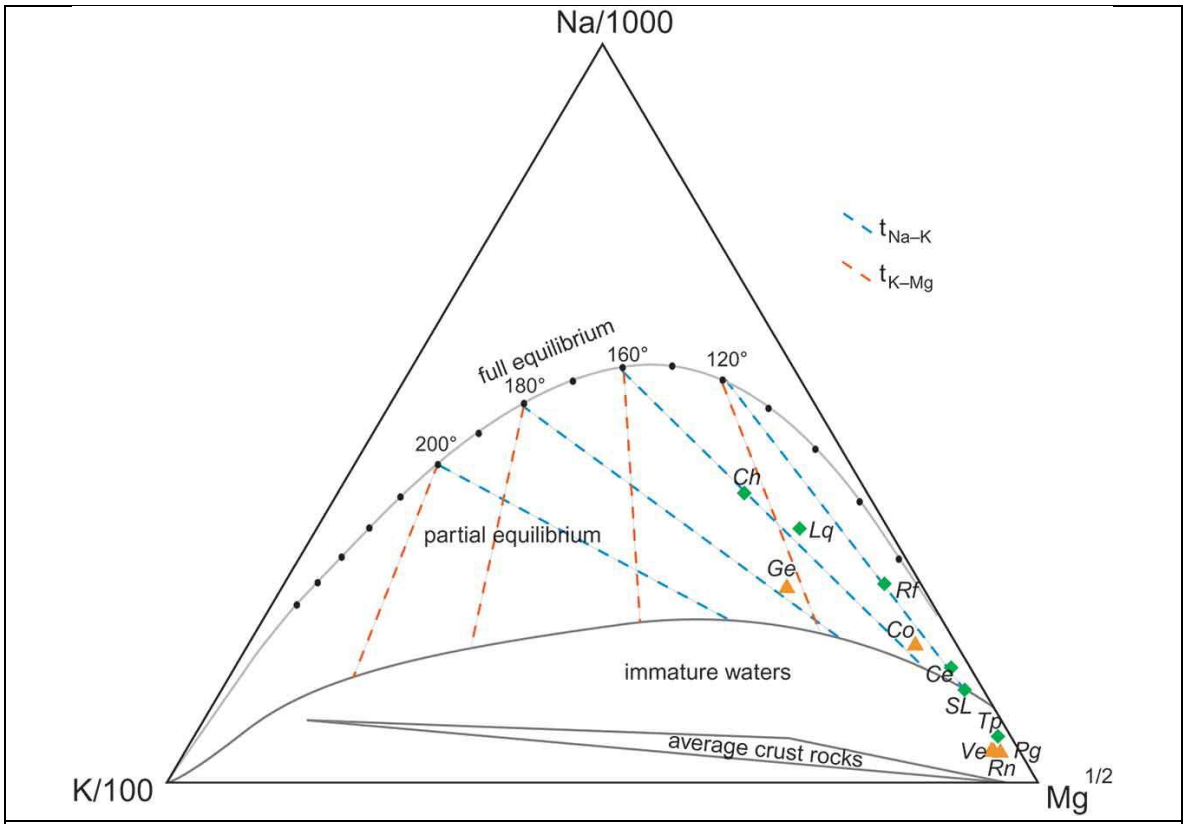

Figure 2.5 | Na–K–Mg geothermometer diagram (Giggenbach 1988) of Villarrica–Chihuio area geothermal fluids. It shows the estimation for reservoir temperatures and assesses equilibrium state.

Activity diagrams and reaction model

The aqueous activities of Na^+, K^+, and H^+ for the thermal springs are plotted in the activity diagrams for the system $Na_2O–K_2O–SiO_2–H_2O$ at reservoir temperature (150°C) in Fig. 2.6. The system $Na_2O–K_2O–SiO_2–H_2O$ is commonly used for analysis of fluid–rock interaction under hydrothermal conditions (e.g. Druschel and Rosenberg 2001; Bignall et al. 2004). In the activity diagrams, the equilibrium lines limit the stability fields of the minerals. The reactions occurring during fluid–rock interaction buffer the chemical composition of fluids and constrain it to (partial and local) equilibrium conditions. Thermal water of Villarrica–Chihuio in the activity diagram lie close to the Albite–Adularia equilibrium line whereas the meteoric water samples lie on the kaolinite stability field (Fig. 2.6). Moreover, the two magmatic-tectonic-geothermal domains lie on differentiable clusters.

Table 3. Isotopic data of thermal and meteoric fluids from Villarrica–Chihuio.

Site	Sample ID	Feature type	$\delta^{18}O$	δD
Liquiñe	Lq	Hot spring	−9.79	−65
Liquiñe[a]	Lq-P	Hot spring	−9.5	−63
San Luis	SL	Hot spring	−9.65	−65.1
Chihuio	Ch	Hot spring	−10.14	−68.5
Cerrillos	Ce	Hot spring	−9.55	−65.3
Palguin	Pg	Hot spring	−9.66	−67.4
Palguin	Pg-GS	Hot spring	−10.33	−71.9
Palguin[a]	Pg-P	Hot spring	−10.15	−69
Coñaripe	Co	Hot spring	−8.47	−55.5
Coñaripe	Co-04	Hot spring	−8.49	−56.5
Coñaripe	Co-01	Hot spring	−8.5	−57
Vergara	Ve	Hot spring	−9.89	−70.1
Geométricas	Ge	Hot spring	−10.1	−70
Chihuio River	Cm	River	−10.04	−68
San Luis	Sm	Cold spring	−9.6	−67.1

Notes: Delta oxygen and hydrogen are referred to V-SMOW, and expressed as parts per million values.
[a]Data from Pérez (1999).

Forward reaction modelling of the fluid–rock interaction on the two hypothesized heating mechanisms reveals the main chemical changes on the fluid phase and the mineral precipitating (Fig. 2.7). These models allow identification of the main processes governing the chemical evolution of fluids in both magmatic-tectonic-geothermal domains. For the LOFS domain, the fluid–rock interaction during deep convection of meteoric waters in areas of high heat flow is modelled as a system composed by the local meteoric water and granitoid in reservoir conditions (150°C). The results of the model show that as reaction progresses, pH increases up to a value of 8 and sodium (Na^+) concentration increases by an order of magnitude. Cl, SO_4, and dissolved SiO_2concentrations remain relatively unchanged (Fig. 2.7(A)). For the ALFS domain, the heat and mass transfer from a magmatic body is modelled by considering the absorption of a magmatic gas end-member (based on a volcanic fluid condensate mixed 1:10 with pure water; (Symonds et al. 1990; Reed 1997; Smith et al. 2010) reacting at 150°C with an unaltered andesite of the SVZ (Risacher et al. 2011).

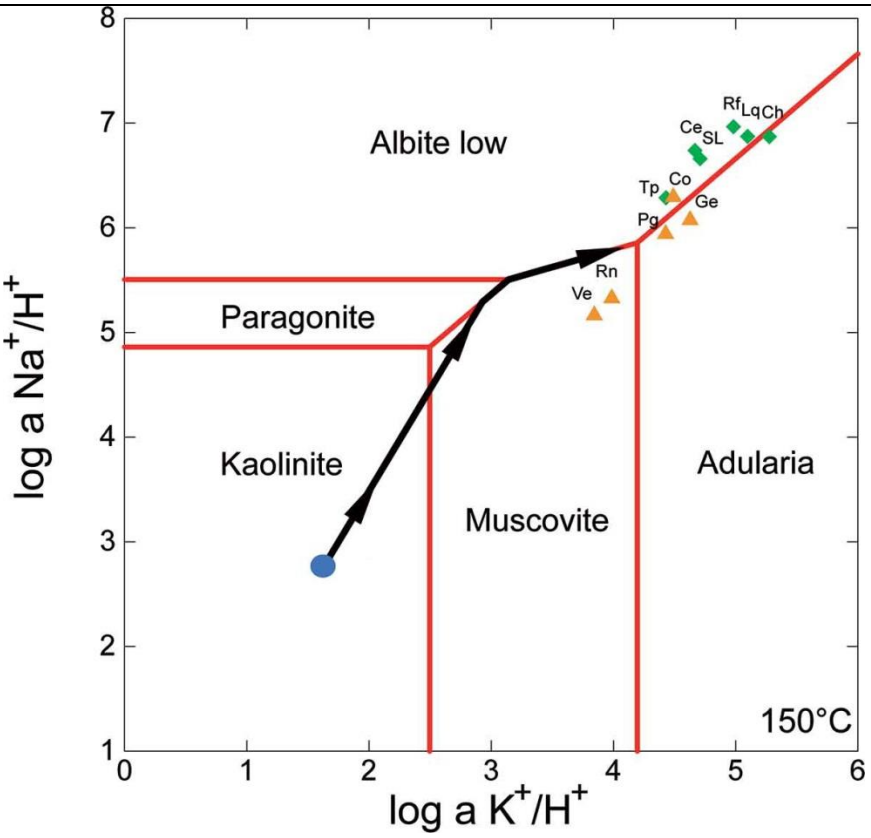

Figure 2.6 | Activity diagram for the system Na_2O–K_2O–SiO_2–H_2O at reservoir temperature (150°C) with the aqueous activities of Na^+, K^+, and H^+ for thermal springs. Stability of hydrothermal minerals is limited by equilibrium lines. The arrow shows the reaction path of meteoric water reacting with local granitoids. P = 1.013 bars; activity of quartz = 1; activity of H_2O = 1.

The results of the model show that as reaction progresses, there is a pH increase and cation (Na^+, K^+) concentration increases by an order of magnitude (Fig. 2.7(B)). SO_4 concentration decreases by two orders of magnitude, related to the precipitation of alunite, barite, and pyrite (Fig. 2.7(B)). As expected, conservative elements (B, Cl) do not get modified by fluid–rock interaction and its ratio stays constant even with dilution. Dissolved SiO_2 is buffered by the solubility of quartz (thermally dependent) and its concentration remains relatively constant.

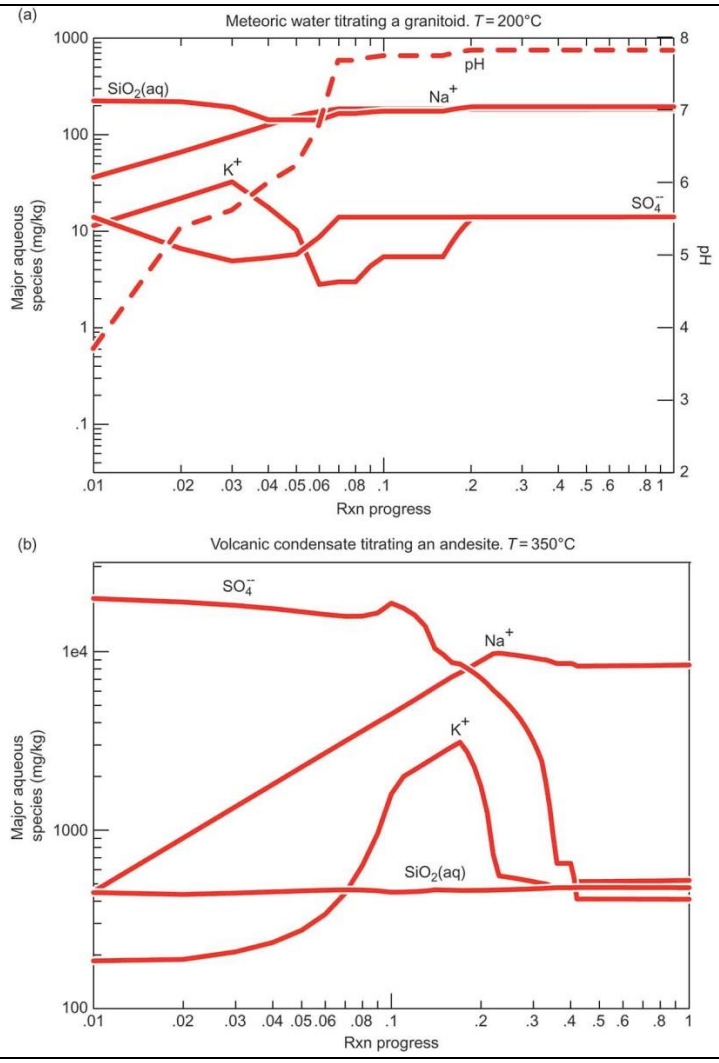

Figure 2.7 | Results of the geochemical modelling showing the effect of the heating mechanism in the chemical evolution of fluids. (A) Meteoric water titrating granitoids at 200°C, simulating the reaction path of geothermal fluids of the LOFS domain. (B) Titration of an andesite from the Villarrica–Chihuio area (Risacher et al. 2011) by a magmatic fluid (based on a volcanic fluid condensate mixed 1:10 with pure water; Symonds et al. 1990; Reed 1997; Smith et al. 2010) at 350°C, simulating the reaction path of geothermal fluids of the ALFS domain.

Discussions

Interplay of faults system and fluid flow

From the analysis of fault systems, volcanic activity, and hydrothermal systems, we have identified two distinctive magmatic-tectonic-geothermal domains: the LOFS domain and the ALFS domain (Fig. 2.1(B); Table 1). Although these domains are not completely independent of each other, they reflect the different natures of the geothermal systems, which are defined by their heat sources. We propose that the nature of the heat source for

the geothermal systems of the LOFS domain is the high heat flux in an intra-arc region, which is transferred by conduction to the deep circulating fluids (Fig. 2.8 and 2.9). In the ALFS domain, in turn, magmatically enhanced advective transport dominates heat and mass flow (Fig. 2.8 and 2.9). The WNW-striking ancient faults, which are misorientated with respect to the prevailing stress field, provide conditions for magma reservoir development. Although these two distinctive domains show contrasting features, the ultimate heat source for both of them is the melt in the MASH zone (Hildreth and Moorbath 1988; Annen et al. 2006).

The contrasting lithologies have different behaviours for fluid flow. The volcaniclastic units have anisotropic permeability architecture because of bedding, autobreccias, and contacts. Thus, it is likely that fluid flow takes place along bedding planes, i.e. subhorizontal (e.g. Rowland and Sibson 2004). In contrast, the pristine crystalline basement has low intrinsic permeability and limits fluid flux to fault–fracture networks. Fault–fracture networks in the damage zone of the LOFS may increase permeability by orders of magnitude within crystalline rocks (Barton et al. 1995). This is also supported by recent seismic activity of faults in the LOFS domain, which shows a causal relationship between fluid flow and earthquakes (Legrand et al. 2010).

Most of the geothermal areas are spatially associated with regional fault systems, and the hot spring alignments exhibit a similar trend (Table 1). This is consistent with the idea of a first order control exerted by brittle deformation on hydrothermal fluid flow (e.g. Sibson 1996; Curewitz and Karson 1997; Cox 2010). The latter suggests that geothermal fluid flow is concentrated in fracture networks once the initial porosity is destroyed by hydrothermal alteration (e.g. Sibson 1996; Hanano 2004; Cox 2010). Thus, the secondary architecture permeability overprints the intrinsic permeability anisotropies originated by stratification in porous rocks. Fault–fracture networks, consisting of faults, extensional fractures, and extensional shear-fractures are conduits for hydrothermal fluid flow.

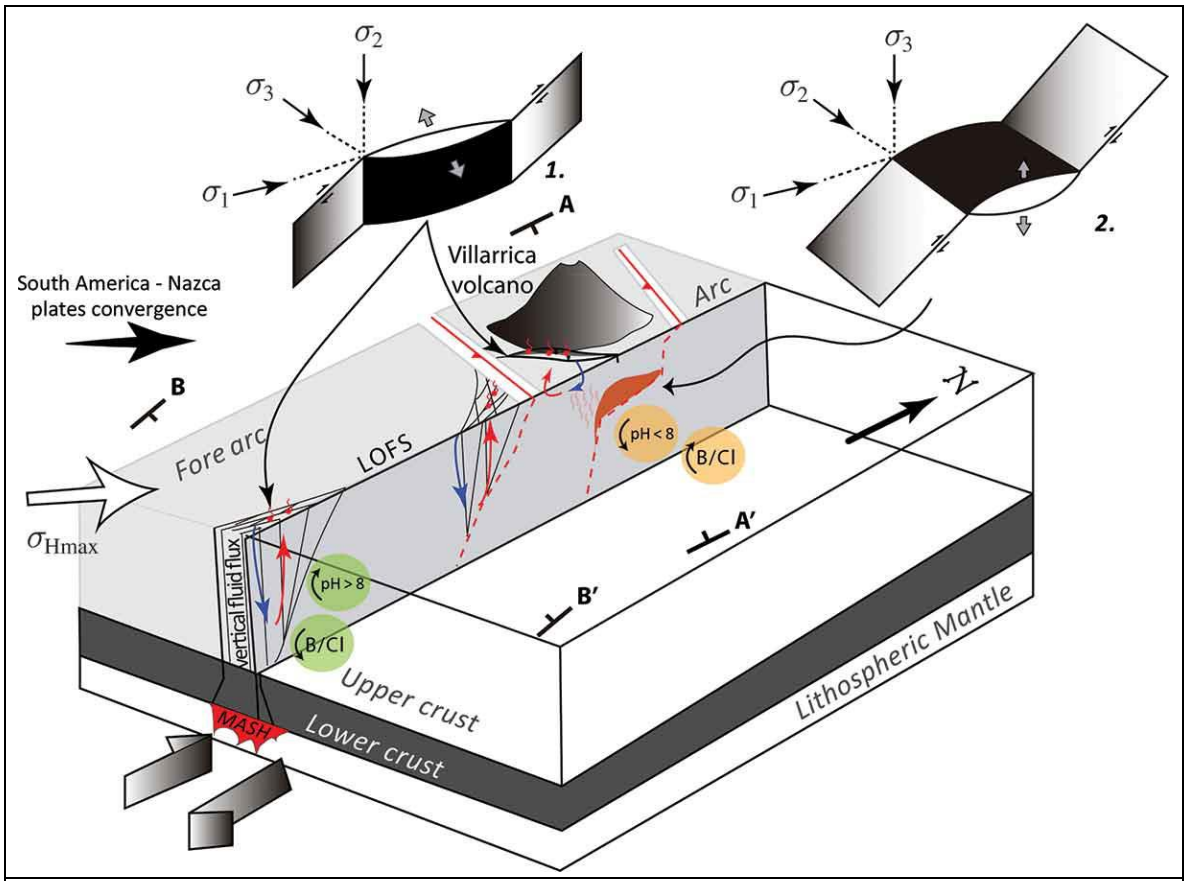

Figure 2.8 | Illustration summarizing the physical and chemical processes governing the two magmatic-tectonic-geothermal domains in the Villarrica–Chihuio area. The nature of the heat source for the geothermal systems of the LOFS domain is the high heat flux in an intra-arc region, which is transferred by conduction to the deep circulating fluids. In the ALFS domain, magmatically enhanced advective transport dominates heat and mass flow. The chemical signature of fluids is shown in circles for the LOFS domain (green) and ALFS domain (orange). Note: Blue arrows = cold meteoric water; red arrows = thermal fluids; σ_{Hmax} = direction of the maximum horizontal stress.

Activation and preservation of fault–fracture networks as highly permeable conduits require the condition of fluid pressure $P_f \sim \sigma_3$ (Sibson 1996). In these networks, the directional permeability follows a direction parallel to σ_2, which is perpendicular to the slip vector (Sibson 1996). Therefore, in the damage zone of the strike–slip LOFS domain (σ_1~N60E; Lavenu and Cembrano 1999; Rosenau et al. 2006), the vertical permeability is enhanced. These are the ideal conditions to form a deep convection cell. However, in the ALFS domain the permeability is only enhanced under fluid overpressure conditions, i.e. when fluid pressure (P_f) is higher than lithostatic pressure (P_l), because $\sigma_3 = \sigma_v = \rho g h = P_l$. When this condition is met, fault–fracture networks mainly promote lateral circulation of

fluids. At shallow levels (<2 km) and hydrostatic conditions, it is more likely to activate tension fractures or shear fractures instead of misorientated faults (Cox 2010; Rowland and Simmons 2012). That is the case of geothermal fluids at shallow levels in both domains, transported through ENE-tension fractures as reflected by ENE-aligned hot springs (Fig. 2.8; Table 1). The recharge of the systems with meteoric water is also likely to occur through ENE-tension fractures of fault–fracture networks.

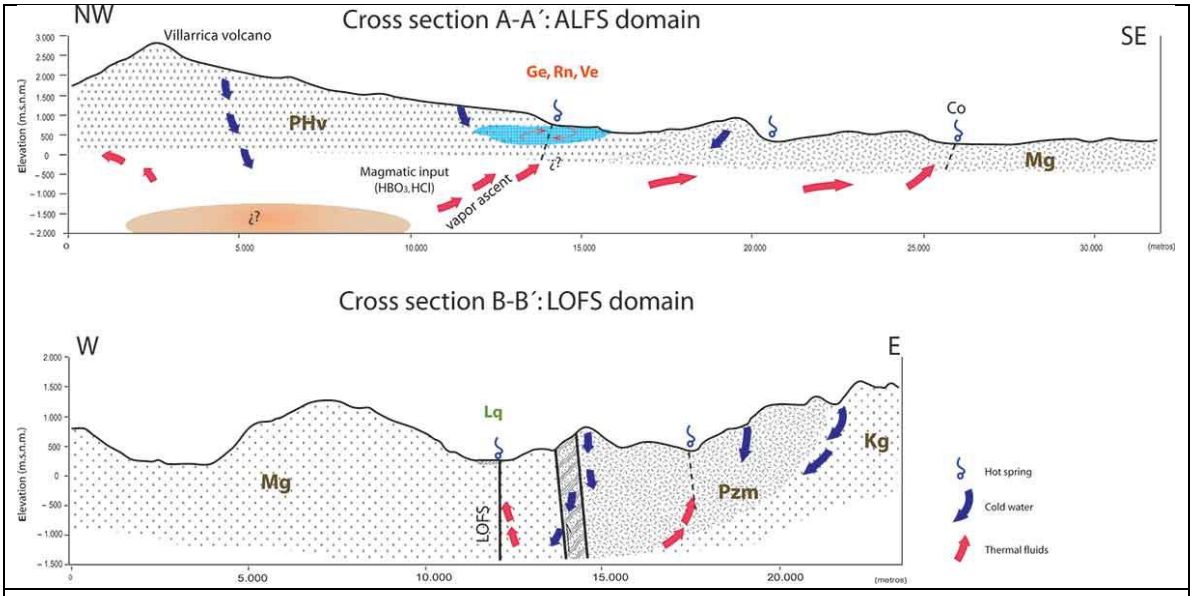

Figure 2.9 | Conceptual model of the geothermal systems for the (A) LOFS domain and (B) ALFS domain. PHv = Pleistocene–Holocene volcanic units; Mg = Miocene granitoids; Kg = Cretacic granitoids; Pzm = Palaeozoic metamorphic rocks.

We propose that these magmatic-tectonic-geothermal domains are also represented in the rest of the SVZ. Evidence to support this idea is the high geothermal resource potential areas, genetically related to WNW volcanic chains, such as Nevados de Chillán (250°C; Lahsen et al. 2010), Tolhuaca volcano (250°C; Melosh et al. 2012), and Puyehue Cordón–Caulle (300°C, Sepúlveda et al.2007). Thus the ALFS domain hosts geothermal systems heated by a shallow magmatic reservoir and favours the development of high enthalpy resources. However, detailed structural and chemical analysis should be combined to further quantify the effect of faults and fractures on those geothermal systems. Emphasis is required in those fluids least affected by shallow dilution (geothermal reservoirs) with the determination of the open fracture disposition and the local stress fields.

Chemical evolution of geothermal fluids

The origin of water in Villarrica–Chihuio thermal fluids at the surface is practically only meteoric water without a significant contribution of magmatic fluids, as shown by isotope data (Fig. 2.4). Moreover, thermal waters display very small or no $\delta^{18}O$ shift with respect to GMWL, despite this shifting normally occuring due to fluid–rock interaction at geothermal temperatures. The lack of $\delta^{18}O$ shift may be produced by an insufficient temperature for isotopic exchange and/or may be indicative of a system with very high water/rock ratios or a system that does not have enough time to equilibrate with the surrounding rocks (Druschel and Rosenberg 2001), together with the effect of mixing of meteoric water at shallow depths.

The main source of Cl and B for the geothermal systems in volcanic areas is the mass transfer from igneous intrusions through absorption of gaseous magma containing HCl and H_3BO_3 (Giggenbach 1988, 1997; Arnórsson et al. 2007). However, experiments show that water–rock interaction (rock leaching) could also introduce Cl and B in thermal water by itself but in lower quantities (Ellis and Mahon 1977). Once added, either from magma degassing or rock dissolution (or both), Cl and B preferentially remains in the liquid phase due to its non-volatile and conservative nature at geothermal conditions. Therefore, the two clusters of B/Cl ratio support the hypothesis of different heat transfer processes.

Regarding the role of the heating mechanism in the chemical evolution of geothermal fluids, several authors have classified geothermal systems based on their geodynamical context (Giggenbach and Glover 1992; Goff and Janik 2000; Druschel and Rosenberg 2001; Reyes et al. 2010). For instance, Goff and Janik (2000) recognized young igneous and tectonic systems. In the young igneous geothermal systems, the heat sources are magmatic intrusions which transfer heat and mass to the deep circulating meteoric water driven convectively to the surface, emerging as hot springs (e.g. Giggenbach 1984). In these systems, the chemical evolution of fluids is controlled by the absorption of volcanic fluids, mixing with meteoric water, and heat–fluid–rock interaction. In the tectonic geothermal systems, the fluid flow is restricted to fault–fracture networks and the heat source is the conductive heat transfer from the host rock (e.g. Druschel and Rosenberg 2001). Tectonic systems are normally associated with alkaline geothermal waters, such as the examples of Bakreswar in Eastern India (Majumdar et al. 2009), Idaho, USA (Druschel and Rosenberg 2001), Western Canada (Grasby et al. 2000), and Western Tianshan, China (Bucher et al. 2009). In these cases, dissolved components are generated by water–rock interaction. Some of these waters are alkaline sodic-sulphated, and SO_4results from leaching of fractured granites (Druschel and Rosenberg 2001; Bucher et al. 2009).

In geothermal systems associated with volcanism, the mixed volcanic condensate (H_2O, CO_2, HCl, and SO_4-rich) and heated meteoric waters are separated in two phases through adiabatic decompression, allowing the ascent of a gaseous phase rich in sulphur (H_2S). The condensation of the primary magmatic volatiles or the secondary steam phase into ground-surface waters forms steam-heated waters (Giggenbach 1988, 1997). The clustering of the geothermal discharges of the ALFS domain in the $Cl–SO_4–HCO_3$ anion ternary diagram (Fig. 2.2), together with decreasing SO_4/Cl, SO_4/HCO_3 ratios away from the Villarrica volcano (Table 1), is consistent with a steam-heated interpretation for these discharges. However, steam-heated waters are in general acid fluids ($pH < 4$) (Giggenbach 1991), with only a few exceptions (Smith et al. 2010). The prominent degassing from the crater lake of the Villarrica volcano (460 ± 260 tons/day SO_2; Witter et al. 2004) validates this interpretation. Absorption and condensation of the gaseous phase rich in sulphur species and low in chloride causes the $NaSO_4$ type waters, with a higher B/Cl ratio for the discharges of the ALFS domain.

The result of the geochemical model of a volcanic condensate interacting with a local andesite, emulating the ALFS domain, shows that the slightly alkaline pH (7.8–8.7) of these waters, not typical of the steam-heated waters, may result from neutralization by water–rock interaction and fluid mixing with groundwater. Increasing the reaction progress, SO_4 dissolved decreases due to alunite, barite, and pyrite precipitation and fluid phase local equilibrium (Fig. 2.7). Also, the pH increases from values around 3 to almost neutral pH. These processes have also been proposed for the alkaline sulphated geothermal waters of the Solomon Islands (Smith et al. 2010). This effect may be increased by dilution at shallow depth with meteoric water, considering the Villarrica–Chihuio area rainy climate (>3000 mm rain/year). Dilution is also consistent with the low content of dissolved solids (<550 mg/l ppm) and chloride (<85 ppm) with respect to thermal springs of mature systems. Another pH increasing mechanism, namely CO_2 lost, is unlikely in the absence of boiling pools in the studied area. Therefore, the chemical evolution of fluid from the ALFS domain is consistent with a magmatic contribution of heat and mass and neutralization by water–rock interaction and fluid mixing with groundwater.

The contribution of a magmatic source of fluids is not evident in the LOFS domain data. The lower B/Cl ratio, B and Cl absolute concentrations, and higher Na/H and K/H activity ratios may reflect the complete lack of magmatic contribution and considerable fluid–rock interaction. The geological features of the LOFS domain, emplaced in the granitic rocks farther than 25 km from the nearest stratovolcano, where migration of the magmatic fluids is unlikely, supports this idea.

The geochemical model of a local meteoric water sample reacting with granite presents an increasing of Na and K and high pH. Therefore, the chemical evolution of fluid

from the LOFS domain is consistent with a component contribution only from fluid–rock interaction and heating due to conductive heat transfer in a deep convective cell (Fig 2.8 and 2.9).

Both conceptual models proposed for the ALFS and LOFS domain contrast with the seawater origin of thermal water in SVZ proposed by Risacher et al. (2011). Alternatively, we propose that the interplay of volcanism and tectonics defines the nature and origin of geothermal systems and that the contribution of a seawater signature through rain is negligible, at least when geothermal systems are as far as 150 km from the ocean.

Conclusions

We have identified two magmatic-tectonic-geothermal domains based on the nature and kinematics of fault systems, volcanic activity, and rock types: the ALFS domain and the LOFS domain. The chemistry of the fluids shows contrasting signatures in these domains in conservative elements (Cl–B–Li) and activity diagrams. We propose that the role of fault systems on the geochemical evolution of geothermal fluids occurs through the development of magmatic-tectonic-geothermal domains, which ultimately defines the heat source. Reaction path modelling validates the hypothesis of two different heating mechanisms controlling the chemical evolution of fluids.

- In the LOFS domain, fault–fracture networks related to the damage zone of the deep seated NNE-striking master fault increases vertical permeability in the crystalline basement. These fracture networks promote development of deep (<3 km) convection cells and heat–fluid–rock interaction after the infiltration of meteoric water (Fig. 2.8). The ultimate heat transfer mechanism of fluids is by conduction from the crystalline host rock in the high heat flow realm of the intra-arc (Fig. 2.9). The heat–fluid–rock interaction and the lack of direct magmatic contribution imprints a signature of low B/Cl ratios and high pH in the composition of the geothermal fluids. The hot springs discharge from the faulted crystalline basement.
- In the ALFS domain, the WNW-striking inherited basement faults, which are strongly disorientated with respect to the prevailing stress field, provide suitable conditions for the development of magma reservoirs. These crustal magmatic reservoirs are the source of heat and mass for the geothermal systems. The mass transfer results in a signature of higher B/Cl ratios and neutral pH in the chemistry of the geothermal fluids compared to those of the LOFS domain. Therefore, the geochemical evolution in the ALFS domain can be represented as meteoric water absorption of magmatic gases, interaction with volcanic rocks, and dilution (Fig. 2.8 and 2.9). The discharge of these systems is through volcanic units, which may promote lateral fluid flow.

- At shallow levels (<2 km) under hydrostatic conditions, the fluid flow is though NE-tension fractures optimally orientated for reactivation where discharge (hot springs) and recharge (meteoric waters) of fluids in the geothermal systems is likely to occur.

Our conceptual model of the effects of crustal deformation on the geochemical evolution of fluids might be applicable to the rest of the Southern Volcanic Zone, where the most prominent geothermal resources are genetically related to WNW volcanic chains.

Bibliography

Adriasola, A.C., Thomson, S.N., Brix, M.R., Hervé, F. and Stöckhert, B. 2006. Postmagmatic cooling and late Cenozoic denudation of the North Patagonian Batholith in the Los Lagos region of Chile, 41°−42°15′S. International Journal of Earth Sciences, 95(3): 504–528. v–9 doi:10.1007/s00531-005-0027

Annen, C. 2006. The genesis of intermediate and silicic magmas in deep crustal hot zones. Journal of Petrology, 47(3): 505–539. Blundy, J.D., and Sparks, S.J.v doi:10.1093/petrology/egi084

Arnórsson, S. 2000. Isotopic and chemical techniques in geothermal exploration, development and use. Sampling methods, data handling and interpretation, 351Vienna: International Atomic Energy Agency.

Arnórsson, S., Stefánsson, A. and Bjarnason, J.Ö. 2007. "Fluid-fluid interaction in geothermal systems, in". In Reviews in Mineralogy and Geochemistry Edited by: Liebscher, A. and Heinrich, C.A. Vol. 65, 259–312. v

Barton, C.A., Zoback, M.D. and Moos, D. 1995. Fluid flow along potentially active faults in crystalline rock. Geology, 23: 683–686. v doi:10.1130/0091-7613(1995)023<0683

Bethke, C.M. 1996. Geochemical reaction modeling, concepts and applications, 397New York: Oxford University Press.

Bignall, G., Sekine, K., and Tsuchiya, N. 2004. Fluid-rock interaction processes in the TeKopia geothermal field (New Zealand) revealed by SEM-CL imaging.Geothermics, 33(5): 615–635. v doi:10.1016/j.geothermics.2004.03.001

Bons, P.D., Elburg, M.A. and Rivas-Gomez, E. 2012. A review of the formation of tectonic veins and their microstructures.Journal of Structural Geology, 43: 33–62. v

Bucher, K., Zhang, L. and Stober, I. 2009. A hot spring in granite of the Western Tianshan, China. Applied Geochemistry, 24(3): 402–410. v doi:10.1016/j.apgeochem.2008.12.021

Cembrano, J., Hervé, F. and Lavenu, A. 1996. The Liquiñe-Ofqui fault zone. A long-lived intra-arc fault system in southern Chile: Tectonophysics, 259: 55–66. v

Cembrano, J. and Lara, L. 2009. The link between volcanism and tectonics in the southern volcanic zone of the Chilean Andes.A review: Tectonophysics, 471(1–2): 96–113. v doi:10.1016/j.tecto.2009.02.038

Cembrano, J., Lavenu, A., Reynolds, P., Arancibia, G., López, G. and Sanhueza, A. 2002. Late Cenozoic transpressional ductil deformation north of the Nazca -South America- Antartica triple junction. Tectonophysics, 354: 289–314. v

Cembrano, J. and Moreno, H. 1994. Geometría y naturaleza contrastante del volcanismo cuaternario entre los 38° S y 46° S: ¿Dominios compresionales y tensionales en un régimen transcurrente?. Proceedings Chilean Geological Congress, 7th, 1: 240–244. inv

Cox, S. 2010. The application of failure mode diagrams for exploring the roles of fluid pressure and stress states in controlling styles of fracture-controlled permeability enhancement in faults and shear zones. Geofluids, 10: 217–233. v

Craig, H. 1963. "The isotopic geochemistry of water and carbon in geothermal areas". In Nuclear geology on geothermal areas: Pisa, Consiglio Nazionale delle Ricerche, Laboratorio di Geologia Nucleare Edited by: Tongiorgi, E. 17–53.

Curewitz, D. and Karson, J.A. 1997. Structural settings of hydrothermal outflow. Fracture permeability maintained by fault propagation and interaction: Journal of Volcanology and Geothermal Research, 79(3–4): 149–168. v

D'Amore, F. 1991. Applications of geochemistry in geothermal reservoir development. Series of Technical Guides on the Use of Geothermal Energy, UNITAR/UNDP Centre on Small Energy Resources and United Nations Institute for Training and Research, : 408

Druschel, G.K. and Rosenberg, P.E. 2001. Non-magmatic fracture-controlled hydrothermal systems in the Idaho Batholith.South Fork Payette geothermal system: Chemical Geology, 173(4): 271–291. v doi:10.1016/S0009-2541(00)00280-1

Ellis, A.J. and Mahon, W. 1977. Chemistry and geothermal systems, 392New York: Academic Press.

Folguera, A., Ramos, V.A. and Melnick, D. 2002. Partición de la deformación en la zona del arco volcánico de los Andes neuquinos (36–39°S) en los últimos 30 millones de años. Andean Geology, 29: 151–165. v

Giggenbach, W.F. 1984. Mass transfer in hydrothermal alteration systems - a conceptual approach. Geochimica et CosmochimicaActa, 48(12): 2693–2711. v doi:10.1016/0016-7037(84)90317-X

Giggenbach, W.F. 1988. Geothermal solute equilibra. Derivation of Na-K-Mg-Ca geoindicators. Geochemica et Cosmochimica Acta, 52: 2749–2765. v

Giggenbach, W.F. 1991. "Chemical techniques in geothermal exploration". In Application of geochemistry in geothermal reservoir development: New York, UNITAR/UNDP publication Edited by: D'Amore, F. 119–142.

Giggenbach, W.F. 1997. "The origin and evolution of fluids in magmatic-hydrothermal systems". In Geochemistry of hydrothermal ore deposits, Edited by: Barnes, H. 737–796. New York: John Wiley and Sons Inc. Publication.

Giggenbach, W.F. and Glover, R.B. 1992. Tectonic regime and major processes governing the chemistry of water and gas discharges from the rotorua geothermal field, New Zealand. Geothermics, 21(1–2): 121–140. v [CSA]

Giggenbach, W.F. and Goguel, R.L. 1989. Collection and analysis of geothermal and volcanic water and gas discharges, 81New Zealand, Chemistry Division, Department of Scientific and Industrial Research Petone.

Glodny, J., Echtler, H., Collao, S., Ardiles, M., Burón, P. and Figueroa, O. 2008. Differential Late Paleozoic active margin evolution in South-Central Chile (37°S–40°S) – the Lanalhue Fault Zone. Journal of South American Earth Sciences, 26(4): 397–411. v doi:10.1016/j.jsames.2008.06.001

Goff, F. and Janik, C.J. 2000. “Geothermal systems”. In Encyclopedia of volcanoes, Edited by: Sigurdsson, H., Houghton, B., McNutt, S., Rymer, H. and Stix, J. 817–834. London: Academic Press.

Grasby, S. 2000. The influence of water–rock interaction on the chemistry of thermal springs in western Canada. Applied Geochemistry, 15(4): 439–454. Hutcheon, I., and Krouse, H.vdoi:10.1016/S0883–2927(99)00066–9 , [CSA]

Hackney, R., Echtler, H., Franz, G., Götze, H.-J., Lucassen, F., Marchenko, D., Melnick, D., Meyer, U., Schmidt, S., Tášrová, Z., Tassara, A. and Wienecke, S. 2006. “The segmented overriding plate and coupling at the south-central Chilean margin (36° and 42°S)”. In The andes—active subduction orogeny, Edited by: Oncken, O., Chong, G., Franz, G., Giese, P., Götze, H.-J., Ramos, V.A., Strecker, M. and Wigger, P. 355–374. New York: Springer. doi:10.1007/978-3-540-48684-8_17

Hanano, M., 2004, Contribution of fractures to formation and production of geothermal resources: Renewable and Sustainable Energy Reviews, v. 8, p. 223–236

Hauser, A. 1997. Catastro y Caracterización de las Fuentes de Aguas Minerales y Termales de Chile. Servicio Nacional de Geología y Minería Boletín, 50: 90 v(In Spanish)

Heinrich, C.A. 2007. Fluid-fluid interactions in magmatic-hydrothermal ore formation. Reviews in Mineralogy and Geochemistry, 65(1): 363–387. v

Hildreth, W. and Moorbath, S. 1988. Crustal contributions to arc magmatism in the Andes of Central Chile. Contributions to Mineralogy and Petrology, 98(4): 455–489. v doi:10.1007/BF00372365

Lahsen, A. 1986. Geoquímica de áreas geotermales de la cordillera de los Andes del sur de Chile, entre los 39°S y 40°S.Comunicaciones, 36: 9–20. v(In Spanish)

Lahsen, A., Muñoz, N. and Parada, M.A. 2010. Geothermal development in Chile, Bali, , Indonesia: Proceedings World Geothermal Congress.

Lange, D., Cembrano, J., Rietbrock, A., Haberland, C., Dahm, T. and Bataille, K. 2008. First seismic record for intra-arc strike-slip tectonics along the Liquiñe-Ofqui fault zone at the obliquely convergent plate margin of the southern Andes. Tectonophysics, 455(1–4): 14–24. v

Lara, L.E., Lavenu, A., Cembrano, J. and Rodríguez, C. 2006. Structural controls of volcanism in transversal chains: Resheared faults and neotectonics in the Cordón Caulle–Puyehue area (40.5°S), Southern Andes. Journal of Volcanology and Geothermal Research, 158(1–2): 70–86. v doi:10.1016/j.jvolgeores.2006.04.017

Lara, L.E. and Moreno, H. 2004. Geología preliminar del área Liquiñe-Neltume. Servicio Nacional de Geología y Minería Carta Geológicade Chile, Serie Geología Básica 83, scale 1:100,000, 1 sheet. 101 p. text (In Spanish),

Lara, L.E., Naranjo, J.A. and Moreno, H. 2004. Rhyodacitic fissure eruption in Southern Andes (Cordón Caulle; 40.5°S) after the1960 (Mw: 9.5) Chilean earthquake. A structural interpretation: Journal of Volcanology and Geothermal Research, 138: 127–138. v

Lavenu, A. and Cembrano, J. 1999. Compressional- and transpressional-stress pattern for Pliocene and Quaternary brittle deformation in fore arc and intra-arc zones (Andes of Central and Southern Chile). Journal of Structural Geology, 21: 1669–1691. v doi:10.1016/S0191-8141(99)00111-X

Legrand, D., Barrientos, S., Bataille, K., Cembrano, J. and Pavez, A. 2010. The fluid-driven tectonic swarm of Aysen Fjord, Chile (2007) associated with two earthquakes (Mw=6.1 and Mw=6.2) within the Liquiñe-Ofqui Fault Zone. Continental Shelf Research, 31: 154–161. v doi:10.1016/j.csr.2010.05.008

López-Escobar, L., Cembrano, J. and Moreno, H. 1995. Geochemistry and tectonics of the Chilean Southern Andes basaltic quaternary volcanism (37–46°S). Andean Geology, 22(2): 219–234. v

Majumdar, N., Mukherjee, A.L. and Majumdar, R.K. 2009. Mixing hydrology and chemical equilibria in Bakreswar geothermal area, Eastern India. Journal of Volcanology and Geothermal Research, 183(3–4): 201–212. v doi:10.1016/j.jvolgeores.2009.03.014

Mark, G., Wilde, A., Oliver, N.H.S., Williams, P.J. and Ryan, C.G. 2005. Modeling outflow from the Ernest Henry Fe oxide Cu–Au deposit. Implications for ore genesis and exploration: Journal of Geochemical Exploration, 85(1): 31–46. v doi:10.1016/j.gexplo.2004.09.002

Melnick, D., and Echtler, H.P., 2006, Morphotectonic and geologic digital map compilations of the south-central Andes (36–42°S), in Oncken, O., Chong, G.,

Franz, G., Giese, P., Götze, H.-J., Ramos, V.A., Strecker, M., and Wigger, P., eds., The Andes – active subduction orogeny: New York, Springer-Verlag, p. 565–568

Melnick, D., Folguera, A. and Ramos, V. 2006. Structural control on arc volcanism: The Caviahue–Copahue complex, Central to Patagonian Andes transition (38°S). Journal of South American Earth Sciences, 22: 66–88. v doi:10.1016/j.jsames.2006.08.008

Melosh, G., Moore, J. and Stacey, R. 2012. "Natural reservoir evolution in the Tolhuaca geothermal field, Southern Chile". InProceedings, Workshop on Geothermal Reservoir Engineering, 36th, Stanford, , California: SGP-TR–194..

Moreno, H. and Lara, L.E. 2007. Geología del Complejo Volcánico Mocho-Choshuenco, X Región de los Lagos. Carta Geológica de Chile, Serie Geología Básica, No. 107, scale 1:50,000, 1 sheet, : 27 text

Moreno, H. and Lara, L. 2008. Geología del área Pucón-Curarrehue, Carta Geológica de Chile. Servicio Nacional de Geología y Minería, scale 1:100,000, 1 sheet, : 36 text

Moreno, M., Melnick, D., Rosenau, M., Bolte, J., Klotz, J.Echtler, H. 2011. Heterogeneous plate locking in the South–Central Chile subduction zone. Building up the next great earthquake: Earth and Planetary Science Letters, 305(3–4): 413–424. Baez, J., Batailled, K., Chena, J., Bevise, M., Hasef, H., and Onckena, O.v doi:10.1016/j.epsl.2011.03.025

Moreno, M., Rosenau, M. and Oncken, O. 2010. 2010, Maule earthquake slip correlates withpre-seismic locking of Andean subduction zone. Nature, 467: 198–202. v doi:10.1038/nature09349 [PubMed],

Nemčok, M., Moore, J.N., Christensen, C., Allis, R., Powell, T., Murray, B. and Nash, G. 2007. Controls on the Karaha–Telaga Bodas geothermal reservoir, Indonesia. Geothermics, 36(1): 9–46. v

Potent, S. 2003. Kinematik und Dynamikneogener Deformationsprozesse des südzentralchilenischen Subduktions systems, nördlichste Patagonische Anden (37°–40°S) [Ph.D. thesis], 159Universitat Hamburg.

Pérez, Y. 1999. Fuentes de Aguas Termales de la Cordillera Andina del centro - sur de Chile (39-42° Sur). Servicio Nacional de Geología y Minería Boletín, 54: 65 v(In Spanish)

Reed, M.H. 1997. “Hydrothermal alteration and its relationship to ore fluid composition”. In Geochemistry of hydrothermal ore deposits, Edited by: Barnes, H. 303–366. New York: John Wiley and Sons Inc. Publication.

Reyes, A.G., Christenson, B.W., and Faure, K., 2010, Sources of solutes and heat in low-enthalpy mineral waters and their relation to tectonic setting, New Zealand: Journal of Volcanology and Geothermal Research, v. 192, no. 3–4, p. 117–141. doi:10.1016/j.jvolgeores.2010.02.015

Risacher, F., Fritz, B. and Hauser, A. 2011. Origin of components in Chilean thermal waters. Journal of South American Earth Sciences, 31(1): 153–170. v doi:10.1016/j.jsames.2010.07.002

Rosenau, M. 2004. Tectonics of the southern Andean intra-arc zone (38°-42°S) [Ph.D. thesis], 159Freie Universitat Berlin.

Rosenau, M., Melnick, D. and Echtler, H. 2006. Kinematic constraints on intra-arc shear and strain partitioning in the southern Andes between 38°S and 42°S latitude. Tectonics, 25(4): 1–16. v doi:10.1029/2005TC001943

Rowland, J.V. and Sibson, R.H. 2004. Structural controls on hydrothermal flow in a segmented rift system, Taupo Volcanic Zone, New Zealand. Geofluids, 4(4): 259–283. v

Rowland, J.V. and Simmons, S.F. 2012. Hydrologic, magmatic, and tectonic controls on hydrothermal flow, taupo volcanic zone, New Zealand. Implications for the formation of epithermal vein deposits: Economic Geology, 107(3): 427–457. v

Sepúlveda, F., Lahsen, A. and Powell, T. 2007. Gas geochemistry of the Cordón Caulle geothermal system, Southern Chile.Geothermics, 36: 389–420. v

Sibson, R.H. 1994. “Crustal stress, faulting and fluid flow”. In Geological Society Special Publication, Edited by: Parnell, J. Vol. 78, 69–84. doi:10.1144/GSL.SP.1994.078.01.07. inv1

Sibson, R.H. 1996. Structural permeability of fluid-driven fault-fracture meshes. Journal of Structural Geology, 18: 1031–1042. v

Smith, D.J., Jenkin, G.R.T., Naden, J., Boyce, A.J., Petterson, M.G. and Toba, T. 2010. Anomalous alkaline sulphate fluids produced in a magmatic hydrothermal system—

Savo, Solomon Islands. Chemical Geology, 275(1–2): 35–49. Darling, W.G., Taylor, H., and Millar, I.L.v doi:10.1016/j.chemgeo.2010.04.011

Stern, C. 2004. Active Andean volcanism: Its geologic and tectonic setting. Andean Geology, 31(2): 161–206. v

Stern, C.R., Moreno, H., Lopez-Escobar, L., Clavero, J.E., Lara, L.E., Naranjo, J.A., Parada, M.A. and Skewes, M.A. 2007. "Chilean volcanoes". In The Geology of Chile, Edited by: Moreno, T. and Gibbons, W. 149–180. Geological Society of London.

Symonds, R.B., Rose, W.I., Gerlach, T.M., Briggs, P.H. and Harmon, R.S. 1990. Evaluation of gases, condensates, and SO2 emissions from Augustine volcano, Alaska: The degassing of a Cl-rich volcanic system. Bulletin of Volcanology, 52: 355–374. v

Thomson, S.N. 2002. Late Cenozoic geomorphic and tectonic evolution of the Patagonian Andes between latitudes 42°S and 46°S: An appraisal based on fission-track results from the transpressional intra-arc Liquiñe-Ofqui fault zone. Geological Society of America Bulletin, 114: 1159–1173. v

Wibberley, C.A.J., Yielding, G. and Toro, G. 2008. Recent advances in the understanding of fault zone internal structure. A review: Geological Society, London, Special Publications, 299(1): 5–33. v

Witter, J.B., Kress, V.C., Delmelle, P. and Stix, J. 2004. Volatile degassing, petrology, and magma dynamics of the Villarrica Lava Lake, southern Chile. Journal of Volcanology and Geothermal Research, 134: 303–337. v

Chapter 3. The interplay between hydrothermal alteration and brittle deformation: insights from the evolution of an Andean Geothermal System

Abstract

The physical and chemical evolution of hydrothermal fluids controls the formation and sustainability of high-enthalpy geothermal resources. The interplay between brittle deformation and hydrothermal alteration plays a key role in such evolution by forming or clogging permeable pathways and modifying fluid and rock chemistry during fluid flow. However, the feedback mechanisms of such interplay and their effects on the duration and thermal structure of hydrothermal systems are poorly constrained. Here we aim at elucidating such interplay by studying the evolution of the Tolhuaca geothermal system in the southern Andes. We first unraveled the physical and chemical evolution of the system by using temperature measurements in the deep wells and geochemical analyses of borehole fluid samples to constrain present-day fluid conditions. In addition, we reconstructed the paleo-fluid temperatures and chemistry from microthermometry and LA-ICP-MS analysis of fluid inclusions taken from well-constrained parageneses in vein samples retrieved from a ~1000 m borehole core. We then explored the effect of hydrothermal alteration on the conditions of fault rupture and on the long-term thermal structure of the system by using rock failure conditions calculations and numerical simulations of heat and fluid flow. Based on mineralogical observations, fluid inclusions determinations and borehole data we identify four stages (S1-S4) of progressive hydrothermal alteration that involved: (S1) an early heating event, (S2) the formation of a clay-rich cap in the upper zone (<670 m) and the development of a propylitic alteration assemblage at higher depth, (S3) boiling, flashing and brecciation and (S4) fluid mixing and boiling. The evolution of hydrothermal alteration at Tolhuaca has produced a structural and hydrological compartmentalization of the system by the development of a low-permeability, low-cohesion clay-rich cap in the upper zone. Calculation of critical fluid pressures required to produce brittle rupture indicate that within the clay-rich cap, the creation or reactivation of highly permeable extensional fractures is inhibited. Contrastingly, in the deep upflow zone the less pervasive formation of clay minerals has contribuited retain rock strength and dilatant behavior during slip, contributing to sustained permeability conditions. Numerical simulations of heat and fluid flow support our observations and suggest that the presence of a low permeability clay-cap has helped increase the duration of high-enthalpy conditions by a factor of three in the deep upflow

zone at Tolhuaca, when compared with an evolutionary scenario where a clay-cap was not developed. Such effect is enhanced in numerical simulations when hydrothermal reservoirs develop near stratovolcanoes relative to flat areas. These data demonstrate that the dynamic interplay between fluid flow, crack-seal processes and hydrothermal alteration are key factors in the evolution of the reservoir at the flank of the Tolhuaca volcano. We conclude that the favorability for developing geothermal resources in southern Chile is enhanced, among other factors, by the formation of a low-permeability upper zone that substantially increase the duration of high enthalpy conditions at the geothermal reservoir.

Introduction

In hydrothermal systems, the interplay between heat-fluid-rock interaction processes and brittle deformation plays a critical role in defining the physical and chemical evolution of fluids. Such evolution governs the processes that sustain high-enthalpy geothermal resources and form gold deposits in the epithermal environment (Rowland and Simmons, 2012; Simmons and Brown, 2007). Previous studies have documented that hydrothermal alteration and fault systems activity compartmentalize hydrothermal systems and may both enhance or inhibit hydrothermal fluid flow (Nemčok et al., 2007; Davatzes and Hickman, 2010; Rowland and Simmons, 2012). Although such studies have provided evidence that both permeability and mineralization are strongly affected by heat-fluid-rock interaction processes, a model that integrates the feedback mechanisms involved and their effect on the condition for fault rupture is currently lacking. Furthermore, the effect in the duration and thermal structure of the hydrothermal system that such interaction may produce– and thus, in the exploitable geothermal energy– remains largely unconstrained. The goal of this study is therefore to assess the effects of the interplay between the heat-fluid-rock interaction and the brittle deformation in the evolution of high enthalpy hydrothermal systems.

An excellent natural laboratory to study such interplay is the Andean Cordillera of Central-Southern Chile, where hydrothermal systems occur in close spatial relationship with active volcanism as well as major seismically-active fault systems. The nature of the relationship between active tectonics and volcanism in this region is the result of interaction between the crustal structures of the basement and the ongoing regional stress field (Cembrano and Lara, 2009), which is primarily controlled by the oblique convergence of the Nazca and South America Plates. Between 39° and 46°S, the volcanic and hydrothermal activity is controlled by the NNE- trending, 1,200 km long Liquiñe-Ofqui Fault System (LOFS) and the NW-trending Arc-Oblique Fault System (ALFS), which host ~25% of geothermal features in the Chilean Andes (Sánchez et al., 2013; Cembrano and Lara, 2009). Within this setting, the active Tolhuaca geothermal field in the northern termination of the

LOFS (Fig. 3.1) has recorded the typical sequence of hydrothermal alteration of high enthalpy systems. The deep exploration drillings performed by MRP-Chile (former GGE Ltd.) allows the investigation of a hydrothermal system not yet affected by geothermal production or re-injection (Melosh et al., 2012).

In this study we first unravel the physical and chemical evolution of the Tolhuaca geothermal system by using temperature measurements in the deep wells and geochemical analyses of fluid samples retrieved from the reservoir to constrain present-day fluid conditions. In addition, we reconstructed paleo-fluid temperature and chemistry from microthermometry and LA-ICP-MS data of fluid inclusions from a deep borehole core. The relative temporal and spatial distribution of hydrothermal alteration at Tolhuaca was first determined using optical petrography, scanning electron microscopy (SEM) and x-ray diffraction (XRD). The effect of hydrothermal alteration on the mechanical behavior of altered rocks was calculated using failure conditions for two end-member scenarios, namely, with and without a low-cohesion, low-permeability clay-cap. The same end-members were considered when analyzing the effect of hydrothermal alteration on the thermal structure of the Tolhuaca geothermal system by using numerical simulations of heat and fluid flow. By integrating these data, our analysis points to constrain the favorable conditions leading to the development of high enthalpy geothermal resources in the Southern Andes.

Geological setting

The main tectonic features in the southern Andes volcanic zone are the LOFS and the ALFS (Fig. 3.1) (Cembrano and Lara, 2009; Rosenau et al., 2006). The LOFS is a major intra-arc fault system that dominates the SVZ between 38°S and 47°S (Cembrano, 1996; Rosenau et al., 2006). The LOFS accommodates strain along the intra-arc by dextral strike shearing along the NNE-striking master fault and normal and dextral strike–slip in subsidiary ENE-striking faults (Lavenu and Cembrano, 1999; Rosenau et al., 2006). Fault–slip data and stress tensors for Pleistocene deformation along the northern portion of the LOFS consistently show a subhorizontal maximum principal compressive stress (σ_{Hmax}) trending N60°E (Lavenu and Cembrano, 1999; Rosenau et al., 2006). NNE-striking master faults are favorably orientated for dextral shear with respect to the prevailing stress field and ENE-striking tension fractures likely form under relatively low differential stress (Lavenu and Cembrano, 1999; Cembrano and Lara, 2009). In the above-described tectonic setting, the WNW-striking faults of the ALFS are severely misorientated with respect to the prevailing stress field and have been interpreted as crustal weaknesses associated with pre-Andean faults reactivated as sinistral-reverse strike–slip faults during arc development

(Rosenau et al., 2006; Cembrano and Lara, 2009). In this context, the nature and origin of hydrothermal systems is strongly dependent on structurally controlled mechanisms of heat transfer that define contrasting magmatic-tectonic-hydrothermal domains (Sánchez et al., 2013). The Tolhuaca volcano is likely to be related to the ALFS which provide suitable conditions for the development of magma reservoirs and therefore a sustained supply heat and mass to sustain high enthalpy geothermal systems.

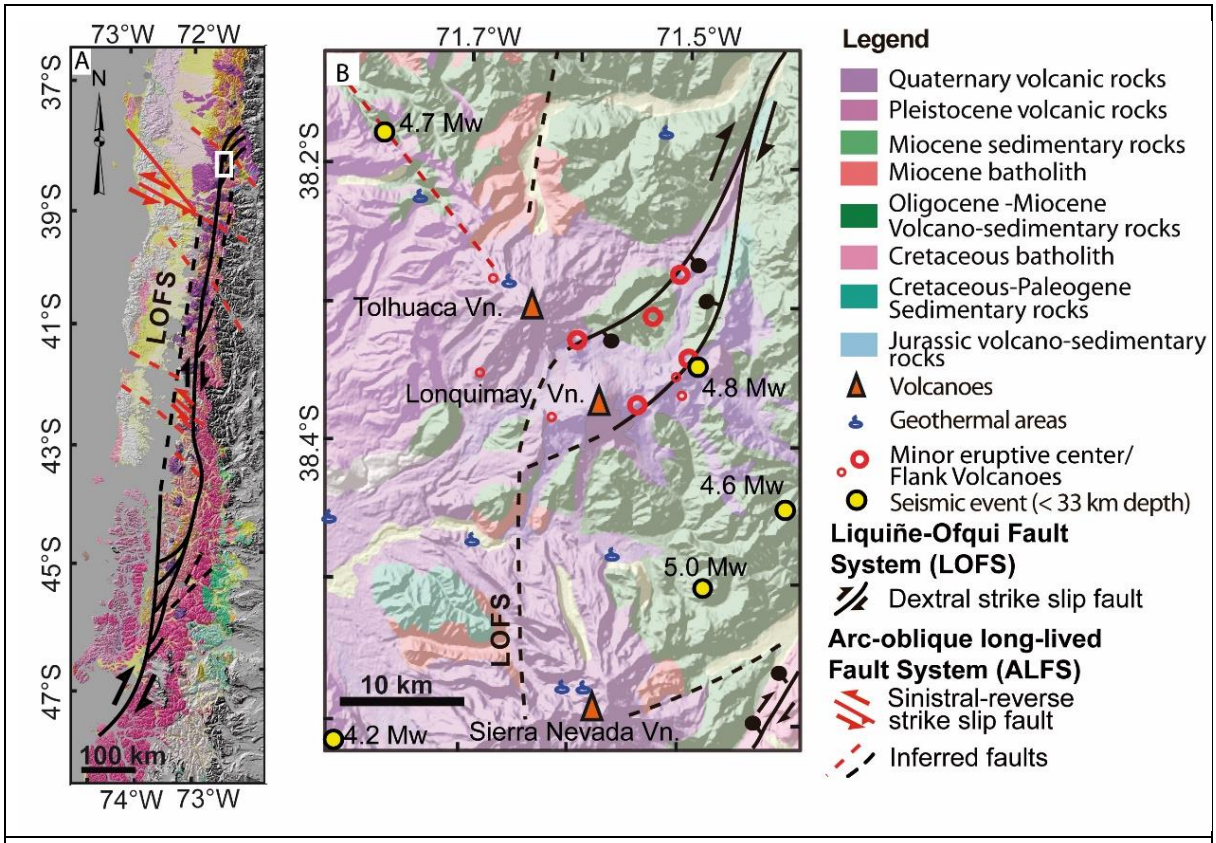

Figure 3.1 | Geodynamic and structural setting of the Tolhuaca geothermal system. **a,** Digital Elevation Model showing the location and extent of the Liquiñe-Ofqui Fault System (LOFS; in black) and the Arc-Oblique Fault System (ALFS; in red) (Sánchez et al., 2013). **b,** Simplified geological map and major structural systems LOFS and ALFS. The spatial and genetic association with the mayor stratovolcanoes, monogenetic cones and geothermal areas are shown (Perez-Flores et al., 2013).

In the area near the Tolhuaca volcano, the basement of the Pleistocene–Holocene volcanic arc is the Miocene volcano-sedimentary rocks (Fig. 3.1) (Cembrano and Lara,

2009), which have intrinsic porosity and permeability enabling the development of a hydrothermal reservoirs. Plutonic rocks associated to the Miocene Batholith serves as impermeable host rock for the hydrothermal systems unless are highly fractured.

The Tolhuaca volcano is a composite stratovolcano that rises ~ 900 m over the basement and has been affected by glacial erosion. In the summit several NW-trending aligned craters with different conservation states indicate a migration of the volcanic activity from SE towards the NW (Thiele et al., 1987). The latest eruptive phases are in the NW extreme and correspond to NW-trending fissure (~2 km long) and a pyroclastic cone. Lavas are predominantly basaltic andesites and andesites, with minor presence of basalts and dacites (Thiele et al., 1987). The volcanic flanks present several thermal features including sulfataras areas with fumaroles, boiling pools and hot springs.

Methods

Mineral paragenesis

Geological mapping and drillcore logging studies were performed in the Tol-1 borehole core of 1073 m depth drilled by MRP Geothermal Chile Ltda (formerly GGE Chile SpA) (Melosh et al., 2012). Fourty-seven representative samples were taken for thin section inspection and fluid inclusions studies. The mineral paragenesis was determined using a combination of SEM and petrographical observations. The mineralogical results were contrasted and complemented with previous studies of the geothermal system that include XRD data (Melosh et al., 2010; Melosh et al., 2012).

Borehole temperatures and fluid chemistry

Temperature measurements of 4 deep wells were used to constrain subsurface temperature of the geothermal system at Tolhuaca. Water and gas samples were collected in January 2013 using sampling procedures after Giggenbach and Goguel (1989). Samples were analyzed for major cations and anions, and trace elements at Actlabs Laboratories, Canada, using a Varian-730-ES Axial ICP-OES system, a Dionex ICS-1000 ion chromatography system and a sector field HR-ICP-MS system (Thermo Element 2), respectively.

Fluid inclusion microthermometry and microanalysis

The thermodynamic conditions of paleo-fluids at Tolhuaca were reconstructed by using microthermometric determinations and microanalytical data from fluid inclusions assemblages hosted in quartz and calcite veins from the Tol-1 borehole core. Detailed fluid

inclusions petrography using optical microscopy and SEM-based cathodoluminescence studies (in euhedral quartz crystals) were performed in order to constrain the different Fluid Inclusions Assemblages (FIAs), and their relation to the mineral paragenesis. A Fluid Inclusion Assemblage is a group of petrographically associated fluid inclusions that formed simultaneously.

Fluid inclusion microthermometry was perforemed partially at the Institute of Geochemistry and Petrology of the ETH of Zürich and partially at the Universidad Católica del Norte, using a Linkam THMSG-600 heating-freezing stage in both institutes. The stages were calibrated with synthetic fluid inclusions of pure H_2O (final ice melting temperature: 0.0 °C, homogenization temperature: 374.0 °C) and CO_2 (final CO2 ice melting temperature: − 56.6 °C). Inclusions were cooled until − 196 °C to test for the presence of CO_2 or CH_4. Salinities were derived from final ice melting temperatures and are calculated as wt.% equivalent (eq.) NaCl (Bodnar, 1993). In total, 243 fluid inclusions from 48 FIAs were measured.

Chemical microanalysis of individual fluid inclusions was performed using a laser ablation system (193 nm ArF excimer laser) connected to a quadrupole ICP -MS (Perkin Elmer Elan 6100 DRC) at the fluid inclusions laboratory in ETH-Zürich (technical details in Günther et al., 1998). As the detection limits of LA-ICPMS microanalysis are strongly dependent on fluid inclusion size, successful analysis of low-salinity fluids required fluid inclusion sizes of at least 40–60 μm and the optimization of LA-ICPMS settings (e.g. dwell time) for the enriched components in the present-day fluid (e.g., B, As) and metals of interest (e.g., Cu, Zn, Au).

Pressure-temperature-enthalpy evolution

Numerical models of coupled heat and fluid flow were computed using HYDROTHERM (Hayba and Ingebritsen, 1994) to simulate the evolution of a Tolhuaca-like hydrothermal system. Model characteristics, including rock properties, temperature-dependent permeability and initial and boundary conditions are similar to those used by Hayba and Ingebritsen (1997). Topography and clay cap spatial distribution was set as in Tolhuaca (Melosh et al., 2012). The modeled heat source of the system is a magma body (~0.5 km^3; at 900°C) that instantly intrudes to a depth of ~3 km beneath the volcano summit. Host rock and clay-cap were defined by permeabilities of 10^{-15} m^2 and 10^{-18} m^2, respectively, within the domain of brittle rock behavior (T<350°C). The deeper wells at Tolhuaca intercepted dikes, supporting the idea of a magmatic intrusion as a heat source (Melosh et al., 2012). Several numerical experiments were computed to calibrate the model using the present-day pressure-temperature-enthalpy distribution by varying intrusion depth and the occurrence or absence of an impermeable barrier (clay-cap). In order to estimate the

effect of a low-permeability clay-cap in the thermal evolution of the system, two selected models (with and without the clay-cap) were analyzed.

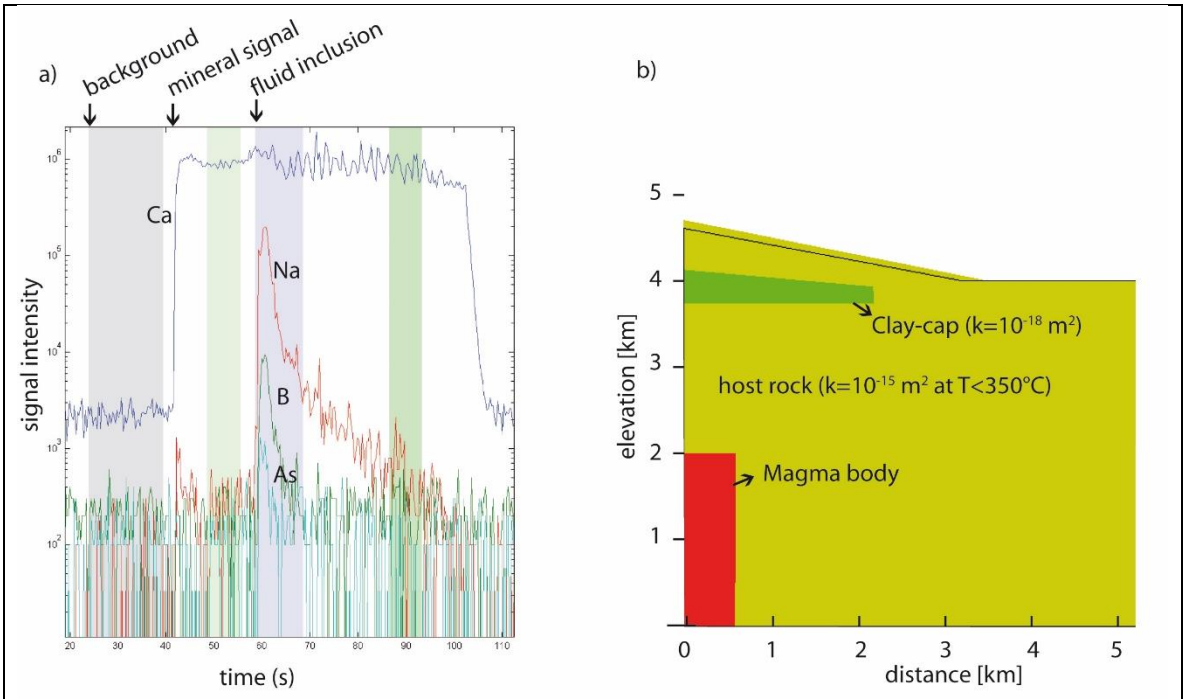

Figure 3.2 | Methods details **a,** LA-ICPMS transient signals of a fluid inclusion hosted in calcite. The peaks of different elements show the ablation of the host mineral (Ca) followed by the opening of the fluid inclusion enriched in Na, B and As. Vertically colored bands indicate the timeframe of background, host mineral and fluid inclusion selected for data reduction. **b,** Geometry of the numerical model of coupled heat and fluid flow computed using HYDROTHERM. Model characteristics are similar to those used by Hayba and Ingebritsen (1997). Topography and clay cap spatial distribution was set as in Tolhuaca.

Critical pore pressure that triggers fault rupture

The fluid-activated valve is the mechanism that triggers fault rupture driven by a fluid pressure increase up to failure conditions (Sibson et al., 1988). To determine the critical pore pressure (Wiprut and Zoback, 2000) at which a fault element will begin to slip the coulomb frictional failure was used (Secor, 1965):

$$P_f^{crit-Shear} = \sigma_n - (\tau - C)/\mu \qquad (1)$$

where μ is the coefficient of sliding friction and C is cohesive strength and σ_n, τ are normal stress and shear stress respectively. To determine the critical pore pressure at which fracture element will begin to open as an extensional fracture, the criterion for hydraulic extension was used (Secor, 1965):

$$P_f^{crit-Ext} = \sigma_n + T \quad (2)$$

where T is tensile strength.

In order to analyze the effect of a low-cohesion clay cap on the failure conditions, the critical pore fluid pressure was calculated considering rock properties of two end-members, intact rock and hydrothermally altered rock. The intact rock case considers T= 5 MPa, C=10 MPa and μ=0.75. The hydrothermally altered rock considers T= 5 MPa, C=0.3 MPa and μ=0.36 (Neuzil, 1994).

The magnitude of stress field was estimated by using a compilation of the absolute stress magnitudes measured *in-situ* (Zang et al., 2012). Based on the kinematic analysis of fault-slip data from Tol-1 borehole that indicates a normal strain regime (Perez-Flores et al., 2013) we used the stress magnitudes compiled by Zang et al. (2012), for normal faulting regime described as:

$$Sv=260 \text{ bar/km}, S_h=0.57S_V, S_H=0.87S_V \quad (3)$$

where Sv, S_h and S_H are vertical, minimum horizontal and maximum horizontal stress component, respectively. Although are not *in-situ* measurements in the Tolhuaca field, are useful as an approximation of the stress field to analyze the effect of hydrothermal alteration.

To calculate the effect of the fracture orientation in the critical pore pressure that would trigger rupture, the calculations were performed in a 3D space. Thus, σ_n, τ , $P_f^{crit-Ext}$ and $P_f^{crit-Shear}$ were computed for an equidistant grid of planes in the 3D space and plotted in equal area stereonets.

Results

Paragenesis and structural segmentation

Geological mapping and drillcore logging reveal that the Tolhuaca geothermal system is characterized by a mineralogical and structural compartmentalization (Fig. 3.3 and 3.4).

Three hydrothermal alteration zones have been recognized: a shallow argillic alteration zone (0-300 m), characterized by clay minerals (smectite, interlayered chlorite-smectite) and iron oxides; an intermediate sub-propylitic alteration zone (300-670 m), dominated by widespread and pervasive occurrence of interlayered chlorite-smectite and stilbite; and a deep propylitic zone (670-1073 m), characterized by the occurrence of

epidote and chlorite. The intensity of alteration in the groundmass and phenocrysts is variable, even at thin-section scale. However, the highest intensity is observed in the shallow region (~100 m depth) near the location of the "steam-heated" aquifer.

Four paragenetical stages (S1, S2, S3 and S4) are recognized in the different alteration zones, which are consistent with previous studies (Melosh et al., 2012; Melosh et al., 2010). In the shallow zone (0-300 m depth), the earliest stage S1 consists on a sequence of iron-oxides (hematite?), bands of amorphous silica and/or chalcedony and later pyrite (with minor chalcopyrite). Stage S2 is dominated by clay mineral alteration (smectite, minor interlayered chlorite-smectite) and stilbite. Stage S3 is represented by "lattice-bladed" calcite and euhedral quartz. In Stage S4, different silica polymorphs (microcrystalline and amorphous silica) are observed.

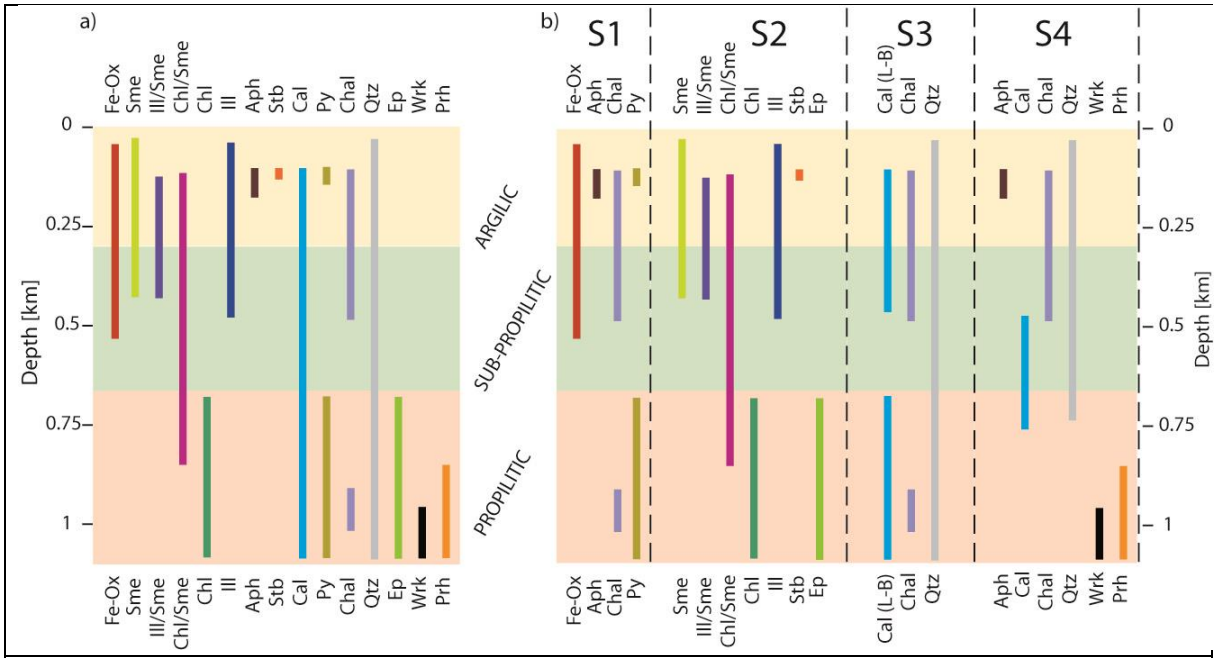

Figure 3.3 | a, Mineral associations identified in the Tol-1 borehole core. Three zones of distinctive hydrothermal minerals association are identified: argilic, sub-propilitic and propilitic. **b,** Paragenetic sequence considering four stages, S1 to S4. Abbreviations are, FeOx: Iron oxides, Aph: Amourphous silica, Py: Pyrite, Chal: Chalcedony, Qtz: Quartz, Chl: Chlorite, Sme: Smectite, Illi: Illite, Stb: Stilbite, Cal: Calcite, Prh: Prehnite, Wrk: Wairakite, Ep: Epidote, (L-B): "lattice-bladed" calcite texture.

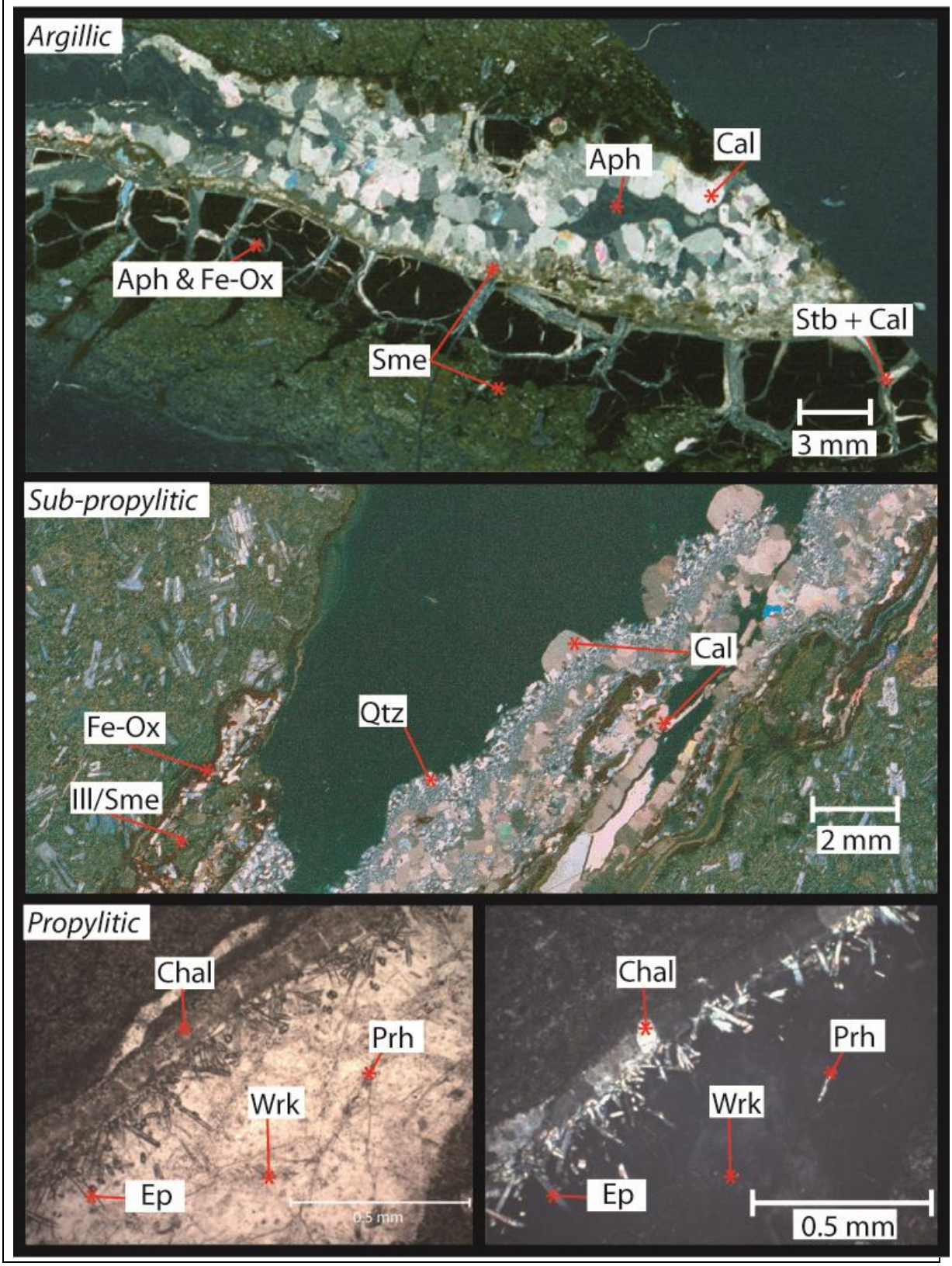
Argillic
Aph
Cal
Aph & Fe-Ox
Sme
Stb + Cal
3 mm
Sub-propylitic
Cal
Qtz
Fe-Ox
Ill/Sme
2 mm
Propylitic
Chal
Prh
Wrk
Ep
0.5 mm
Chal
Prh
Wrk
Ep
0.5 mm

Figure 3.4 | Photomicrographs of a representative samples taken from the three hydrothermal alteration zones. Abbreviation of minerals is similar to Figure 3.3.
Top: Argilic Zone (104 m). Early amorphous silica bands with colloform texture interlayered with iron oxides, cut by two-direction-cleavage-zeolite and calcite micro veins (<0.5 mm) forming a mineral breccia texture. Pyrite and chalcopyrite occurrence is restrained to the amorphous silica and iron oxides bands. A green yellowish halo of interlayered clay minerals (chl/sme) forms towards the main vein up to the brecciated outer part. In the inner part, the latter stages are represented by bladed calcite and late amorphous silica with moss texture unaffected by clay alteration.
Center: Sub-Propylitic Zone (410.6 m). Complex history of mineral brecciation comprising chalcedony bands, iron oxides and interlayered clay minerals (chl/sme). Calcite and quartz with different textures are alternating in the inner part of the vein. Size of quartz crystals increases towards the center of the vein, from microcrystalline to euhedral.
Bottom: Propylitic Zone (947.8 m). A chalcedony band is followed by prismatic euhedral epidote and wairakite. The main vein is cut obliquely by micro-veins of prehnite.

In the intermediate sub-propylitic zone (300-670 m), stage S1 consists on iron-oxides followed by chalcedony bands. Stage S2 is dominated by a pervasive alteration to clay minerals (interlayered chlorite-smectite). Stage S3 is represented by calcite alternating with microcrystalline quartz. Unlike the other zones, "lattice-bladed" calcite is absent. A final stage S4 records the precipitation of calcite and euhedral quartz. Therefore, in the upper part of the system (<670 m) a clay-rich cap was formed at stage S2, comprising minerals which have intrinsically low permeability.

In the deep propylitic zone (>670 m), stage S1 is represented by a sequence of pyrite and chalcedony and/or microcrystalline quartz. Stage S2 consists on chlorite and epidote. Stage S3 is characterized by the occurrence of quartz (euhedral, plumose and microcrystalline) and lattice-bladed calcite. The latest stage (S4) is marked by the occurrence of wairakite and late prehnite.

Secondary permeability is mainly represented by veins, veins-faults, fractures and, to a lesser extent, by textures related to dissolution of plagioclase during the formation of epidote in the deepest parts of system. The occurrence and characteristics of the structures that affect secondary permeability also show segmentation into three zones. In the shallow argillic zone, secondary permeability is characterized by a relatively higher frequency of open fractures, normal faults and veins and absence of shear fractures. At the base of this zone (~301 m) there is a 30 cm-thick cataclastic zone that underlies 10 m of abundant hydrothermal breccias. The intermediate sub-propylitic clay-rich zone (300-670 m) is characterized by the highest shear fracture frequency, and few quartz and calcite veins. Low-angle (≤ 35°) structures in the borehole core are mostly restricted to this level. The

deep propylitic zone (>670 m) presents a low-shear fracture density and the highest vein frequency. The aforentioned veins are filled of quartz, calcite and epidote.

Present-day P-T-H-X conditions: borehole data

Borehole temperature and temperature gradient data from four deep wells reveal that segmentation also affects the heat transfer regime (Fig. 3.5). The shallow argillic zone presents a steep temperature gradient (< 150°C/km) and hosts a "steam-heated" aquifer with high vapor content between 100 and 200 m depth (Melosh et al., 2012). The inverse temperature gradient from two wells indicates lateral fluid flow and meteoric water infiltration. The intermediate sub-propylitic clay-rich zone is characterized by a relatively constant, conductive-type gradient of 20-30°C/km occurring in most of the wells. In the propylitic zone starts the transition to an almost isothermal gradient of < 5°C/km, typical of convective heat transfer regimes characterized by liquid saturated conditions at the top of the convection cell.

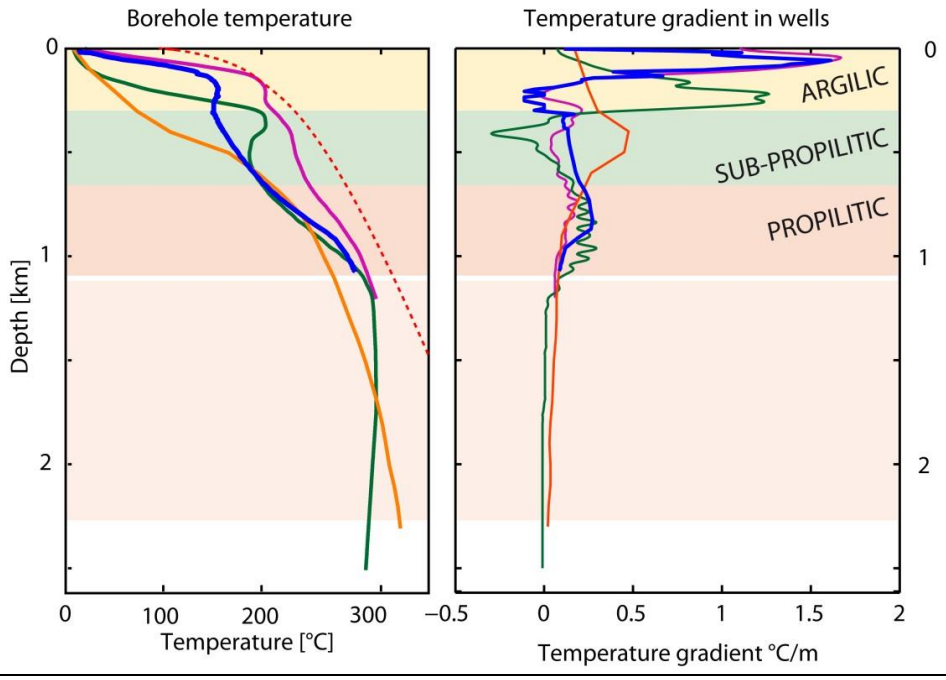

Figure 3.5 | Present-day temperature conditions of the Tolhuaca system and their relation with the three structural-mineralogical zones. The permeability conditions define the contrasting dominant heat transfer mechanism for each zone. **a,** Temperature with depth for Tol-1 (blue) and other three deep wells. Boiling curve (dashed red line) is shown for reference. **b,** Temperature gradient with depth.

Borehole fluid chemistry at the reservoir was constrained by sampling a deep geothermal well. The main chemical characteristics of the liquid phase are low salinity (Na=182 mg/kg; Cl=266 mg/kg), low sulfur content (SO_4=8.7 mg/kg) and relatively high concentrations of metals including Au (1.57 µg/kg), Ag (0.018 µg/kg), Cu (0.07 µg/kg) and Zn (7.5 µg/kg). Boron (219 mg/kg) and As (25.6 mg/kg) content are particularly high, and may reflect a magmatic-vapor contribution.

Paleo-fluid P-T-H-X conditions: fluid inclusions data

The fluid inclusions study focused on the quartz and calcite crystals that are well constrained within the paragenetic sequence. Fluid inclusion investigations combining petrography, microthermometry and LA-ICPMS microanalysis were done on eleven veins and fault-veins from the paragenetical stages S2, S3 and S4 comprising the three mineralogical-structural segments. The earlier paragenetical stage S1 has complicated growth patterns with scarce fluid inclusions, making very difficult to establish a reliable time sequence for the different FIAs. Primary and pseudo-secondary fluid inclusions were used to define FIAs in crystals with a well-constrained position in the paragenetical sequence. Some secondary FIAs were measured but considered only for interpretations related to the latest alteration stage (S4). No clathrate melting was observed upon heating to room temperature, excluding the presence of substantial concentrations of CO_2 in the fluid inclusions.

Four different types of fluid inclusions (FI) were identified (Fig. 3.6), and all of them are aqueous two-phase (liquid–vapor) inclusions: (1) FI hosted in massive quartz or euhedral quartz associated to stages S2 and S3, of 10-30 µm size and typically have oval or negative crystal shapes, (2) FI osted in lattice-bladed calcite associated to stage S3, of 10-120 µm size and typically have elongated oval or negative crystal shape, (3) FI hosted in syn-kinematic or late calcite associated to stage S4, of 20-100 µm size and typically have negative crystal shape, (4) pseudosecondary FI trapped synchronous to prehnite precipitation that crosscut quartz crystals. These FI are associated to stage S4 and typically have round to oval shapes with a size of 10-15 µm. Most of the successful quantitative chemical analyses by LA-ICP-MS were obtained in large FI from types (2) and (3).

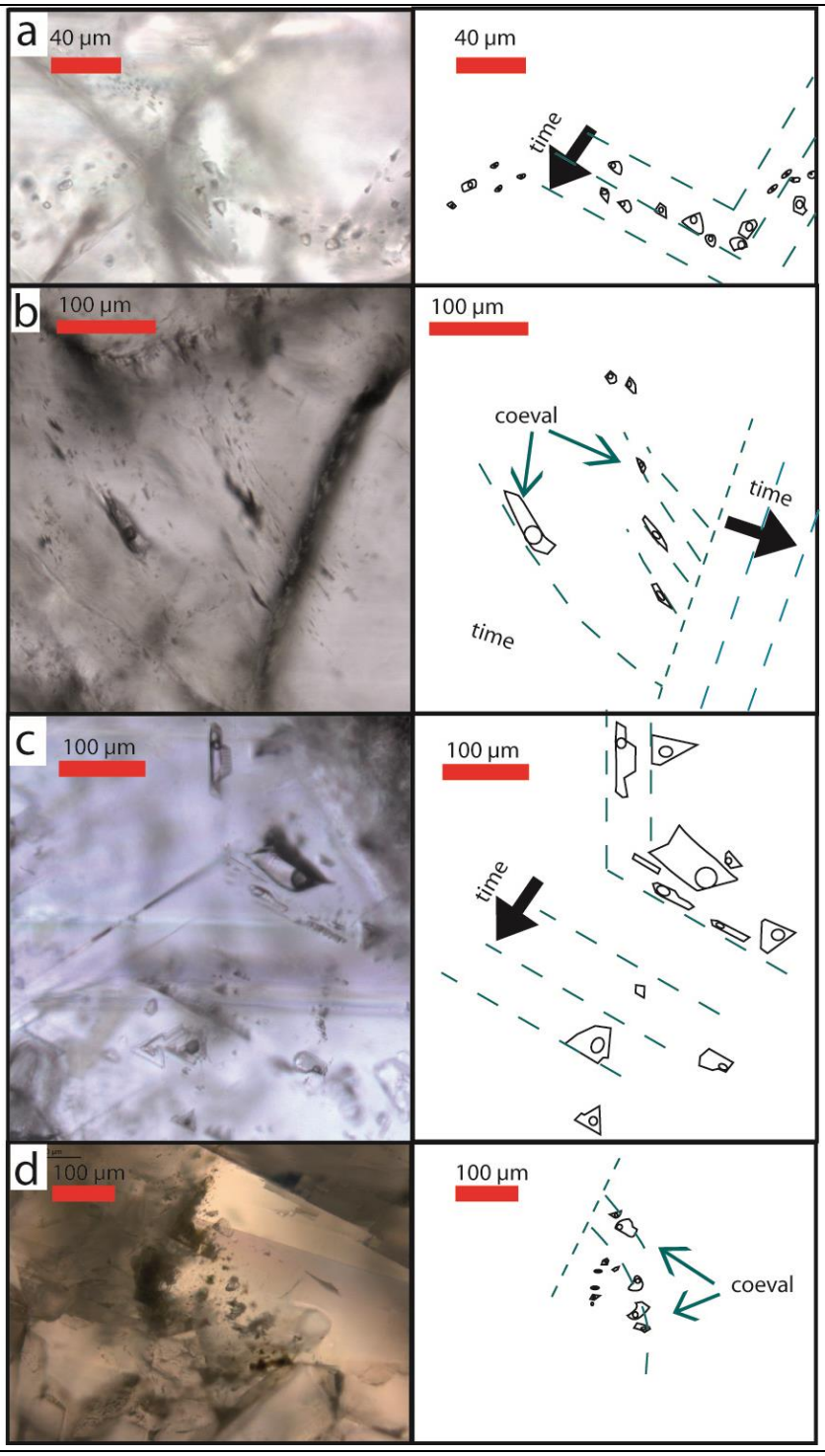

Figure 3.6 | Fluid inclusions assemblages (FIAs) types. **a,** Fluid inclusions hosted in euhedral quartz associated to stage S3. **b,** Fluid inclusions hosted in lattice-bladed calcite associated to stage S3. **c,** Fluid inclusions hosted in syn-kinematic calcite associated to stage S4. **d,** Pseudosecondary fluid inclusions trapped synchronous to prehnite precipitation that crosscut quartz crystals associated to stage S4.

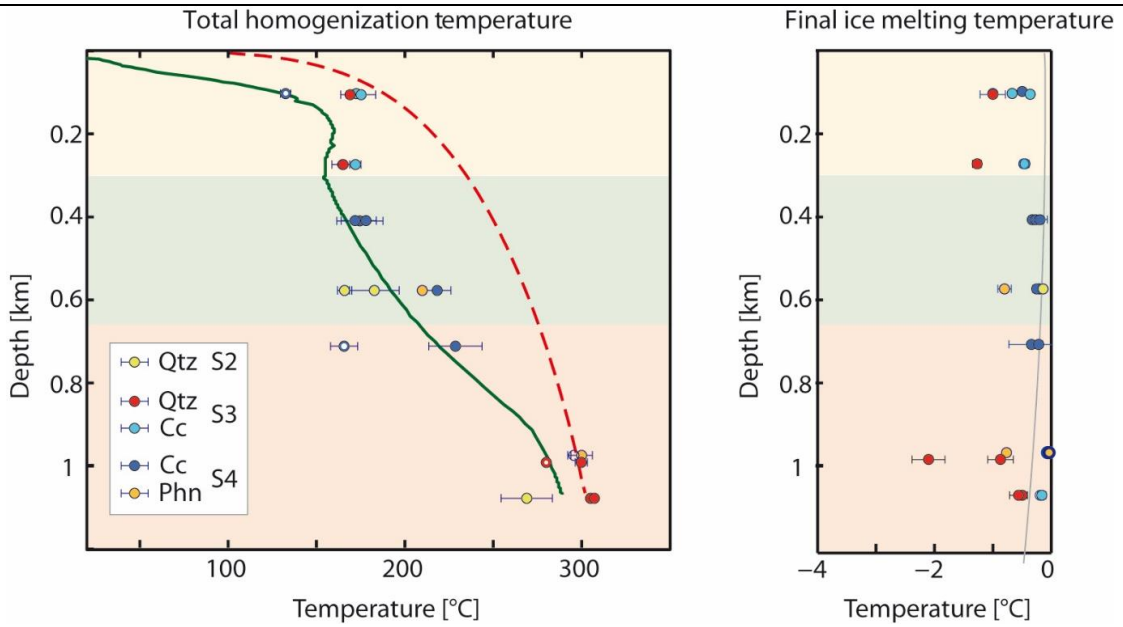

Figure 3.7 | Paleo fluid conditions from fluid inclusions data. Solid circles show the average homogenization and final ice melting temperatures of FIAs. Error bars indicate 1-sigma standard deviation and colors depict the paragenetical stage. The boiling temperature as a function of depth (dashed red line) and present-day borehole temperature of Tol-1(green line) are shown for reference.

The average total homogenization (Th_{tot}) and final ice melting (Tm_{ice}) temperatures for each FIAs are plotted versus depth in Figure 3.7. The temperatures of first ice melting were close to -23°C, indicating the presence of NaCl–H_2O dominated fluids. All fluid inclusions show final ice melting in the temperature range between -2.3 and -0.0°C, corresponding to salinities of 0 to 3.8 wt.% eq. NaCl. The presence of substantial concentrations of CO_2 in the fluid inclusions is excluded because no clathrate melting was observed upon heating to room temperature.

Microthermometric data shows a correlation within ±40°C between Th and temperature log. The Th_{tot} from fluid inclusion assemblages related to stage S3 indicate that the boiling temperature was reached, which is consistent with mineral textures. Changes in Th_{tot} from stage S3, S4 to borehole temperature indicate a slight cooling (< 20°C) (Fig. 3.7). A slight increase in apparent salinity (≤ 2 wt.% eq. NaCl) with depth might indicate the presence of CO_2 lowering freezing temperature. The Th_{tot} measured in the latest paragenetic stage are relatively coincident with present borehole temperatures (Fig. 3.7).

Table 3.1 | Fluid chemistry data from microanalysis of fluid inclusions and measurements from a liquid sample retrieved from a deep well. Data is normalized to sodium in molal ratios to avoid error introduced by internal standards. b.d.: bellow detection limit

Fluid Assemblage	*Inculsion*	*Depth*	*Paragenetic Stage*	$B^{11}/^{23}Na$	$^{65}Cu/^{23}Na$	$^{66}Zn/^{23}Na$	$^{75}As/^{23}Na$
2V-C10		99.29	S4	2.14E-01	b.d.	b.d.	b.d.
4A-CP1		106.61	S3	1.54E-01	b.d.	b.d.	1.60E-03
4A-CP1		106.61	S3	2.18E-02	b.d.	b.d.	b.d.
13A-CP2		274.85	S3	2.47E-01	b.d.	b.d.	b.d.
13A-CP2		274.85	S3	1.96E-01	b.d.	b.d.	b.d.
13A-CP2		274.85	S3	1.88E-01	b.d.	b.d.	b.d.
45Y-C4		1078.8	S4	1.58E-01	b.d.	1.43E-01	8.92E-03
27A-CK8		712.7	S4	b.d.	b.d.	b.d.	3.43E-02
20E-CK8		409.96	S4	8.00E-03	3.88E-03	1.46E-02	b.d.
20E-CK8		409.96	S4	3.16E-02	b.d.	b.d.	b.d.
19A-CK8		410.6	S4	3.17E-01	2.53E-03	5.95E-03	2.03E-03
19A-CK8		410.6	S4	2.60E-01	b.d.	b.d.	b.d.
19A-CK8		410.6	S4	1.42E-01	b.d.	b.d.	b.d.
19A-CK8		410.6	S4	8.38E-01	b.d.	b.d.	b.d.
19A-CK8		410.6	S4	1.25E+00	b.d.	b.d.	b.d.
24E-QT6		578.26	S2	3.43E-02	b.d.	b.d.	b.d.
Wellbore				4.45E+00	5.49E-05	4.12E-02	5.62E-02

Paleo-fluid chemistry was constrained on near ten of the hundreds of fluid inclusions analyzed. Elements analyzed were Cu, Zn, B and As due to the restricted amount of sample fluid (<10 ng) contained in the small (<80 μm) and low salinity (<3 wt.% eq. NaCl) fluid inclusions. To the best of our knowledge these are the first quantitative chemical data of single fluid inclusions in an active geothermal system. The element-to-sodium molar ratios value and the average of all FIAs determined using LA-ICPMS are plotted with their standard deviations in Figure 3.8. Those are compared to present-day fluid chemistry obtained from the analysis of a deep well fluid sample. Fluid inclusion chemical data are shown in molar ratios and not in absolute concentrations to avoid the error introduced when the apparent salinity used as internal standard, considering that the error is more relevant for low-salinity fluids. The dataset of fluid chemistry is presented in Table 3.1.

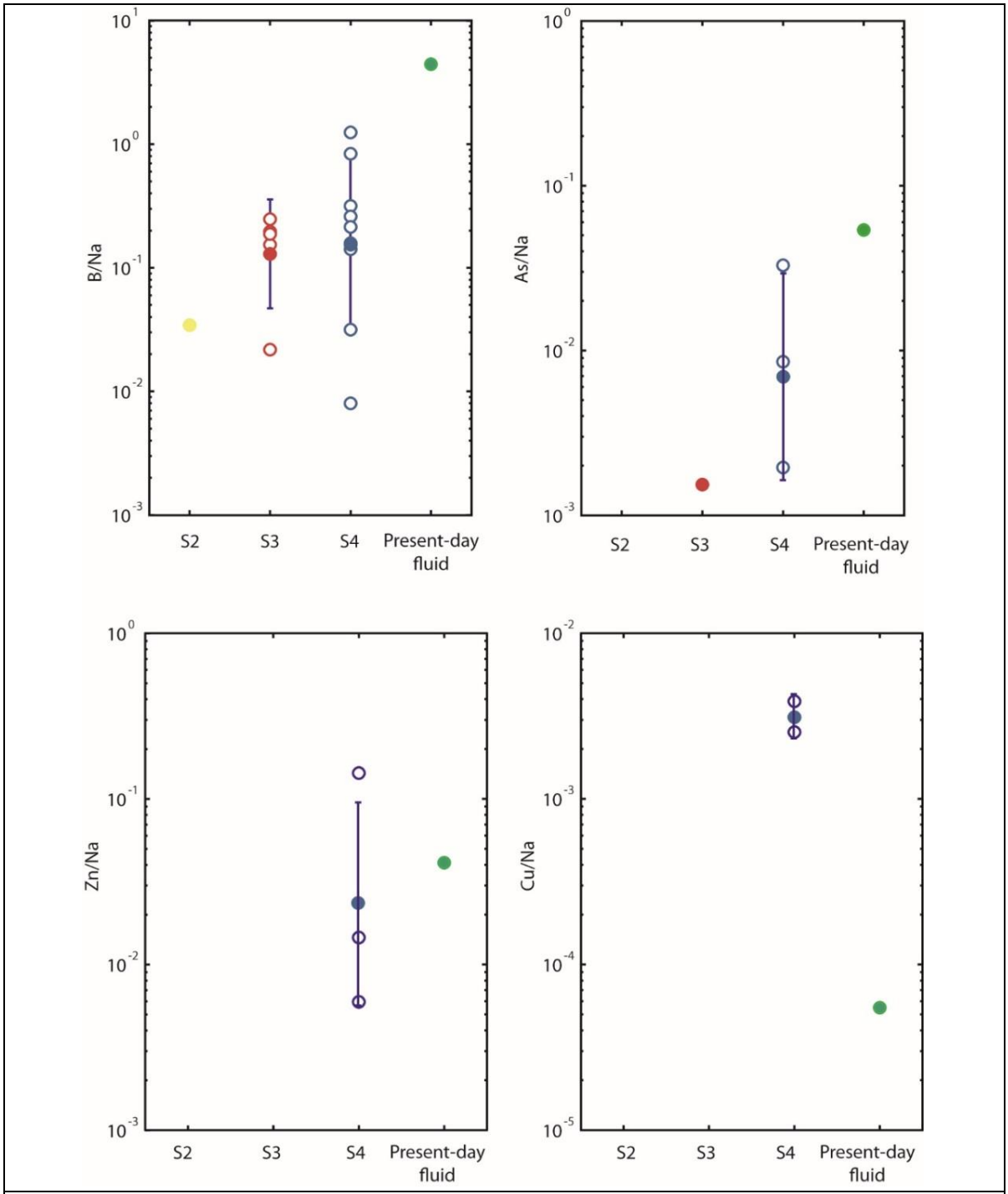

Figure 3.8 | Past (FIAs) and present-day (borehole fluid) fluid chemistry evolution for selected elements in molal ratios normalized to sodium. The horizontal axes display the different stages of the paragenetical sequence linked to the FIAs. Solid circles show the mean molal ratios for measured FIAs, whereas open circles are single-inclusion data. The green solid circles show present-day fluid chemistry.

Our results show that past and present-day fluids at Tolhuaca clearly differ in terms of chemical composition (Fig. 3.8). While present-day reservoir fluids are rich in Au, B and As, but Cu-poor (B/Na ~ $10^{0.5}$, As/Na ~ $10^{-1.1}$, Cu/Na ~ $10^{-4.2}$), the paleofluids trapped in fluid inclusions are Cu-rich but poor in B and As (B/Na ~ 10^{-1}, As/Na ~ 10^{-2}, Cu/Na ~ $10^{-2.5}$ in average) (Fig. 3.8). Zinc content does not show significant variations.

Critical fluid pressure for fault rupture

To assess the effects of the hydrothermal alteration on faulting conditions we calculate the critical fluid pressure (P_f^{crit}) that would trigger rupture in faults (Wiprut and Zoback, 2000) by combining mesoscopic failure criteria (Secor, 1965; Cox, 2010) with the estimation of the stress field in Tolhuaca.

The minimum and maximum fluid pressure required to rupture an extensional and a shear fault were calculated for two scenarios. One scenario mimics intact rocks conditions and the other scenario mimics hydrothermally altered rock conditions with preexistent fractures. Mechanical properties of altered rock were obtained from Neuzil (1994). The minimum fluid pressure corresponds to planes optimally oriented for rupture whereas the maximum correspond to fault planes severely misoriented for rupture. Based on the kinematic analysis of fault-slip data from Tol-1 borehole that indicates a N60E-striking bulk fault plane solution with normal strain regime (Perez-Flores et al., 2013), we assume that stress conditions of an extensional regime end-member (Zang et al., 2012) are representative of the stress field in Tolhuaca. Therefore, calculations for shear failure are related to the rupture of normal faults.

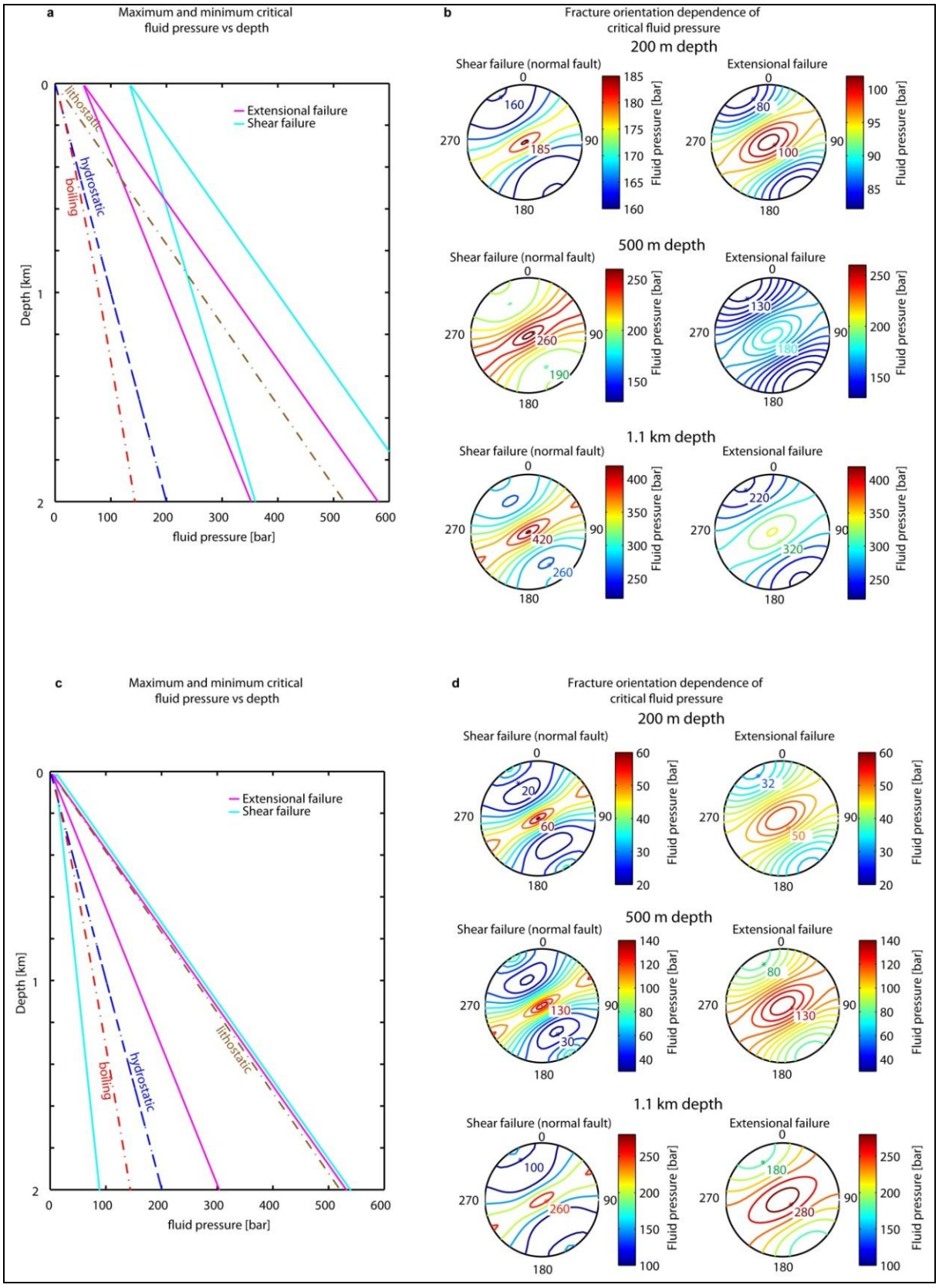
a
Maximum and minimum critical fluid pressure vs depth
Extensional failure
Shear failure
lithostatic
hydrostatic
boiling
Depth [km]
fluid pressure [bar]
b
Fracture orientation dependence of critical fluid pressure
200 m depth
500 m depth
1.1 km depth
Shear failure (normal fault)
Extensional failure
Fluid pressure [bar]
c
Maximum and minimum critical fluid pressure vs depth
Extensional failure
Shear failure
lithostatic
hydrostatic
boiling
Depth [km]
fluid pressure [bar]
d
Fracture orientation dependence of critical fluid pressure
200 m depth
500 m depth
1.1 km depth
Shear failure (normal fault)
Extensional failure
Fluid pressure [bar]

Figure 3.9 | Critical pore fluid pressures that trigger fault rupture (P_f^{crit}) under two scenarios. Calculations considering shear and extensional failure modes in a normal-faulting stress regime. **a,** Dependence on depth of the maximum (optimally oriented plane) and minimum (severely misoriented plane) critical P_f^{crit} for the intact rock scenario. Boiling, hydrostatic and lithostatic fluid pressure is shown for reference. **b,** Dependence on orientation of P_f^{crit} for 200 m, 500 m and 1.1 km with the fluid pressure in bar. Panels **c** and **d** are equivalent to **a** and **b**, respectively, but for the hydrothermally altered rock scenario.

Our calculations of the maximum and minimum P_f^{crit} for the two scenarios are shown in Figure 3.9. In the unaltered scenario, extensional fractures requires less fluid pressure to rupture than shear faults within the shallower ~2 km. At deeper conditions, with higher differential stress and confining pressure, shear failure requires lower fluid pressures to rupture. In the hydrothermally altered scenario, where cohesionless fractures are present, shear failure rupture for an optimally oriented preexisting fracture requires significant less fluid pressure than extensional fractures at any depth.

The dependence of P_f^{crit} on the orientation of the fracture plane is depicted for three representative depths (0.2, 0.5 and 1.1 km) of the alteration zones (Fig. 3.9). The difference of P_f^{crit} between the optimally oriented and the severely misoriented fracture planes increase significantly with depth. Therefore, at shallow depth is likely to have a wider range of faults and fractures orientation.

Effects of the clay-cap on thermal structure: Numerical simulations

In order to explore the effect of the development of a low-permeability clay-cap on the physical evolution of the Tolhuaca geothermal system, we performed numerical simulation of coupled heat and fluid flow using HYDROTHERM (Hayba and Ingebritsen, 1994). The modeled heat source of the system is a magma body that instantly intrudes to a depth of ~3 km beneath the volcano summit. The deeper wells intercepted dikes, supporting the idea of a magmatic intrusion as a heat source for Tolhuaca (Melosh et al., 2012). Several numerical experiments were computed to calibrate the model using the present-day pressure-temperature-enthalpy distribution by varying intrusion depth.

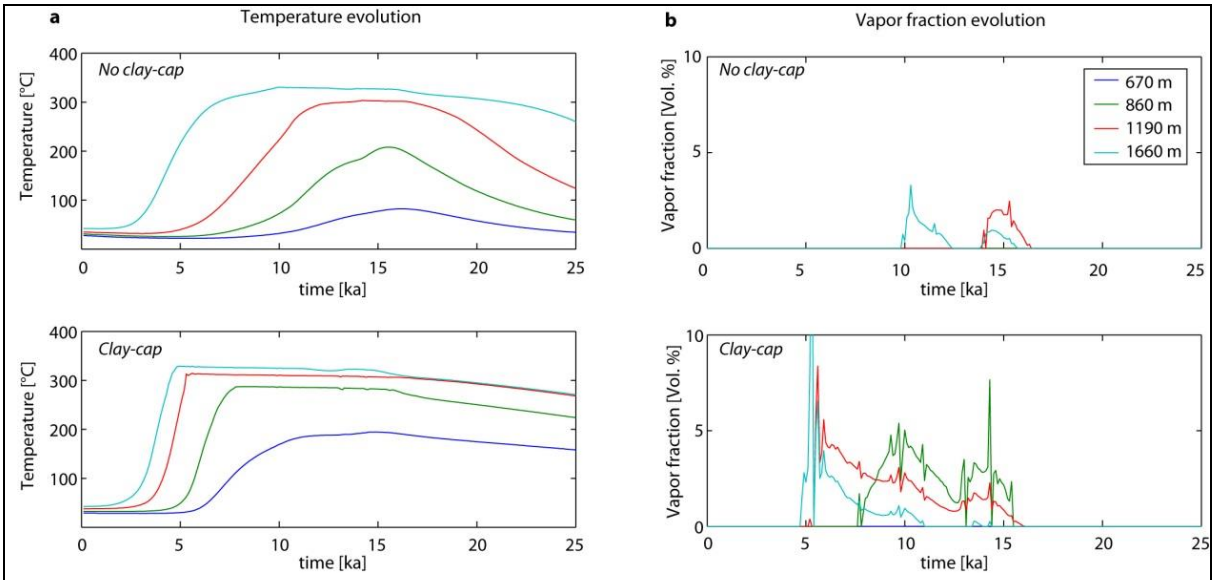

Figure 3.10 | Evolution of P-T-H conditions simulated for a Tolhuaca-like system under two scenarios, namely, with and without a low permeability clay-cap. Four selected depths (colored) depict the thermal structure in the vertical axis. **a,** Temperature evolution. The constant and horizontal temperature path mark two-phase fluid conditions (boiling). **b,** Volumetric vapor fraction. These parameters indicate the location and duration of the two-phase reservoir.

Two scenarios were considered, namely, with and without the presence of a low-permeability clay cap. The main differences between both scenarios are depicted in temperature and vapor fraction evolution (Fig. 3.10). In the absence of a low-permeability layer the system reach boiling conditions (maximum temperature for depth) only in the deep regions (> 1.1 km) after 10 ka for a short period (~3 ka). Contrastingly, in the presence of a low-permeability layer (clay-cap) the system heats up faster and reaches boiling conditions (flat and constant temperature) near 5 ka at reservoir depth (~0.9–2 km) and a vapor fraction of up to 15 vol. %. Boiling conditions disappear after 15 ka. Such a different evolution is mainly produced by the barrier effect that the low-permeability layer has on the cold meteoric water down-flow.

Discussion

Evolution of the Tolhuaca geothermal system

Based on the mineral paragenesis we identify four stages of hydrothermal alteration occurring during the evolution of the Tolhuaca geothermal system. Such paragenesis is in general agreement with previous studies at Tolhuaca (Melosh et al., 2010; Melosh et al., 2012). Our results indicate that the mineralogical changes affected the mechanical

properties of the rock and developed the current compartmentalized system. For a better visualization of the evolution proposed, the different stages of mineralization are represented in a cartoon of an idealized vein in Figure 11(a). In addition, a first order estimation of the physical conditions (temperature and vapor fraction) for the different stages obtained from numerical simulations is shown in Figure 11(b).

Stage S1 represents the early heating event with the precipitation of iron-oxides, quartz and chalcedony. The ubiquitous co-precipitation of quartz polymorphs suggest widespread boiling and flashing (Moncada et al., 2012). Boiling in most of the hydrothermal system and the formation of hydrothermal breccias might be related to a catastrophic event which occurred at end of S1. At the beginning of the stage S1, the buoyancy-driven hydrothermal fluid flow focused on interconnected open pores in the fresh volcaniclastic units. New hydrofractures were formed and increased permeability when pressure reached the critical values to trigger rupture in faults (fluid pressure in Figure 3.9). Such pressure increase was driven either by a complete infill of open pores with hydrothermal minerals (e.g., quartz, calcite) or an increase in heat supply which transiently sustained an increase in fluid pressure. Geometry and kinematic of new hydrofractures depended on the stress regime, mechanical properties of rocks (e.g., rock strength, friction coefficient) and pore fluid pressure. In the shallow levels (<500 m), the low differential stress promoted the development permeable fractures of almost any orientation (Rowland and Simmons, 2012), where the critical pore fluid pressure for fault rupture is almost the same in the optimally oriented (minimum) and severely misoriented (maximum) planes (Fig. 3.9). We propose that the transient event causing brecciation and flashing conditions at the end of stage S1 might be related to depressurization due to the retreat of glaciers during the late Pleistocene or flank collapse, as proposed for the Karaha-Telaga Bodas geothermal systems in Indonesia (Moore et al., 2008).

Stage S2 represents the alteration of volcanic and volcanoclastic rocks to form the typical hydrothermal mineral assemblages of geothermal systems related to volcanic activity (Browne, 1978; Simmons and Browne, 2000). Stage S2 also marks the beginning of the structural, hydraulic and chemical compartmentalization of the system. The varying physical and chemical conditions of hydrothermal fluids with depth controlled the segmentation of heat-fluid-rock interaction processes. A main control on those processes is the maximum temperature which is limited by the liquid-saturated conditions in the most commonly occurring liquid-dominated systems. Therefore, at stage S2 in the shallow levels (< 670 m) that had lower temperature (<200°C) hydrothermal alteration developed an argillic hydrothermal mineral assemblage with smectite (illite/smectite; interlayered chlorite/smectite), calcite and chalcedony/amorphous silica, as commonly recognized in geothermal fields (Simmons and Browne, 2000). In the deep upflow zone (>700 m), the

rock-dominated conditions of near neutral fluids and higher temperature (≥250°C) produce the propylitic assemblage with chlorite, epidote, quartz, calcite and pyrite.

In the shallow levels, the low-strength clay minerals which have intrinsically low permeability (10^{-23} – 10^{-17} m^2) (Neuzil, 1994) created an impermeable clay-cap and reduced cohesion of existent fractures. Because the presence of a cohesionless fault optimally oriented for reactivation precludes all other forms of brittle failure in intact rock (Cox, 2010; Rowland and Simmons, 2012), the impermeable effect of clay minerals is sustained by inhibiting the creation of highly permeable extension fractures (Fig. 3.9). Thus, deformation accommodated in the clay-cap is unlikely to increase permeability. Contrastingly, in the deep upflow zone the less intense presence of clay minerals retain rock strength and the dilatant behavior during slip (Wyering et al. 2014). Shear faults in rocks with brittle behavior also are hydraulically conductive fractures (Barton et al., 1995) and increase permeability by either sustaining faults aperture and/or producing damage zones (Kim, 2004). Such conditions promote the creation of hydraulically conductive fractures, allowing permeability regeneration (Davatzes and Hickman, 2010) and maintaining the conditions required for fluid advection ($k>10^{-16}$) (Rowland and Sibson, 2004).

Stage S3 records an event of boiling and flashing evidenced by "lattice-bladed" calcite, quartz with plumose texture and the coexistence of quartz polymorphs. Brecciation also occurs in the propilitic zone, revealing a transient change in the physical conditions that trigger fault rupture. The total homogenization temperature data from fluid inclusions assemblages related to stage S3 supports such interpretation by indicate that the boiling temperature was reached.

Stage S4 reflects a compartmentalized system, where the argillic, sub-propylitic and propylitic zones have decoupled evolutions. The argillic and sub-propylitic zones revealed gentle boiling conditions in euhedral quartz, which alternate with flashing episodes, evidenced by the co-precipitation of quartz polymorphs. In the deep propylitic zone, prehnite after epidote suggest a cooling event which might be produced by the influx steam-heated or meteoric waters. This is consistent with microthermometric data indicating a temperature decrease from stages S3, S4 to present-day temperature (Fig 3.7). Homogenization temperature data related to stage S4 are coincident with present borehole temperatures.

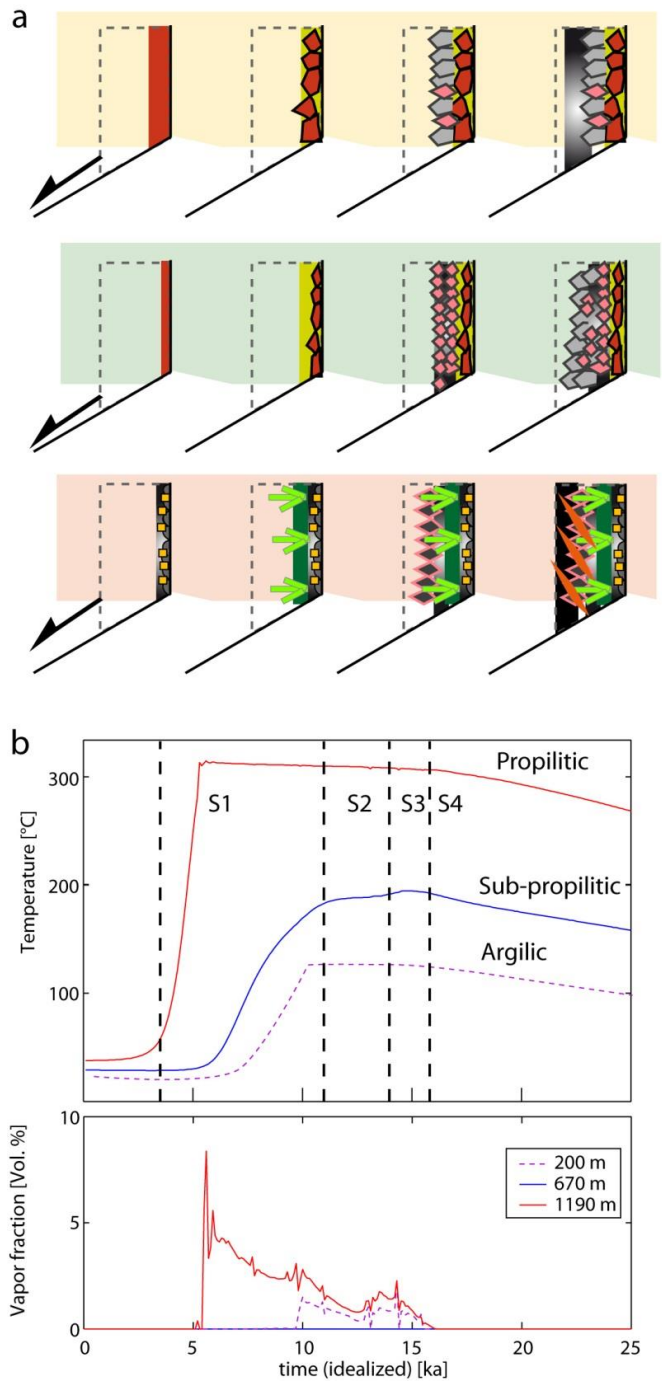

Figure 3.11 | Mineralogical and physical evolution of the Tolhuaca geothermal system. **a,** Cartoon of an idealized vein representing the different stages of mineralization in the three structural-mineralogical zones. **b,** Estimation of the physical conditions for the different stages obtained from numerical simulations of a Tolhuaca-like geothermal system.

The heat transfer mechanism is also affected by the compartmentalization as revealed by the contrasting vertical temperature gradient (Fig. 3.5). Convection dominates in the propylitic zone, whereas in the sub-propylitic zone the constant gradient indicates a conductive heat transfer regime. The vapor phase formed in the boiling reservoir is able to migrate through the low-permeability clay-cap, reaching the meteoric water level and forming a steam-heated aquifer in the argillic zone. Within this zone, lateral fluid flow and meteoric water infiltration was favored by the presence of open fractures, as indicated by the inverse temperature gradient and localized steep temperature changes. Total homogenization temperature data from fluid inclusion are within a range of ±40°C from present-day borehole temperatures and show a similar temperature gradient, indicating that the vertical compartmentalization had already occurred when the fluid inclusions were trapped.

Figure 3.11(a) describes, in a more regional scale, the main features required to develop a high enthalpy geothermal system related to long-lived arc-oblique fault systems (ALFS) and the LOFS (Sánchez et al., 2013). The severely misoriented ALFS for reactivation under the present-day stress field provides suitable conditions for the development of magma reservoirs and therefore a sustained supply heat and mass to fuel high enthalpy geothermal systems. In a local scale, the main features of the Tolhuaca geothermal system including lithology, faults, isotherms and the resulting compartmentalization of the system are depicted in the Figure 3.11(b). Focused fluid flow is restricted to high damage zones near faults whereas distributed flow occurs in intact rock and propylitic zones. Only vapor goes through the low permeability clay-cap, forming the steam heated aquifer and feeding fumaroles. Such heterogeneities compartmentalize fluid flow (Rowland and Sibson, 2004) and develop convection cells limited laterally by high permeability conduits and vertically by the clay-cap (Fig. 3.11). Granites are likely to behave as impermeable barriers for fluid flow and may act as the lower limit for the large scale hydrothermal convection.

Chemical evolution of fluids

Geochemical analyses of fluid samples retrieved from the deep wells indicate that present-day fluids match the classification for neutral chloride geothermal fluids with low salinity and relatively high content of metals. The high B and As contents are likely to be supplied by a magmatic-vapor contribution (Pokrovski et al., 2013). Such interpretation is supported by the helium isotopes data of a mantle-like signature from fumaroles in Tolhuaca (He^3/He^4 = 6.5 Ra) (Dobson et al., 2013). Those are common features on active geothermal systems and low-sulphidation epithermal environments (Simmons et al., 2005).

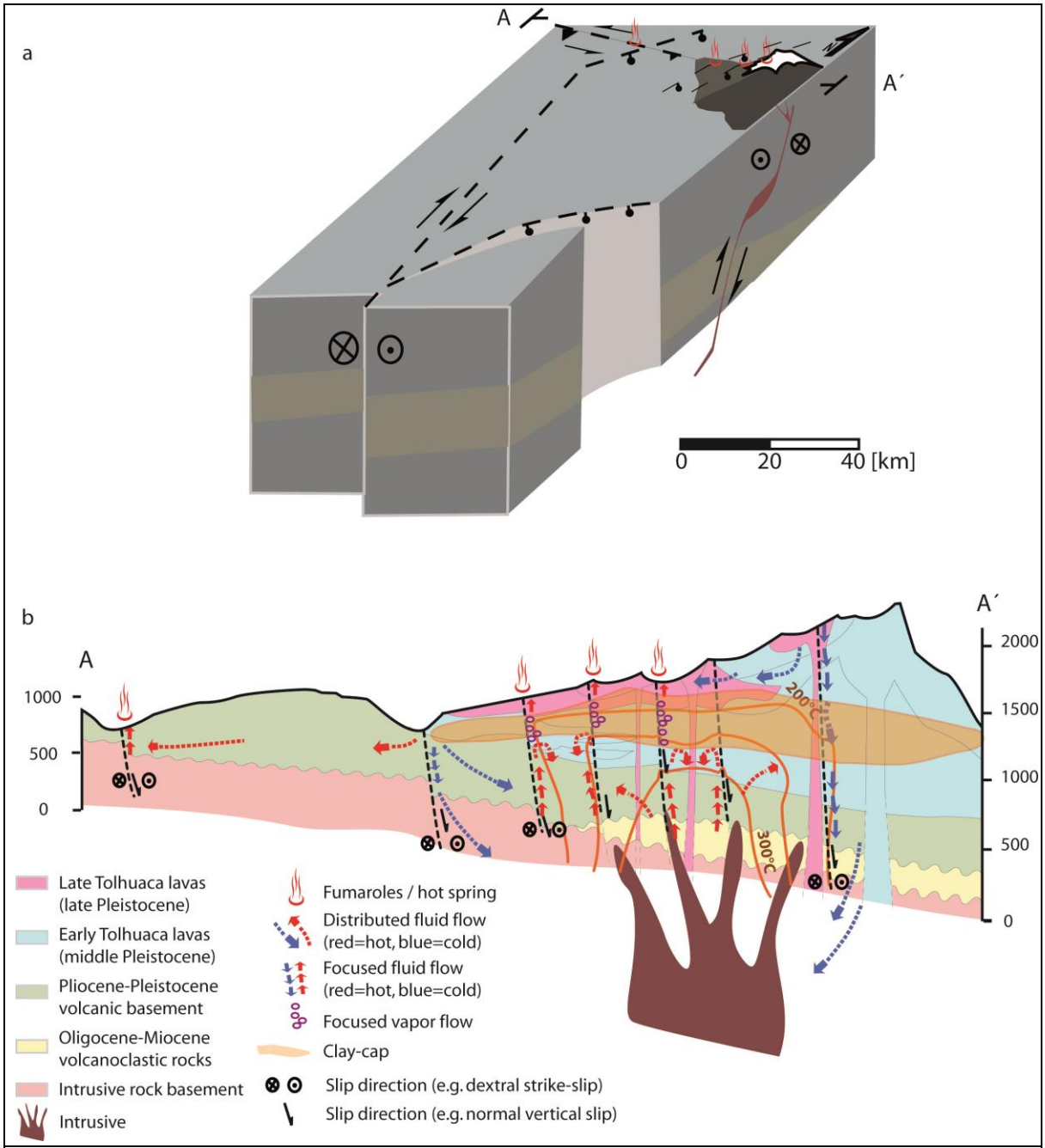

Figure 3.12 | a, Block model showing the context of the Tolhuaca volcano related to long-lived arc-oblique fault systems (ALFS) and the LOFS. The severely misoriented ALFS provides the suitable conditions for the development of magma reservoirs which are the heat source for geothermal systems. **b,** Conceptual model of the Tolhuaca geothermal system describing the compartmentalization of the system and its main features. Focused fluid flow is restricted to high damage zones near faults whereas distributed flow occurs in intact rock and propylitic zones. Such heterogeneities develop convection cells limited laterally by high permeability conduits and vertically by the clay-cap.

The comparison between paleo-fluid chemistry and present-day borehole fluids reveals significant differences. Paleo-fluids are Cu-rich but poor in B and As and present-day fluids are rich in Au, B and As, but Cu-poor (Fig. 3.8). Simple boiling models cannot explain the aforementioned fluctuations in fluid chemistry at Tolhuaca because molal ratios in the liquid phase of non-volatiles as Cu/Na, B/Na and As/Na are almost not affected during a boiling path. Those non-volatiles elements remain in the liquid phase during boiling at epithermal conditions as reaveled by their liquid-vapor partitioning coefficient (Pokrovski et al., 2013).

These data are consistent with recent studies documenting abrupt chemical and isotopic changes recorded in hydrothermal sulfides from epithermal Au (Deditius et al., 2009; Peterson and Mavrogenes, 2014) and porphyry Cu(Au) (Reich et al., 2013) deposits. Oscillatory trace metal signatures recorded in pyrite from such deposits reveal geochemical decoupling of As and Cu where Cu-rich, As-poor bands alternate with As-rich, Cu-poor bands. Preliminary electron microprobe analyses (EMPA) and X-ray maps in pyrites from Tolhuaca show similar features. Therefore, we interpret such fluctuation as the result of transient supply of metal-rich, magmatically-derived fluids where As, Au and Cu are geochemically decoupled (Rowland and Simmons, 2012; Wilkinson et al., 2009).

Effects of the hydrothermal alteration on the physical evolution of the system

Our calculations on fault rupture conditions provides an estimation of the effect that hydrothermal alteration has on the fluid pressure required to create or reactivate extensional and shear fractures. In the clay cap, the lower fluid pressure required to shear cohesionless faults optimally oriented for reactivation precludes the formation of other forms of brittle failure, such as highly permeable extension fractures. Thus, deformation accommodation in the clay cap does not increase permeability significantly.

The difference of P_f^{crit} between the optimally oriented and the severely misoriented fracture planes increase significantly with depth. At shallow depth (< 300 m) where such difference is small, the two rupture types occur in a wide range of orientations. At a higher depth, a small deviation from the optimal orientation produces a larger increase on the P_f^{crit} and therefore faults/fractures are likely to be nearer the optimal orientation. If fluid pressure reaches the extreme condition to rupture a severely misoriented extensional fracture, a breccia is formed. However, it is likely that breccias form before reaching the extreme condition.

At a depth higher that 2 km for intact rocks, rupture as shear faults requires lower fluid pressures than as extensional fractures. Such a limiting condition for extensional

fractures may have an effect on the maximum depth of highly permeable regions for the epithermal environment.

Hydrothermal reservoirs are dominated, in general, by extensional fractures oriented perpendicular to the minimum stress direction (σ_3), especially nearby the high permeability regions which are indicated by circulation loss (Nemčok et al., 2007). Such geometry of fault and fracture networks would enhance fluid flow in σ_2 direction (Sibson, 1996; Rowland and Sibson, 2004). In a normal stress regime as proposed for Tolhuaca (Perez-Flores et al., 2013) that implies an asymmetric increase on lateral and vertical permeability related to mesoscopic normal faults.

The interplay between hydrothermal alteration and fault kinematic has been interpreted to occur in a similar way in other active geothermal systems (Nemčok et al., 2007; Davatzes and Hickman, 2010). For example, in Karaha–Telaga Bodas geothermal field (Indonesia), the clay-cap is characterized by strike-slip and normal faults and tensile fractures, while the reservoir shows only tensile fractures and normal faults (Nemčok et al., 2007). Moreover, the depth at which there is a change in fault kinematics between clay-cap and geothermal reservoir zones corresponds approximately to the first appearance of epidote.

Our numerical simulations indicate that the development of a low-permeability clay-cap layer modifies the thermal structure and evolution of the geothermal system. The intrusion of a shallow (<4 km) magma body results in an increase in enthalpy of the fluid and a decrease in fluid pressures as a result of a transition from the hydrostatic pressure gradient to a liquid-saturated (boiling) environment at the propylitic zone (>670 m depth). The presence of a low permeability clay-cap increases the duration of liquid-saturated conditions (boiling temperatures) by a factor of three at the Tolhuaca reservoir depth (propylitic zone) and extends significantly the lifespan of the hydrothermal system. As in high relief regions the driven force for meteoric water down-flow increases, the effect of a low-permeability layer is enhanced in hydrothermal systems that develop near the flank of stratovolcanoes, compared to flat areas.

Thus, our results show that the favorability for developing geothermal resources in the southern Andes is highly dependent on, among other factors, the formation of a low-permeability upper zone that substantially increase the duration of high enthalpy conditions at the geothermal reservoir. Such implications extend to the field of ore deposits, because the liquid-saturated condition at shallow depth is fundamental to enhance precipitation of precious metals in the epithermal environment through boiling (Moncada et al., 2012; Simmons et al., 2005).

Concluding remarks

Our results indicate that the evolution of the Tolhuaca geothermal system is strongly influenced by the interplay between heat-fluid-rock interaction processes and brittle deformation. We recognized three hydrothermal alteration zones: a shallow argillic alteration zone; an intermediate sub-propylitic alteration zone and a deep propylitic zone. Based on mineralogical observations, fluid inclusions determinations and borehole data we identify four stages (S1-S4) of progressive hydrothermal alteration that involved: (S1) an early heating event; (S2) the development of a clay-cap in the upper zone (<670 m) and a deeper level affected by propylitic alteration, configuring the beginning of the structural, hydraulic and chemical compartmentalization of the system; (S3) boiling, flashing and brecciation; and (S4) fluid mixing and boiling. Borehole temperature data reveals that the heat transfer mechanism is also affected by the vertical compartmentalization. Thus convection dominates in the propylitic zone, whereas in the sub-propylitic zone the constant gradient indicates a conductive heat transfer regime.

The quantitative chemical analyses of fluid inclusions and present-day (well) fluids reveal a strong chemical change during the evolution of the Tolhuaca system. While the paleofluids trapped in fluid inclusions are Cu-rich but poor in B and As, present-day reservoir fluids are rich in Au, B and As, but Cu-poor. We interpret such fluctuation as the result of transient supply of metal-rich, magmatically-derived fluids where As, Au and Cu are geochemically decoupled.

The compartmentalization of the Tolhuaca geothermal system produces focused fluid flow in the damage zones near faults whereas distributed flow in the intact host rock and the propylitic zone. Clay-cap acts as a vertical barrier inhibiting fluid flow. Therefore convection cells are developed, limited laterally by high permeability conduits and vertically by the clay-cap.

The clay-rich zone not only compartmentalizes fluid flow but also change the mechanical response to deformation. Our calculations on the critical fluid pressure required to fault rupture indicate that in the clay-rich region the creation or reactivation of highly permeable extension fractures is inhibited. Contrastingly, in the deep upflow zone the less intense presence of clay minerals with the precipitation of mineral epidote and quartz, retain rock strength and the dilatant behavior during slip and contributes in sustaining permeability. Such structural and hydrological configuration naturally develops by a combination of high permeability and a sustained heat source.

The numerical models of coupled heat and fluid flow performed to analyze the effect of hydrothermal alteration on the thermal evolution of the system indicate that a low-permeability clay-cap triplicates the duration of liquid-saturated conditions (boiling

temperatures) at the Tolhuaca reservoir and extends the life-time of the hydrothermal system. Such effect of a low-permeability layer is enhanced in hydrothermal system near stratovolcanoes compared to flat areas.

Bibliography

Barton, C.A., Zoback, M.D., and Moos, D., 1995, Fluid flow along potentially active faults in crystalline rock: Geology, v. 23, no. 8, p. 683, doi: 10.1130/0091-7613(1995)023<0683:FFAPAF>2.3.CO;2.

Barton, C.A., Zoback, M.D., and Moos, D., 1995, Fluid flow along potentially active faults in crystalline rock: Geology, v. 23, no. 8, p. 683, doi: 10.1130/0091-7613(1995)023<0683:FFAPAF>2.3.CO;2.

Bodnar, R.J., 1993. Revised equation and table for determining the freezing point depression of H2O-NaCl solutions. Geochimica et Cosmochimica Acta, v. 57, p. 683–684, doi:10.1016/0016-7037(93)90378-A

Browne, P.R.L., 1978. Hydrothermal Alteration in Active Geothermal Fields. Annu. Rev. Earth Planet. Sci. 6, 229–248. doi:10.1146/annurev.ea.06.050178.001305

Cembrano, J., 1996, The Liquiñe Ofqui fault zone: a long-lived intra-arc fault system in southern Chile: Tectonophysics, v. 259, no. 1-3, p. 55–66, doi: 10.1016/0040-1951(95)00066-6.

Cembrano, J., and Lara, L., 2009, The link between volcanism and tectonics in the southern volcanic zone of the Chilean Andes: A review: Tectonophysics, v. 471, no. 1-2, p. 96–113, doi: 10.1016/j.tecto.2009.02.038.

Cox, S.F., 2010, The application of failure mode diagrams for exploring the roles of fluid pressure and stress states in controlling styles of fracture-controlled permeability enhancement in faults and shear zones: Geofluids, p. 217–233, doi: 10.1111/j.1468-8123.2010.00281.x.

Davatzes, N.C., and Hickman, S.H., 2010, The Feedback Between Stress, Faulting, and Fluid Flow: Lessons from the Coso Geothermal Field, CA, USA, *in* Proceedings World Geothermal Congress 2010 Bali, Indonesia, 25-29 April 2010,.

Deditius, a. P., Utsunomiya, S., Ewing, R.C., Chryssoulis, S.L., Venter, D., and Kesler, S.E., 2009, Decoupled geochemical behavior of As and Cu in hydrothermal systems: Geology, v. 37, no. 8, p. 707–710, doi: 10.1130/G25781A.1.

Dobson, P.F., Kennedy, B.M., Reich, M., Sanchez, P., and Morata, D., 2013, Effects of Volcanism, Crustal Thickness, and Large Scale Faulting on the He Isotope Signatures of Geothermal Systems in Chile, *in* 38th Workshop on Geothermal Reservoir Engineering, p. SGP–TR–198.

Giggenbach, W.F., and Goguel, R.L., 1989, Collection and analysis of geothermal and volcanic water and gas discharges: DSIR Report CD-2401.

Hayba, D.O., and Ingebritsen, S.E., 1994, The computer model HYDROTHERM, a three-dimensional finite-difference model to simulate ground-water flow and heat transport in the temperature range of 0 to 1200 °C: U.S. Geol Survey Water-Res Invest Report 94-12252.

Hedenquist, J.W., and Lowenstern, J.B., 1994, The role of magmas in the formation of hydrothermal ore deposits: Nature, v. 370, no. 6490, p. 519–527, doi: 10.1038/370519a0.

Kim, Y., 2004, Fault damage zones: Journal of Structural Geology, v. 26, no. 3, p. 503–517, doi: 10.1016/j.jsg.2003.08.002.

Lavenu, A., and Cembrano, J., 1999, Compressional- and transpressional-stress pattern for Pliocene and Quaternary brittle deformation in fore arc and intra-arc zones (Andes of Central and Southern Chile): Journal of Structural Geology, v. 21, no. 12, p. 1669–1691, doi: 10.1016/S0191-8141(99)00111-X.

Melosh, G., Cumming, W., Benoit, D., Wilmarth, M., Colvin, A., Winick, J., Soto-, E., Sussman, D., Urzúa-Monsalve, L., Powell, T., and Peretz, A., 2010, Exploration results and resource conceptual model of the Tolhuaca Geothermal Field, Chile, *in* Proceedings World Geothermal Congress 2010 Bali, Indonesia, 25-29 April 2010,.

Melosh, G., Moore, J., and Stacey, R., 2012, Natural reservoir evolution in the Tolhuaca geothermal field, southern Chile, *in* 37th Workshop on Geothermal Reservoir Engineering Stanford University, Stanford, California, January 31 - February 1, 2012, SGP-TR-194.

Moncada, D., Mutchler, S., Nieto, a., Reynolds, T.J., Rimstidt, J.D., and Bodnar, R.J., 2012, Mineral textures and fluid inclusion petrography of the epithermal Ag–Au deposits at Guanajuato, Mexico: Application to exploration: Journal of Geochemical Exploration, v. 114, p. 20–35, doi: 10.1016/j.gexplo.2011.12.001.

Moore, J.N., Allis, R.G., Nemčok, M., Powell, T.S., Bruton, C.J., Wannamaker, P.E., Raharjo, I.B., and Norman, D.I., 2008, The evolution of volcano-hosted geothermal systems based on deep wells from Karaha-Telaga Bodas, Indonesia: American Journal of Science, v. 308, no. 1, p. 1–48, doi: 10.2475/10.2008.01.

Nemčok, M., Moore, J.N., Christensen, C., Allis, R., Powell, T., Murray, B., and Nash, G., 2007, Controls on the Karaha–Telaga Bodas geothermal reservoir, Indonesia: Geothermics, v. 36, no. 1, p. 9–46, doi: 10.1016/j.geothermics.2006.09.005.

Neuzil, C.E., 1994, How permeable are clays and shales? Water Resources Research, v. 30, no. 2, p. 145–150, doi: 10.1029/93WR02930.

Perez-Flores, P., Veloso, E.E., Cembrano, J.M., Sánchez, P., Iriarte, S., and Lohmar, S., 2013, Paleomagnetic Reorientation of Structural Elements in Drill Cores: an example from Tolhuaca Geothermal Field (abstract), *in* AGU Fall Meeting Abstracts.

Peterson, E.C., and Mavrogenes, J. a., 2014, Linking high-grade gold mineralization to earthquake-induced fault-valve processes in the Porgera gold deposit, Papua New Guinea: Geology, v. 42, no. 5, p. 383–386, doi: 10.1130/G35286.1.

Pokrovski, G.S., Borisova, a. Y., Bychkov, a. Y., 2013. Speciation and Transport of Metals and Metalloids in Geological Vapors. Rev. Mineral. Geochemistry 76, 165–218. doi:10.2138/rmg.2013.76.6

Reich, M., Deditius, A., Chryssoulis, S., Li, J.-W., Ma, C.-Q., Parada, M.A., Barra, F., and Mittermayr, F., 2013, Pyrite as a record of hydrothermal fluid evolution in a porphyry copper system: A SIMS/EMPA trace element study: Geochimica et Cosmochimica Acta, v. 104, p. 42–62, doi: 10.1016/j.gca.2012.11.006.

Rosenau, M., Melnick, D., and Echtler, H., 2006, Kinematic constraints on intra-arc shear and strain partitioning in the southern Andes between 38°S and 42°S latitude: Tectonics, v. 25, no. 4, p. 1–16, doi: 10.1029/2005TC001943.

Rowland, J. V., and Sibson, R.H., 2004, Structural controls on hydrothermal flow in a segmented rift system, Taupo Volcanic Zone, New Zealand: Geofluids, v. 4, no. 4, p. 259–283, doi: 10.1111/j.1468-8123.2004.00091.x.

Rowland, J. V., and Simmons, S.F., 2012, Hydrologic, Magmatic, and Tectonic Controls on Hydrothermal Flow, Taupo Volcanic Zone, New Zealand: Implications for the Formation of Epithermal Vein Deposits: Economic Geology, v. 107, no. 3, p. 427–457, doi: 10.2113/econgeo.107.3.427.

Sánchez, P., Pérez-Flores, P., Arancibia, G., Cembrano, J., and Reich, M., 2013, Crustal deformation effects on the chemical evolution of geothermal systems: the intra-arc Liquiñe–Ofqui fault system, Southern Andes: International Geology Review, v. 55, no. 11, p. 1384–1400, doi: 10.1080/00206814.2013.775731.

Secor, D.T., 1965, Role of fluid pressure in jointing: American Journal of Science, v. 263, no. 8, p. 633–646, doi: 10.2475/ajs.263.8.633.

Sibson, R.H., 1996, Structural permeability of fluid-driven fault-fracture meshes: Journal of Structural Geology, v. 18, no. 8, p. 1031–1042, doi: 10.1016/0191-8141(96)00032-6.

Sibson, R.H., Robert, F., and Poulsen, K.H., 1988, High-angle reverse faults, fluid-pressure cycling, and mesothermal gold-quartz deposits: Geology, v. 16, no. 6, p. 551, doi: 10.1130/0091-7613(1988)016<0551.

Simmons, S.F., Brown, K.L., 2007. The flux of gold and related metals through a volcanic arc, Taupo Volcanic Zone, New Zealand. Geology 35, 1099. doi:10.1130/G24022A.1

Simmons, S.F., and Browne, P., 2000, Hydrothermal minerals and precious metals in the Broadlands-Ohaaki geothermal system: Implications for understanding low-sulfidation epithermal: Economic Geology, v. 95, p. 971–999.

Simmons, S.F., White, N., and John, D., 2005, Geological characteristics of epithermal precious and base metal deposits: Economic Geology, v. 100th Anni, no. 1, p. 485–522.

Thiele, R., Lahsen, A., Hugo, M., Varela, J., and Munizaga, F., 1987, Estudio geológico regional a escala 1:100.000 de la Hoya Superior y Curso Medio del Río Bío-Bío.

Centrales Quitramán, Huequecura, Aguas Blancas, Pangue, Ralco y Llanquén. Depto. de Geología-ENDESA (In spanish).

Wilkinson, J.J., Stoffell, B., Wilkinson, C.C., Jeffries, T.E., and Appold, M.S., 2009, Anomalously metal-rich fluids form hydrothermal ore deposits.: Science (New York, N.Y.), v. 323, no. 5915, p. 764–7, doi: 10.1126/science.1164436.

Wiprut, D., and Zoback, M.D., 2000, Fault reactivation and fluid flow along a previously dormant normal fault in the northern North Sea: Geology, v. 28, no. 7, p. 595, doi: 10.1130/0091-7613(2000)28<595:FRAFFA>2.0.CO;2.

Zang, A., Stephansson, O., Heidbach, O., and Janouschkowetz, S., 2012, World Stress Map Database as a Resource for Rock Mechanics and Rock Engineering: Geotechnical and Geological Engineering, v. 30, no. 3, p. 625–646, doi: 10.1007/s10706-012-9505-6.

Chapter 4. The optimal windows for seismically-enhanced gold precipitation in the epithermal environment

Abstract

Epithermal gold deposits result from the combination of a sustained flux of metal-rich fluids and an efficient precipitation mechanism. Earthquakes may trigger gold precipitation but their efficiency and time-integrated contribution are poorly constrained. In order to quantify the feedbacks between earthquake-driven fracturing and gold precipitation in the shallow crust, we constrained the physico-chemical evolution of metal-rich fluids in the active Tolhuaca geothermal system, located in the highly seismic Southern Andes of Chile. We combined temperature measurements in the deep wells with geochemical analyses of fluid samples retrieved from the reservoir. In addition, we reconstructed the paleo-fluid conditions and chemistry using microthermometry and LA-ICP-MS data of fluid inclusions from a deep borehole core. The effect of pressure and enthalpy changes on precipitation was evaluated by calculating the solubility of gold in P-H space, and the impact of externally-forced, seismic perturbations on fluid parameters was constrained using a thermo-mechanical piston model for a "suction pump" mechanism, and the critical fluid pressure for a "fluid-activated valve" mechanism. The reconstructed *P-T-H-X* fluid trajectories at Tolhuaca indicate that single-phase convective fluids feeding the hydrothermal reservoir reach the two-phase boundary with a high gold budget (~1-5 ppb) at saturated liquid pressures between 50 and 120 bar. We show that if hydrothermal ore fluids reach this optimal threshold for metal precipitation, small pressure changes (~50 bar) triggered by transient fault-rupture can drop gold solubility by up to two orders of magnitude. Our results indicate that subtle, externally-forced perturbations – equivalent to low magnitude earthquakes (Mw<2) and/or intrinsically-built overpressure of a hydrothermal reservoir under optimal conditions – may significantly enhance gold precipitation rates in the shallow crust and lead to overall increases in metal endowment over time.

Introduction

The interplay between seismic activity, fluid flow and mineral precipitation exerts a first-order control on the strength (Barton et al., 1995; Sibson, 1985) and permeability (Manga et al., 2012) of the crust, and plays a critical role in promoting the development of hydrothermal systems (Weis et al., 2012; Hedenquist and Lowenstern, 1994) and the formation of world class base and precious metal deposits (Richards, 2013; Hedenquist and

Lowenstern, 1994; Sibson et al., 1988). Giant ore deposits form in the crust when critical factors such as distinct tectonic configurations, focused fluid flow and/or reactive host rocks are met to enhance the overall metal endowment (Richards, 2013). External forcing such as earthquakes can have a profound impact on metal precipitation, triggering physical and chemical changes in ore fluids that can enhance the whole process (Rowland and Simmons, 2012; Sibson et al., 1988). This is particularly relevant in shallow crustal settings where giant porphyry copper and epithermal gold mineralization form as a result of phase separation or boiling of a single-phase fluid (Heinrich et al., 2004). In epithermal systems, in particular, precipitation of gold and/or silver may occur either as "gentle boiling" (Williams-Jones et al., 2009; Simmons et al., 2005), where enthalpy increase produces a small vapor fraction near liquid-saturated conditions, or as "flash vaporization" forced by a transient pressure drop that converts most of the original liquid into a low density vapor phase (Moncada et al., 2012; Weatherley and Henley, 2013; Simmons et al., 2005). There is abundant qualitative evidence in the literature documenting that both permeability and mineralization are strongly affected by pressure changes triggered by earthquakes (Sibson et al., 1988; Sibson, 1985; Rowland and Simmons, 2012) and a recent model (Weatherley and Henley, 2013) allows estimation of the magnitude of such pressure fluctuations. Nevertheless, direct estimations of the enhancing effect that earthquakes have on mineralization and a general formulation to describe the optimal conditions for earthquake-enhanced mineralization in seismically active regions are still lacking. This is mainly by the fact that hydrothermal ore deposits are open systems that record a time-integrated sequence of fluid flow events (Sibson et al., 1988; Wilkinson et al., 2009) driven by the complex interplay between mechanical processes affecting the rock, and the changes in the thermodynamic conditions and metal solubility that ore-forming fluids undergo from their magmatic-hydrothermal source to their final deposit trap.

An ideal natural laboratory to study such interplay is the Andean Cordillera of Central-Southern Chile, where hydrothermal systems occur in close spatial relationship with active volcanism as well as major seismically-active fault systems. The nature of the relationship between active tectonics, volcanism and hydrothermal activity in this region is the result of interaction between the crustal structures of the basement and the ongoing regional stress field (Cembrano and Lara, 2009). Near 25% of geothermal features in the Chilean Andes are hosted by the Liquiñe-Ofqui Fault System (LOFS) and the NW-trending Arc-Oblique Fault System (ALFS) (Sánchez et al., 2013; Cembrano and Lara, 2009). Within this setting, the active Tolhuaca geothermal field in the northern termination of the LOFS (Fig. 4.1) hosts a high enthalpy, metal-rich system that has been drilled down to ~3 km depth but is not yet affected by geothermal production or re-injection (Melosh et al., 2012). Therefore, it is a good analogue system that offers a unique opportunity to evaluate

the impact of internal and external triggers on fluid evolution and mineralization in a hydrothermal reservoir.

Material and methods

An ideal natural laboratory to study the interplay between earthquakes, fluid flow and metal precipitation is the Andean Cordillera of Central-Southern Chile, where hydrothermal systems occur in close spatial relationship with active volcanism as well as major seismically-active fault systems. In this region it has been shown that the nature and evolution of volcanic and hydrothermal systems is controlled by the NNE- trending, 1,200 km long Liquiñe-Ofqui Fault System (LOFS) and the NW-trending Arc-Oblique Fault System (ALFS) (Cembrano and Lara, 2009; Sánchez et al., 2013).

Within this setting, the active Tolhuaca geothermal field in the northern termination of the LOFS (Fig. 1) hosts a high enthalpy, metal-rich system that has been drilled down to ~3 km depth but is not yet affected by geothermal production or re-injection (Melosh et al., 2012). Therefore, it is a good analogue system that offers a unique opportunity to evaluate the impact of internal and external triggers on fluid evolution and mineralization in a hydrothermal reservoir.

Present-day conditions and borehole fluid chemistry

Temperature measurements of the deep wells after thermal recovery were used to constrain subsurface temperature of the geothermal system at Tolhuaca. Water and gas samples were collected in January 2013 using sampling procedures after Giggenbach and Goguel (1989). Samples were analyzed for major cations and anions, and trace elements at Actlabs Laboratories, Canada, using a Varian-730-ES Axial ICP-OES system, a Dionex ICS-1000 ion chromatography system and a sector field HR-ICP-MS system (Thermo Element 2), respectively.

Paleofluids physicochemical conditions

We reconstructed the thermodynamic conditions of paleo-fluids at Tolhuaca using microthermometric determinations and microanalytical data from fluid inclusions assemblages hosted in quartz and calcite veins from the Tol-1 borehole core. Homogenization temperatures and apparent salinities were measured using microthermometric techniques in fluid inclusions assemblages (FIA) identified by optical petrography. A Linkam heating-freezing system was used and calibrated using synthetic fluid inclusions as standards for temperature. No clathrate melting has been observed upon heating to room temperature, excluding the presence of substantial concentrations of CO2 in the fluid inclusions. Chemical microanalysis of individual fluid inclusions was performed using a laser ablation system (193 nm ArF excimer laser) connected to a

quadrupole ICP -MS (Perkin Elmer Elan 6100 DRC) at the fluid inclusions laboratory in ETH-Zürich (technical details in Günther et al., 1998).

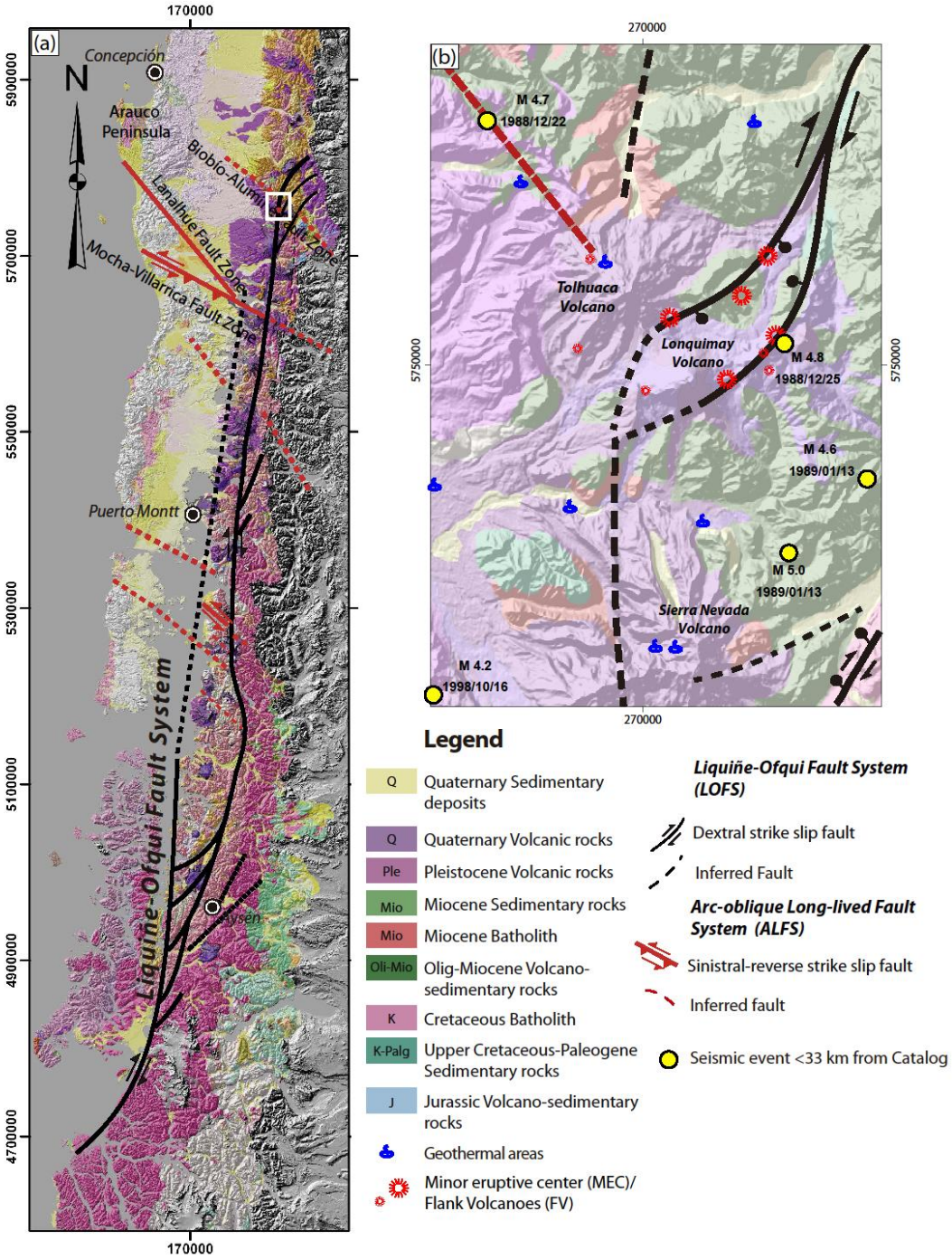

Figure 4.1 | Geodynamic and structural setting of the Tolhuaca geothermal system. (**A**), Digital

Elevation Model showing the location and extent of the Liquiñe-Ofqui Fault System (LOFS; in black) and the Arc-Oblique Fault System (ALFS; in red) (Sánchez et al., 2013). (**B**), Simplified geological map and major structural systems LOFS and ALFS. The spatial and genetic association with the mayor stratovolcanoes, monogenetic cones and geothermal areas are shown (Perez-Flores et al., 2013).

Fluid evolution modeling

Numerical models of coupled heat and fluid flow were computed using HYDROTHERM (Hayba and Ingebritsen, 1994) to simulate the evolution of a Tolhuaca-like hydrothermal system. Model characteristics, including rock properties, temperature-dependent permeability and initial and boundary conditions are similar to those used by Hayba and Ingebritsen (1997). Topography and clay cap spatial distribution was set as in Tolhuaca (Melosh et al., 2012). The modeled heat source of the system is a magma body (~0.5 km^3; at 900°C) that instantly intrudes to a depth of ~3 km beneath the volcano summit. Host rock and clay cap were defined by permeabilities of 10^{-15} m^2 and 10^{-18} m^2, respectively, within the domain of brittle rock behavior (T<350°C). The deeper wells at Tolhuaca intercepted dikes, supporting the idea of a magmatic intrusion as a heat source (Melosh et al., 2012). Several numerical experiments were computed to calibrate the model using the present-day pressure-temperature-enthalpy distribution by varying intrusion depth and the occurrence or absence of an impermeable barrier (clay-cap).

Gold solubility calculations in pressure-enthalpy space

The GEMS geochemical modeling software (Kulik et al., 2012) was used to compute dissolved Au concentrations. The starting fluid composition at the depth of the geothermal reservoir was reconstructed using the phase segregation methodology Scott et al. (2014) (see 2.5 for more details). Reconstructed concentrations: Cl=5.33e-3, S=1.132e-3, Fe=7.646e-7, Ca=3.194e-5, Na=0.1056, K=0.2007, Al=0.50003, As=4.4513e-4, Cu=1.574e-7, Si=1.006, in moles/kg of water. Feldspar-buffered acid-base conditions were assumed, i.e., excess Kfeldspar+albite+muscovite+quartz (Heinrich, 2005). The GEMS code uses the PSI/Nagra database (Hummel et al., 2002) as the core thermodynamic data source, which is complemented with SUPCRT92 (Johnson et al., 1992) for aqueous species and minerals. We updated the Au thermodynamic data for $Au(Cl)_n$, $Au(OH)_n$ and $Au(HS)_n$ species (n=1,2) with recent and self-consistent experimental results (Stefánsson and Seward, 2003b; Stefánsson and Seward, 2003a; Stefánsson and Seward, 2004). Direct calculation of Au solubility with GEMS is restricted to the stability field of aqueous liquid, hereby computed within an equidistant temperature-pressure grid (ΔT=5°C; ΔP=10 bar), ranging from 10-300 bar and 50-375 °C. Calculated Au solubilities are consistent with

updated databases and experimental results (Stefánsson and Seward, 2004) as well as with more recent studies of Au behavior in epithermal environments (Heinrich, 2005).

It is well documented that gold solubility in the two-phase region is strongly affected by the loss of sulfur, the nature of Au-ligands and to a lesser extent by the decrease of aqueous liquid solvent. To account for the effect of H_2S-loss, sulfur depletion was calculated using Henry´s law. Then, the solubility of Au in the aqueous liquid was computed using GEMS for the S-depleted liquid fraction (m_{Au_liquid}) at saturated pressure ($P=P_{sat}$). The Au content in any point within the two-phase region was calculated using:

$$m_{Au\_liq+vap} = m_{Au\_vapor}*f_{vapor}+m_{Au\_liquid}*(1-f_{vapor}) \quad (1)$$

where m is molality of liquid and vapor as subscripted and f_{vapor} is the vapor mass fraction. Due to the low solvation capacity of low-density H_2O (Hurtig and Williams-Jones, 2014), it is reasonable to assume that m_{Au_vapor}~0.

Reservoir sulfur content

As gold solubility calculation is highly dependent of the sulfur content in the fluid, an accurate reconstruction of fluid chemistry under the conditions of the deep reservoir is fundamental. The volatile content of reservoir fluids is modified during fluid flow through the well up to sampling conditions by phase separation (boiling). In "excess enthalpy" wells – i.e., those with higher vapor-to-liquid ratio, than resulting from adiabatic boiling of a vapor-saturated liquid at the measured aquifer temperatures – the effect of phase segregation is considerable (Scott et al., 2014). Phase segregation is driven by adhesion of the liquid phase onto mineral surfaces in the porous, fractured aquifer rock upon rapid depressurization boiling. Non-volatiles components in the liquid such as B, Na, Au and Si are mildly affected by phase segregation, and molal ratios among non-volatiles are completely unaffected. The sampled well at Tolhuaca, as many in high enthalpy geothermal system, is an "excess enthalpy well" and therefore such correction is need for an estimation of sulfur content at reservoir conditions. To estimate the S-content (as SO_4 and H_2S) at pre-sampling conditions the methodology developed by Scott et al. (2014) to reconstruct deep fluid chemistry from excess enthalpy wells was used. Computations were performed with the aid of WATCH program. A sensitivity test was performed by varying the controlling parameters - phase segregation pressure (±10 bar) and reservoir temperature (± 20°C) - and resulting variations in S-content were less than 10%.

Gold precipitation efficiency and gold grades

The percentage of Au precipitated for adiabatic pressure drop and isobaric cooling trajectories was calculated using:

$$\text{Efficiency [\%]} = (m_{Au\_initial} - m_{Au\_final}) / m_{Au\_initial} \quad (2)$$

that reflects the amount of Au precipitated with respect to the initial Au content in the fluid. Where *m* is the molality of the initial fluid (at liquid saturated conditions of the reservoir) and final fluid (at any condition bellow critical pressure and temperature), as subscripted.

Quartz solubility in the liquid region was computed using data from Manning (1994) and calculated within the two-phase region using:

$$m_{SiO2\_liq+vap} = m_{SiO2\_vapor} * f_{vapor} + m_{SiO2\_liquid} * (1-f_{vapor}) \quad (3)$$

where *m* is the molality of SiO_2 and f is the vapor fraction. Taking into account (2) and (3), the gold grade in idealized quartz veins formed through adiabatic pressure drop and isobaric cooling mechanisms is represented by the gold-quartz mass ratio resulting from the precipitation of a certain mass of fluid:

$$\text{Gold grade} = [(m_{Au\_initial} - m_{Au\_final}) * MW_{Au}] / [(m_{SiO2\_initial} - m_{SiO2\_final}) * MW_{SiO2}] \quad (4)$$

where MW_{Au} and MW_{SiO2} are the molecular weights of gold and quartz, respectively. Gold grade units are [mg Au / kg quartz].

The thermodynamic properties of water and steam - such as P, T, H, ρ and f_{vapor} (vapor fraction) - were calculated in P-H space using the freeware Matlab code XSteam (Holmgren, 2007), which implements the IAPWS IF-97 databases.

Transient effect of the "suction pump" mechanism

To estimate the pressure drop triggered by earthquakes (Sibson, 1987) we used the thermo-mechanical piston model (Weatherley and Henley, 2013). This model uses well-established earthquakes fault scaling relationships to calculate the change in volume and fluid pressure within a fault jog initially filled with fluid due to the action of an earthquake of certain magnitude. The least constrained geometrical parameter in the model is the jog length (or step-over distance) arbitrarily considered as 1 m. However, co-seismic pressure drop estimations are only dependent on the relative volume change and are unaffected by variations on the jog length because, by definition, the jog volume increases perpendicular to the jog length. Therefore, the geometrical characteristics of the model used here are identical to those proposed by Weatherley and Henley (2013) although we considered that under epithermal conditions flashing is likely to be an adiabatic and not an isothermal process (Weatherley and Henley, 2013; Henley and Hughes, 2000). Such adiabatic expansion is sustained by heat transfer from wallrock to fluid consequent on the decrease in temperature due to phase change (Henley and Hughes, 2000). Transient fluid pressure and

vapor fraction was computed by combining the relative volume changes triggered by earthquakes (of variable magnitude) with the thermodynamic properties of water.

The time-integrated contribution of earthquake-triggered precipitation to ore deposits formation

Weatherley and Henley (2013) and the results presented in section 4.1 indicate that the co-seismic "suction pump" mechanism related to microseism up to large earthquakes (-2<Mw<8) triggers flashing and precipitation of dissolved species in the fluid (e.g. Au, SiO_2). It is reasonable to assume that the volume of vaporized fluid by the "suction pump" mechanism is at least comparable to the co-seismic volume increase, because the system "flashes" until the pre-seismic pressure is reached via new fluid inflow. The pre-seismic conditions at the reservoir are defined by a liquid-saturated fluid (T_{sat}~300°C, P_{sat}~85 bar, $\rho_{sat\text{-}liq}$~712.1 kg/m^3; Melosh et al., 2012). Therefore, in each seismic event, the amount of precipitated ore is equal to the mass of metal contained in the volume of vaporized fluid:

$$\mathrm{M_{total}} = m_{\mathrm{Au\_liquid}} \rho V_{\mathrm{vap}} \qquad (5)$$

where V_{vap} is the volume of vaporized fluid.

The time-integrated contribution of earthquake-triggered precipitation (M_{total}) to ore deposits formation is fundamentally dependent on the metal content of the fluid (e.g. m_{Au_liquid}) and the incremental magnitude-frequency distribution (or earthquake frequency). For a specific time-span (e.g., 1 ka), this relation can be described as:

$$\mathrm{M_{total}} = m_{\mathrm{Au\_liquid}} \rho \int_{Mw=-2}^{Mw=8} V_{\mathrm{vap}} N dMw \qquad (6)$$

where N is the number of earthquakes in a magnitude range dMw per time-unit.

In order to constrain the earthquake frequency at Tolhuaca, earthquake density distribution data from the southern termination of the LOFS was used (Lange et al., 2008). As a reference, the seismicity of the LOFS during the 2007 Aysen seismic swarm is shown (Legrand et al., 2011), as well as the seismicity of geothermal systems such as Wairakei (Hunt and Latter, 1982), Salton Sea (Brodsky and Lajoie, 2013) and Milos (Fabriol and Beauce, 1997).

Earthquake frequency is scale-dependent and the spatial extension of active geothermal systems is the reasonable scale to estimate the time-integrated contribution of earthquake-triggered precipitation in epithermal deposits. Then, the amount of Au precipitated was computed for variable Au concentrations in the fluid. Different earthquake density distributions were synthetically constructed by increasing and decreasing the earthquake frequency for a constant b-value ~ 1. The comparison between different

earthquake density distributions uses the number of events in Mw=1 relative to the LOFS data.

Intrinsically-built overpressure for the "fluid-activated valve" mechanism

The fluid-activated valve is the mechanism that triggers fault rupture driven by a fluid pressure increase up to failure conditions (Sibson et al., 1988). To determine the critical pore pressure (Wiprut and Zoback, 2000) at which a fault element will begin to slip the coulomb frictional failure was used (Secor, 1965):

$$P_f^{crit-Shear} = \sigma_n - (\tau - C)/\mu \quad (7)$$

where σ_n, τ are normal and shear stresses respectively.

To determine the critical pore pressure at which fracture element will begin to open as an extensional fracture, the criterion for hydraulic extension was used (Secor, 1965):

$$P_f^{crit-Ext} = \sigma_n + T \quad (8)$$

Calculations were made for intact rock failure with tensile strength, T, of 5 MPa, cohesive strength, C, of 10 MPa and the coefficient of sliding friction, μ, of 0.75. Estimations for normal and shear stresses with depth were obtained from a world-wide compilation of absolute stress magnitudes measured *in-situ* by Zang et al., 2012. The best correlation for this function is reached when the tectonic faulting regime (normal, strike-slip, and reverse faulting) is used as discriminator. In a normal faulting regime stress can be described as (Zang et al., 2012):

$$Sv=260 \text{ bar/km}, S_h=0.57S_V, S_H=0.87S_V \quad (9)$$

where Sv, S_h and S_H are vertical, minimum horizontal and maximum horizontal stress component, respectively. To calculate the effect of the fracture orientation in the critical pore pressure that would trigger rupture, the calculations were performed for all the planes in a 3D space and plotted in equal area stereonets. The σ_n, τ, was computed with an *ad-hoc* Matlab routine, partially based on published computer codes (Neves et al., 2009). Then, $P_f^{crit-Ext}$ and $P_f^{crit-Shear}$ was obtained for planes in the 3D space.

Results and discussion

Fluid inclusions and borehole fluid data

Geological mapping, drillcore logging studies and kinematic analysis of fault-slip data have revealed that the Tolhuaca geothermal system is characterized by a structural and mineralogical compartmentalization under a normal-faulting strain regime (Melosh et al., 2012; Perez-Flores et al., 2013). Fluid inclusion microthermometric data in quartz and calcite veins show an early stage of heating, boiling and brecciation that is followed by a cooling stage, in agreement with a previous report by Melosh et al. (2012). Temperatures measured in fluid inclusion assemblages (FIA) from the latest paragenetic stage are coincident with present-day borehole temperatures (Fig. 2A). FIAs data and present-day temperature measurements at geothermal reservoir depths suggest a continuity of "gentle boiling" conditions (Fig. 2A). However, petrographic observations of colloform, plumose and jigsaw mineral textures in quartz veins are indicative of episodes of flashing vaporization (Moncada et al., 2012) triggered by transient pressure drops during the hydrothermal evolution at Tolhuaca.

Fluid chemistry has exerted a first-order control on hydrothermal alteration and mineralogical segmentation at Tolhuaca. Present-day fluids are characterized by low salinity (Na 182 mg/kg; Cl 266 mg/kg) and high concentrations of metals including Au (1.57 µg/kg), Ag (0.018 µg/kg), Cu (0.07 µg/kg) and Zn (7.5 µg/kg) (Fig. 2B). High B and As contents (219 and 25.6 mg/kg, respectively) may be supplied by a magmatic-vapor contribution (Heinrich et al., 2004), which is also supported by a mantle-like ^{3}He isotope signature in the fluids (He^3/He^4 = 6.5 Ra; Dobson et al. (2013)). Paleo-fluid chemistry was only constrained for Cu, Zn, B and As due to the restricted amount of sample fluid (<10 ng) contained in the small (<60 µm), low salinity (<3 wt.% eq. NaCl) fluid inclusions, and is presented as relative element abundance - molar ratio with respect to Na - to avoid errors produced by its transformation into absolute values (Fig. 2B). To the best of our knowledge these are the first quantitative chemical data of single fluid inclusions in an active geothermal system.

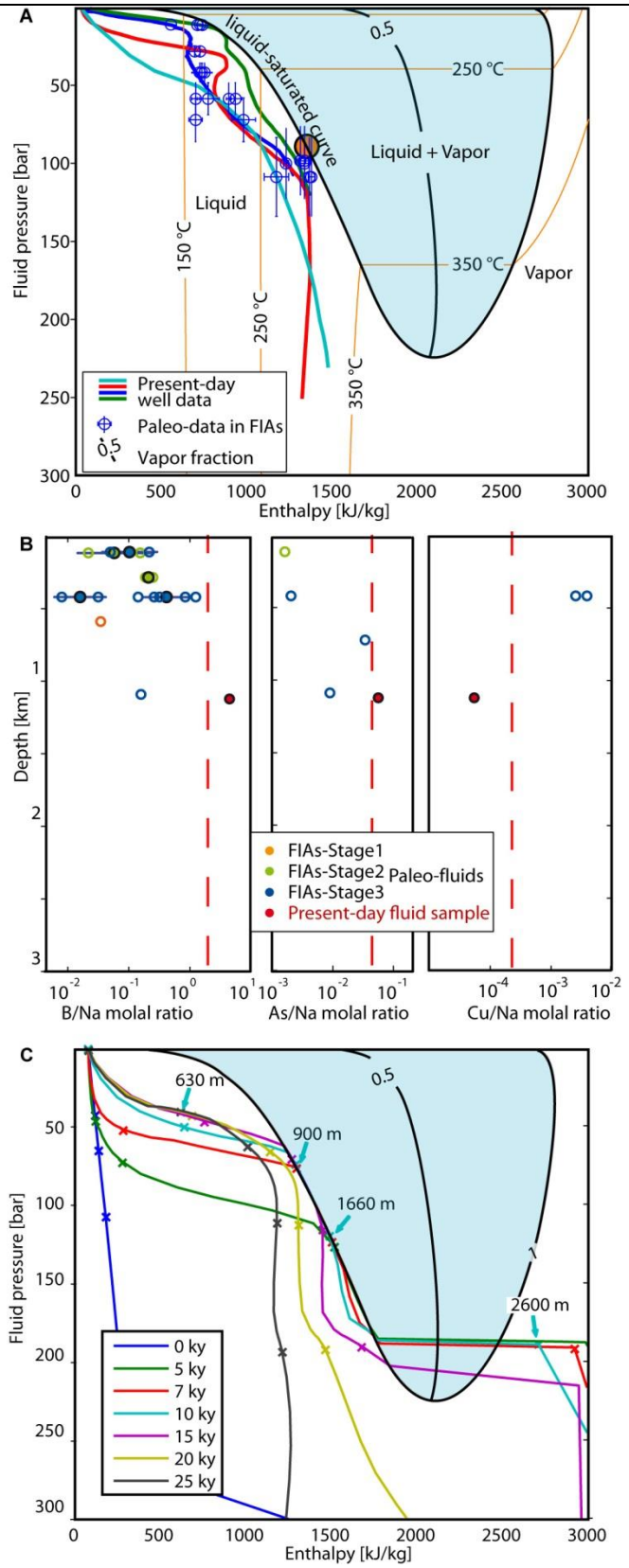
A
liquid-saturated curve
0.5
250 °C
Liquid + Vapor
Liquid
150 °C
250 °C
350 °C
350 °C
Vapor
Present-day well data
Paleo-data in FIAs
Vapor fraction
Fluid pressure [bar]
Enthalpy [kJ/kg]
B
Depth [km]
FIAs-Stage1
FIAs-Stage2
FIAs-Stage3
Paleo-fluids
Present-day fluid sample
B/Na molal ratio
As/Na molal ratio
Cu/Na molal ratio
C
630 m
900 m
1660 m
2600 m
0.5
1
0 ky
5 ky
7 ky
10 ky
15 ky
20 ky
25 ky
Fluid pressure [bar]
Enthalpy [kJ/kg]

Figure 4.2 | Physicochemical evolution of the Tolhuaca hydrothermal system. (**A**)**,** Microthermometric data and present-day conditions in pressure-enthalpy (P-H) space. Blue open circles show the average homogenization temperatures of fluid inclusions with 1-sigma standard deviation. Depth was converted to pressure assuming a hydrostatic gradient, and vertical error bars indicate the difference between hydrostatic and boiling pressure gradient. The colored curves show the temperature profiles obtained in four boreholes at Tolhuaca. The orange circle shows the metastable reservoir conditions. (**B**)**,** Paleofluid (fluid inclusions) and present-day (borehole fluid) chemistry for selected elements in molal ratios normalized to Na. Solid circles show the mean molal ratios for measured FIAs, whereas open circles are single-inclusion data. The red solid circles show present-day fluid chemistry. The segmented red line represents the inferred boundary between paleofluid and present-day conditions. (**C**)**,** Simulated, time-dependent pressure-enthalpy fluid trajectories at Tolhuaca, calibrated with present-day data.

Fluid inclusions and present-day (well) fluids at Tolhuaca are distinctive in terms of chemical composition (Fig 2B). While present-day reservoir fluids are rich in Au, B and As, but Cu-poor (B/Na ~ $10^{0.5}$, As/Na ~ $10^{-1.1}$, Cu/Na ~ $10^{-4.2}$), the paleofluids trapped in fluid inclusions are Cu-rich but poor in B and As (B/Na ~ 10^{-1}, As/Na ~ 10^{-2}, Cu/Na ~ $10^{-2.5}$) (Fig 2B). These data are consistent with recent studies documenting abrupt chemical and isotopic changes recorded in hydrothermal sulfides from epithermal Au and porphyry Cu(Au) deposits (Deditius et al., 2009; Reich et al., 2013; Peterson and Mavrogenes, 2014). Oscillatory trace metal signatures recorded in pyrite from such deposits reveal geochemical decoupling of As and Cu where Cu-rich, As-poor bands alternate with As-rich, Cu-poor bands. The aforementioned fluctuations in fluid chemistry at Tolhuaca cannot be explained by simple boiling models because molal ratios in the liquid phase of non-volatiles as Cu/Na, B/Na and As/Na are almost not affected during a boiling path. Therefore, we interpret such fluctuation as the result of transient supply of metal-rich, magmatically-derived fluids where As, Au and Cu are geochemically decoupled.

Optimal window for gold precipitation

The fluid chemistry variations reported at Tolhuaca suggest that metal solubility is critically affected by *P-T-H* trajectories followed by the metal carrier fluid, which will depend mainly on the permeability distribution and heat source characteristics of the active reservoir. Numerical simulations of the *P-T-H* evolution of a Tolhuaca-like hydrothermal reservoir indicate that the intrusion of a shallow (<4 km) magma body results in an increase in enthalpy of the fluid and a decrease in fluid pressures as a result of a transition from the hydrostatic pressure gradient to a liquid-saturated "gentle boiling" environment at reservoir conditions (Fig. 2C). Such critical conditions at the two-phase boundary are sustained until the waning and cooling of the hydrothermal system, as previous studies have shown (Hayba and Ingebritsen, 1997; Weis et al., 2012)

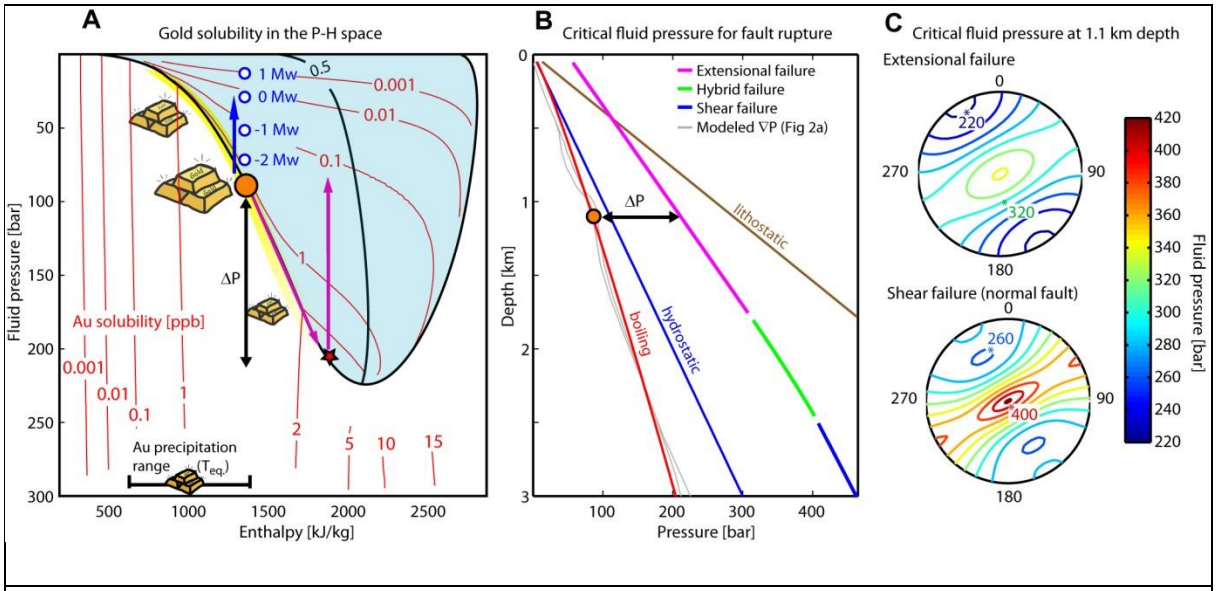

Figure 4.3 | External and internal triggers for Au precipitation in hydrothermal systems. (**A**), Seismically-triggered and internally-forced fluid pathways in P-H space. The red curves show the calculated Au solubilities in parts per billion (ppb) within the single-phase and two-phase (L+V, light blue) fields. The blue arrow shows the adiabatic pressure drop from metastable reservoir conditions (orange circle) to lower pressures (blue/white circles), triggered by a suction pump-like mechanism for different earthquake magnitudes (Mw). The magenta arrows indicate the fluid trajectory driven by the fault-activated valve and the red star shows the overpressure (ΔP, black double arrow) needed for fault rupture. Shaded in yellow is the optimal range for Au precipitation triggered by adiabatic pressure decrease (P~Psat and P<150 bar). (**B**)**,** Critical fluid pressures that trigger fault rupture considering three failure modes in a normal-faulting stress regime as a function of depth. (**C**)**,** Dependence on orientation of the critical pore fluid pressure needed to rupture an extensional and shear fracture, plotted in a stereographic representation under estimated reservoir conditions at Tolhuaca.

To quantify the effect of the different *P-T-H* trajectories on dissolved metal species we calculated the solubility of Au for the liquid and the two-phase regions. This is best described in a pressure-enthalpy (*P-H)* space representation (Fig. 3A), which allows the visualization of vapor fractions in the two-phase region - reduced to a line in the *P-T* space - and an intuitive representation of adiabatic (isoenthalpic) processes. We used the reconstructed chemistry from the Tolhuaca fluid at the estimated reservoir conditions as a reasonable starting point for calculations. Although Au solubility values are highly dependent on fluid chemistry, the topology of the diagram is representative for epithermal conditions. Within most of the two-phase (liquid+vapor) region, Au is only transported by the liquid phase because vapor as a metal carrier is limited to higher pressures (Williams-Jones et al., 2009). In Figure 3A, the calculated isopleths (red lines) show high solubility conditions for Au in the liquid-phase region between ~210 to 370°C (P_{sat} eq. 20 to 220 bar),

as widely recognized for epithermal environments. More interestingly, our results indicate that a subtle adiabatic pressure drop of ~50 bar from liquid-saturated conditions (e.g., orange circle), where saturated liquid pressure (P_{sat}) is less than 100 bar (T_{sat} eq.<310°C), causes a sharp decrease in Au solubility (Fig. 3A, blue vertical arrow; and Fig. 4B). If the adiabatic pressure drop occurs at higher pressures ($P>P_{sat}$~100 bar), the solubility decrease is moderate. Therefore, we recognize an optimal window for efficient Au precipitation (210°C<T_{sat}<310°C) that can be triggered by subtle adiabatic pressure drops, coincident with the documented ore precipitation conditions in epithermal Au deposits (Simmons et al., 2005) (Fig. 3A). Furthermore, the gold-quartz mass ratio resulting from an adiabatic pressure drop within the optimal window (~95% precipitation efficiency for a 50 bar pressure drop) is consistent with observed Au grades in small tonnage, high-grade orebodies (10-100 g Au/t, Simmons et al., 2005) (Fig. 4A and D, red vertical arrow). In turn, isobaric cooling pathways result in similar Au grades that those described in large tonnage, low-grade orebodies (1-2 g Au/t, Simmons et al., 2005) (Fig. 4A and D, green horizontal arrow). It is relevant to note that the increase of gold-quartz mass ratio at pressures higher than 150 bar is caused by the retrograde quartz solubility and does not represent an increase in the Au precipitation efficiency. Such optimal conditions for Au transport and precipitation develop through a combination of sustained heat and high permeability conditions, as numerical simulations indicate (Fig. 2C).

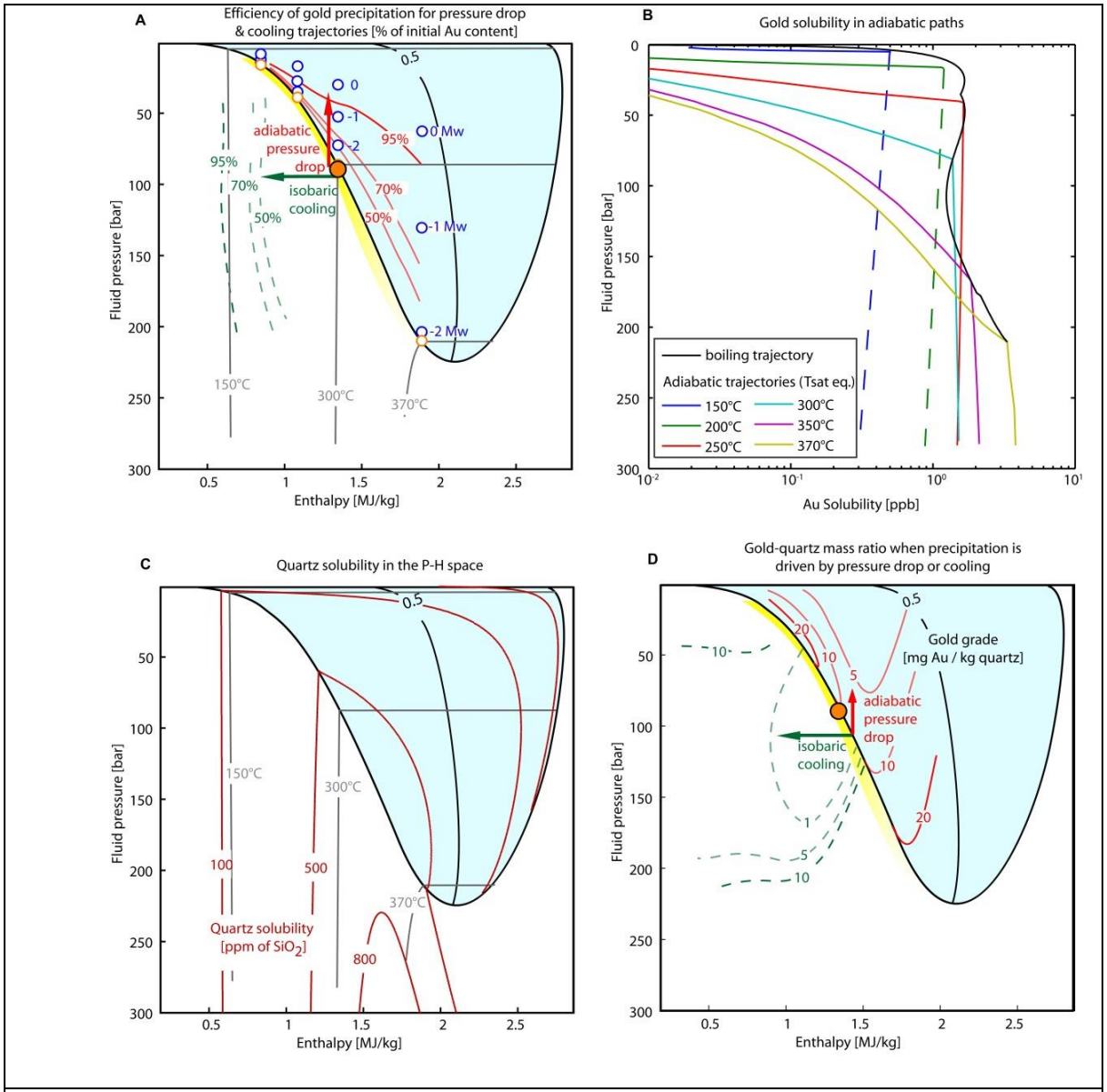

Figure 4.4 | Gold precipitation efficiency in pressure-enthalpy space. **A,** Gold precipitation efficiency (%) driven by adiabatic pressure drop (red arrow and solid red curves) and (ii) isobaric cooling (green arrow and dashed green curves), considering liquid saturated conditions as starting point (orange circle). The transient fluid pressures (blue circles) triggered by suction pump mechanism for different earthquake magnitudes (Mw) and different starting temperatures (200, 250, 300 and 370°C) are shown for reference. Adiabatic pressure drops have the highest efficiencies at P_{sat}<100 bar, whereas isobaric cooling requires a significant temperature decrease (ΔT~150°C) to precipitate most of the dissolved Au. **B,** Gold solubility along six adiabatic paths (colored curves) and under boiling conditions (black curve). The enthalpy of the fluid was converted to the equivalent temperature at saturated liquid conditions. **C,** Quartz solubility in the P-H space depicting its prograde (150<T<350°C) and retrograde (T>350°C) behavior. **D,** Gold-quartz mass ratio resulting from precipitation driven by adiabatic pressure drop and isobaric cooling. The

calculated gold-quartz mass ratio represents the Au grade in an idealized quartz vein. Results are consistent with reported data of Au content in Au-rich (>10 ppm Au) and Au-poor (< 1 ppm Au) quartz veins (Simmons et al., 2005; Sillitoe and Hedenquist, 2003).

Further implications: The enhancing effect of earthquakes

The combination of fluid chemistry data, numerical simulations and thermodynamic modeling at Tolhuaca strongly suggest that metal solubility is critically affected by *P-T-H* trajectories followed by the Au-rich carrier fluid, which will depend mainly on the permeability distribution and heat source characteristics of the active reservoir. Furthermore, and since our results reveal that Au solubility is significantly affected by subtle adiabatic pressure releases (e.g., ~50 bar), the key question is how seismic activity transiently affects the physico-chemical conditions of a hydrothermal reservoir. In the next sections we explore the effects of external triggers on Au precipitation.

The "suction pump" mechanism

We estimated the effect of the externally-forced "suction pump" mechanism assuming a general geometry of a dilational jog that relates earthquake magnitude (Mw) and pressure changes following the methods from Weatherley and Henley (2013). Considering the fact that this is a transient process near the two-phase region, it is reasonable to assume adiabatic and not isothermal conditions (Weatherley and Henley, 2013).

Under the estimated reservoir conditions at Tolhuaca (T_{sat}~300°C, P_{sat}~85 bar, orange circle in Fig. 3A), our calculations indicate that a pressure drop of more than 55 bar, equivalent to a seismic event of Mw=1, would generate a vapor fraction of 0.25 and at least a 2 log-units decrease in Au solubility (Fig. 3A and Fig. 4A). The efficiency of Au precipitation and the grade of the ore-veins formed are highly dependent on the *P-T-H* initial conditions of the hydrothermal reservoir (Fig. 4D), and are optimal at liquid-saturated conditions and pressures below 100 bar (T_{sat} eq.< 310°C). The association of Au precipitation to small magnitude earthquakes, i.e., small slips, is consistent with the observation that low-displacement, second-order fractures predominate as high grade ore-veins in geothermal systems and epithermal Au deposits (Simmons et al., 2005). This supports the idea invoked in petrographic and mineralogical studies of ore textures and fluid inclusions assemblages that flash vaporization is more efficient than gentle boiling for ore precipitation (Moncada et al., 2012). Thus, our results stress the potential relevance of frequent small magnitude earthquakes (Mw<2) on metal precipitation by triggering transient flash vaporization.

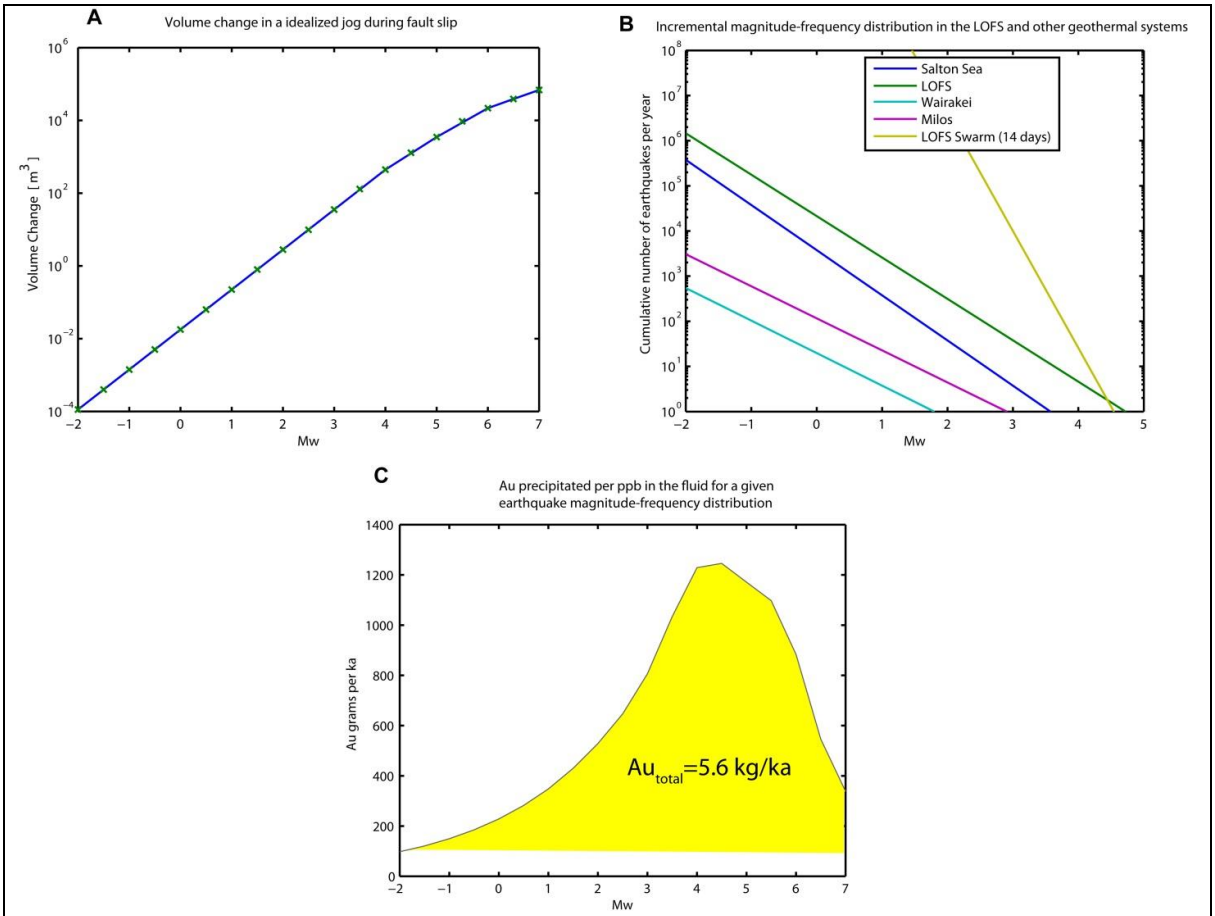

Figure 4.5 | Time-integrated contribution of earthquakes to Au precipitation rates. **A,** Co-seismic volume increase in a jog for different earthquakes magnitudes (Mw). Calculations are based on Weatherley & Henley (2013). **B,** Incremental magnitude-frequency distribution in the LOFS, Chile (Lange et al., 2008). Seismicity in Salton Sea, Milos and Wairakei (WK) geothermal systems are shown as a reference. **C,** Time-integrated contribution of earthquake-triggered precipitation to Au deposits formation in a time span of 1 ka, for a fluid containing 1 ppb of gold using LOFS incremental magnitude-frequency distribution as reference for calculation.

Enhancement of ore forming processes by "suction pump" mechanism

The time-integrated contribution of earthquake-triggered precipitation to Au deposits formation is fundamentally dependent on the Au content of the fluid, the volume affected by flashing and the frequency of seismicity. Due to the lack of adequate record of sufficient spatial and temporal resolution at local scale for the greenfields Tolhuaca, we

used the earthquake density distribution data from the LOFS in its southern termination (Lange et al., 2008) as an estimation of the frequency of tectonic-induced earthquakes in the area. In addition, seismic data from other geothermal systems were used as a comparison. Assuming that dilational jogs on controlling faults are persistent and prone to reactivation during earthquakes, we estimated the mass of fluid affected by an earthquake of a given magnitude by using the piston model.

Our analysis shows that the fault rupture of an earthquake with Mw>2 (that co-seismically affects a dilational jog) would not be significantly more efficient than lower magnitude earthquakes in decreasing the Au solubility in the fluid (Fig. 4A). However, it is documented that the volume directly affected by the adiabatic pressure drop increases exponentially with earthquake magnitude (Fig. 5A) (Leonard, 2010; Weatherley and Henley, 2013). Likewise, the frequency of earthquakes decreases with magnitude following the Gutenberg-Richter law. Therefore, the amount of fluid affected by seismically-triggered flash vaporization over a certain period of time (Fig. 5C) will depend on these two counteracting effects, which in turn are controlled by the slope on the corresponding plots (Fig. 5A&B). In an earthquake frequency vs. magnitude plot, the slope (named b-value) that describes the proportion of small earthquakes relative to large ones, is approximately 1.0 for tectonically-induced sequences and depends inversely on differential stress (Schorlemmer et al., 2005). Fluid-induced earthquakes swarms have a higher b-value that can be as large as 2.5 (Legrand et al., 2011).

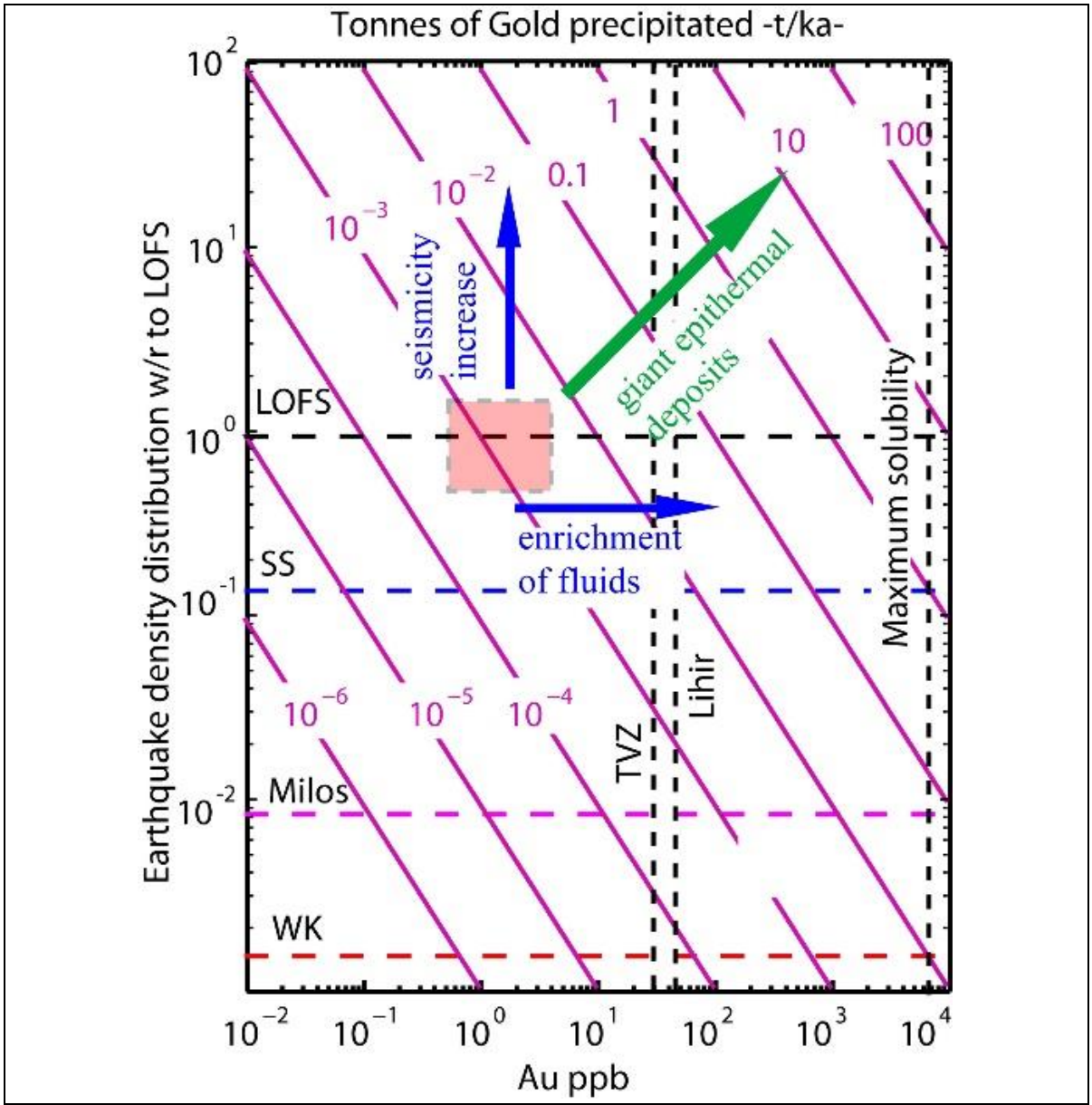

Figure 4.6 | Gold precipitation rates triggered by the suction pump mechanism during earthquakes. Gold precipitation rates (magenta diagonal lines, in tonnes (t) per 1000 years (ka)) are plotted as a function of Au content of the fluid (in ppb) and earthquake density distribution relative to the LOFS. The upper limits for Au content in hydrothermal fluids from geothermal systems and epithermal Au deposits are shown as vertical segmented lines for comparison (Taupo Volcanic Zone, Lihir and maximum solubility data were taken from Simmons and Brown, 2006, 2007; Hurtig and Williams-Jones, 2014). Seismicity at Salton Sea (SS), Milos and Wairakei (WK) geothermal systems are shown for reference. The light-red shaded region constrains the window of seismicity vs. Au precipitation at Tolhuaca.separation model used to evaluate the effects of boiling on dissolved species (B, As, Cu) contents in molal ratios units. The starting chemical and pressure conditions are the present conditions of the reservoir.

In Figure 5C, the time-integrated contribution of earthquake-triggered precipitation was calculated taking into account a Tolhuaca-like Au-bearing fluid (~1 ppb) and the LOFS earthquake magnitude relationship (b-value ~ 1) for a 100,000 years period. The area below the time-integrated contribution curve represents the total Au precipitated (5.6 kg/ka) and reveals that earthquakes with magnitude between 3 Mw and 6 Mw contribute ~60% of the total Au precipitated for a tectonically-induced sequences (Fig. 5C). In order to compare with fluid-induced earthquake swarms, similar calculations were performed using the higher b-values (2.5) of the LOFS seismic swarm (Legrand et al., 2011), indicating that in seismic swarms small magnitude earthquakes (Mw<3) contribute with most of the Au precipitation rates over time.

To visualize the general effect of seismicity and metal supply changes, the amount of Au precipitated was integrated over time for different earthquake density distributions (b-value ~ 1) and variable Au concentrations in the fluid as first order estimations (Fig. 6). According to these calculations, a 10-fold increase in seismicity produces a 10-fold increase in Au precipitation rate for a given Au content in the fluid.

The "fault-valve" mechanism

The fault-valve mechanism also triggers pressure fluctuations, but unlike the "suction pump", it is driven by pore fluid overpressure (Sibson et al., 1988). Borehole pressure measurements in active geothermal system indicate that pressure gradient commonly varies from boiling pressure up to hydrostatic pressure without exceeding 1.2 times the hydrostatic value (Rowland and Simmons, 2012). Such conditions in epithermal systems contrast with those in mesothermal Au deposition environments (T=350-450°C, depth~10 km, Pf~Plit) where fault rupture through the fault valve mechanism transiently enhances fluid migration to shallower levels, dropping fluid pressure towards hydrostatic values that trigger Au precipitation due to a decrease in metal solubility (Sibson et al., 1988). In that sense, suction pump is likely to dominate in epithermal environment whereas fault-activated valve does in mesothermal conditions (Sibson et al., 1988). However, overpressure in epithermal systems may occur if common minerals (quartz and/or calcite) precipitate fast enough to completely infill fractures and hydraulically seal the reservoir, heating up the system. Therefore, a scenario where temperature and pressure increase following a trajectory along the liquid-saturated curve (Fig. 3A, magenta arrow) needs to also be evaluated.

To estimate the effect of the fault-valve mechanism on Au solubility, we calculated the critical fluid pressure ($P_{failure}$) that would trigger rupture in faults (Wiprut and Zoback,

2000) by combining fault activity criteria, world-wide compilations of *in-situ* stress measurements and kinematic analysis of faults in the area.

Our results indicate that for an optimally oriented extensional fault at reservoir conditions similar to those at Tolhuaca (~1.1 km depth), the fluid pressure required ($P_{failure}$=211 bar; red star in Fig. 3A; Figs. 3B, C) is much lower than lithostatic pressure (P_{lit}~286 bar). After reaching rupture conditions, post-failure discharge releases excess energy through an adiabatic and transient pressure drop (Sibson et al., 1988), triggering a sharp solubility decrease (Fig. 3A, magenta vertical arrow). However, if sealing of the hydrothermal reservoir follows an isocoric trajectory (representing a completely closed system with null permeability) and/or the pressure fluctuations are limited to the liquid region ($P>>P_{sat}$), the Au solubility decrease may be insignificant. Therefore, our quantitative estimations of pressure and Au solubility fluctuations driven by the fault-valve mechanism indicate that overpressures may trigger efficient Au precipitation only if the system is at the critical liquid-saturated conditions during overpressure release (red star in Fig. 3A). This result contradicts the common view that changes in physical parameters such as permeability and/or pressure triggered by fault rupture always lead to highly efficient precipitation of Au in hydrothermal systems (e.g., Micklethwaite et al., 2015).

Concluding remarks

This study provides unique data from an active geothermal system to deconvolve the interplay between seismic activity, fluid flow and mineral precipitation in the epithermal environment. By combining borehole data and fluid chemistry at Tolhuaca with thermodynamic modeling and rock mechanics calculations, we conclude that high-enthalpy hydrothermal reservoirs forming in seismically active areas naturally approach an optimal window for Au precipitation. This optimal environment (210°C<T_{sat}<310°C) develops through a combination of sustained heat and high permeability conditions, and can be perturbed by subtle adiabatic pressure decreases (~20-50 bar) leading to efficient precipitation of Au (>90%). Our results show that, although gentle boiling drives some Au deposition, flash vaporization under optimal window conditions maximizes the extraction of most of the Au from ore fluid. We propose that the key conditions for earthquake-enhanced Au precipitation in the shallower portions of hydrothermal systems are defined by a sustained supply of metals from a magmatic-hydrothermal source, an efficient ore transport mechanism that ensures high Au-solubility conditions, followed by transient seismic-perturbation of a hydrothermal reservoir that has reached optimal conditions to maximize flash vaporization. Such conditions result from an ideal interplay between

seismic activity, fluid flow, transient solubility changes and *P-T-H* fluctuations in active continental margins and extensional zones.

Bibliography

Brodsky, E.E., Lajoie, L.J., 2013. Anthropogenic seismicity rates and operational parameters at the Salton Sea Geothermal Field. Science 341, 543–6. doi:10.1126/science.1239213

Cembrano, J., Lara, L., 2009. The link between volcanism and tectonics in the southern volcanic zone of the Chilean Andes: A review. Tectonophysics 471, 96–113. doi:10.1016/j.tecto.2009.02.038

Deditius, a. P., Utsunomiya, S., Ewing, R.C., Chryssoulis, S.L., Venter, D., Kesler, S.E., 2009. Decoupled geochemical behavior of As and Cu in hydrothermal systems. Geology 37, 707–710. doi:10.1130/G25781A.1

Dobson, P.F., Kennedy, B.M., Reich, M., Sanchez, P., Morata, D., 2013. Effects of Volcanism, Crustal Thickness, and Large Scale Faulting on the He Isotope Signatures of Geothermal Systems in Chile, in: 38th Workshop on Geothermal Reservoir Engineering. p. SGP–TR–198.

Fabriol, H., Beauce, A., 1997. Temporal and spatial distribution of local seismicity in the Chipilapa-Ahuachapán geothermal area, El Salvador. Geothermics. doi:10.1016/S0375-6505(97)00016-3

Giggenbach, W.F., Goguel, R.L., 1989. Collection and analysis of geothermal and volcanic water and gas discharges, 4th Ed. ed. DSIR Report CD-2401.

Günther, D., Audétat, A., Frischknecht, R., Heinrich, C.A., 1998. Quantitative analysis of major, minor and trace elements in fluid inclusions using laser ablation-inductively coupled plasmamass spectrometry. J. Anal. At. Spectrom. 13, 263–270. doi:10.1039/a707372k

Hayba, D.O., Ingebritsen, S.E., 1994. The computer model HYDROTHERM, a three-dimensional finite-difference model to simulate ground-water flow and heat transport in the temperature range of 0 to 1200 °C. U.S. Geol Survey Water-Res Invest Report 94-12252.

Hayba, D.O., Ingebritsen, S.E., 1997. Multiphase groundwater flow near cooling plutons. J. Geophys. Res. 102, 12235. doi:10.1029/97JB00552

Heinrich, C.A., 2005. The physical and chemical evolution of low-salinity magmatic fluids at the porphyry to epithermal transition: a thermodynamic study. Miner. Depos. 39, 864–889. doi:10.1007/s00126-004-0461-9

Heinrich, C.A., Driesner, T., Stefánsson, A., Seward, T.M., 2004. Magmatic vapor contraction and the transport of gold from the porphyry environment to epithermal ore deposits. Geology 32, 761. doi:10.1130/G20629.1

Henley, R., Hughes, G., 2000. Underground fumaroles:“ Excess heat” effects in vein formation. Econ. Geol. 95, 453–466.

Holmgren, M., 2007. XSteam: Water and Steam Properties According to IAPWS IF-97.

Hummel, W., Berner, U., Curti, E., Pearson, F.J., Thoenen, T., 2002. Nagra/PSI Chemical Thermodynamic Data Base 01/01. Nagra NTB 02-16, Nagra, Wettingen, Switzerland.

Hunt, T.M., Latter, J.H., 1982. A survey of seismic activity near wairakei geothermal field, New Zealand. J. Volcanol. Geotherm. Res. 14, 319–334. doi:10.1016/0377-0273(82)90068-3

Hurtig, N.C., Williams-Jones, A.E., 2014. An experimental study of the transport of gold through hydration of AuCl in aqueous vapour and vapour-like fluids. Geochim. Cosmochim. Acta 127, 305–325. doi:10.1016/j.gca.2013.11.029

Johnson, J.W., Oelkers, E.H., Helgeson, H.C., 1992. SUPCRT92: A software package for calculating the standard molal thermodynamic properties of minerals, gases, aqueous species, and reactions from 1 to 5000 bar and 0 to 1000°C. Comput. Geosci. 18, 899–947. doi:10.1016/0098-3004(92)90029-Q

Kulik, D. a., Wagner, T., Dmytrieva, S. V., Kosakowski, G., Hingerl, F.F., Chudnenko, K. V., Berner, U.R., 2012. GEM-Selektor geochemical modeling package: revised algorithm and GEMS3K numerical kernel for coupled simulation codes. Comput. Geosci. 1–24. doi:10.1007/s10596-012-9310-6

Lange, D., Cembrano, J., Rietbrock, A., Haberland, C., Dahm, T., Bataille, K., 2008. First seismic record for intra-arc strike-slip tectonics along the Liquiñe-Ofqui fault zone

at the obliquely convergent plate margin of the southern Andes. Tectonophysics 455, 14–24. doi:10.1016/j.tecto.2008.04.014

Legrand, D., Barrientos, S., Bataille, K., Cembrano, J., Pavez, a., 2011. The fluid-driven tectonic swarm of Aysen Fjord, Chile (2007) associated with two earthquakes (Mw=6.1 and Mw=6.2) within the Liquiñe-Ofqui Fault Zone. Cont. Shelf Res. 31, 154–161. doi:10.1016/j.csr.2010.05.008

Leonard, M., 2010. Earthquake Fault Scaling: Self-Consistent Relating of Rupture Length, Width, Average Displacement, and Moment Release. Bull. Seismol. Soc. Am. 100, 1971–1988. doi:10.1785/0120090189

Manning, C.E., 1994. The solubility of quartz in H2O in the lower crust and upper mantle. Geochim. Cosmochim. Acta 58, 4831–4839. doi:10.1016/0016-7037(94)90214-3

Melosh, G., Moore, J., Stacey, R., 2012. Natural reservoir evolution in the Tolhuaca geothermal field, southern Chile, in: 37th Workshop on Geothermal Reservoir Engineering Stanford University, Stanford, California, January 31 - February 1, 2012. SGP-TR-194.

Micklethwaite, S., Ford, a., Witt, W., Sheldon, H. a., 2015. The where and how of faults, fluids and permeability - insights from fault stepovers, scaling properties and gold mineralisation. Geofluids 15, 240–251. doi:10.1111/gfl.12102

Moncada, D., Mutchler, S., Nieto, a., Reynolds, T.J., Rimstidt, J.D., Bodnar, R.J., 2012. Mineral textures and fluid inclusion petrography of the epithermal Ag–Au deposits at Guanajuato, Mexico: Application to exploration. J. Geochemical Explor. 114, 20–35. doi:10.1016/j.gexplo.2011.12.001

Neves, M.C., Paiva, L.T., Luis, J., 2009. Software for slip-tendency analysis in 3D: A plug-in for Coulomb. Comput. Geosci. 35, 2345–2352. doi:10.1016/j.cageo.2009.03.008

Perez-Flores, P., Veloso, E.E., Cembrano, J.M., Sánchez, P., Iriarte, S., Lohmar, S., 2013. Paleomagnetic Reorientation of Structural Elements in Drill Cores: an example from Tolhuaca Geothermal Field (abstract), in: AGU Fall Meeting Abstracts.

Peterson, E.C., Mavrogenes, J. a., 2014. Linking high-grade gold mineralization to earthquake-induced fault-valve processes in the Porgera gold deposit, Papua New Guinea. Geology 42, 383–386. doi:10.1130/G35286.1

Reich, M., Deditius, A., Chryssoulis, S., Li, J.-W., Ma, C.-Q., Parada, M.A., Barra, F., Mittermayr, F., 2013. Pyrite as a record of hydrothermal fluid evolution in a porphyry copper system: A SIMS/EMPA trace element study. Geochim. Cosmochim. Acta 104, 42–62. doi:10.1016/j.gca.2012.11.006

Richards, J.P., 2013. Giant ore deposits formed by optimal alignments and combinations of geological processes. Nat. Geosci. 6, 911–916. doi:10.1038/ngeo1920

Rowland, J. V., Simmons, S.F., 2012. Hydrologic, Magmatic, and Tectonic Controls on Hydrothermal Flow, Taupo Volcanic Zone, New Zealand: Implications for the Formation of Epithermal Vein Deposits. Econ. Geol. 107, 427–457. doi:10.2113/econgeo.107.3.427

Sánchez, P., Pérez-Flores, P., Arancibia, G., Cembrano, J., Reich, M., 2013. Crustal deformation effects on the chemical evolution of geothermal systems: the intra-arc Liquiñe–Ofqui fault system, Southern Andes. Int. Geol. Rev. 55, 1384–1400. doi:10.1080/00206814.2013.775731

Schorlemmer, D., Wiemer, S., Wyss, M., 2005. Variations in earthquake-size distribution across different stress regimes. Nature 437, 539–542. doi:10.1038/nature04094

Scott, S., Gunnarsson, I., Arnórsson, S., Stefánsson, A., 2014. Gas chemistry, boiling and phase segregation in a geothermal system, Hellisheidi, Iceland. Geochim. Cosmochim. Acta 124, 170–189. doi:10.1016/j.gca.2013.09.027

Secor, D.T., 1965. Role of fluid pressure in jointing. Am. J. Sci. 263, 633–646. doi:10.2475/ajs.263.8.633

Sibson, R.H., 1987. Earthquake rupturing as a mineralizing agent in hydrothermal systems. Geology 15, 701. doi:10.1130/0091-7613(1987)15<701:ERAAMA>2.0.CO;2

Sibson, R.H., Robert, F., Poulsen, K.H., 1988. High-angle reverse faults, fluid-pressure cycling, and mesothermal gold-quartz deposits. Geology 16, 551. doi:10.1130/0091-7613(1988)016<0551

Sillitoe, R., Hedenquist, J., 2003. Linkages between volcanotectonic settings, ore-fluid compositions, and epithermal precious metal deposits, in: Simmons, S.F., Graham, I. (Eds.), Volcanic, Geothermal and Oreforming Fluids; Rulers and Witnesses of Processes within the Earth. Society of Economic Geologists Special Publication 10, pp. 315–343.

Simmons, S.F., Brown, K.L., 2006. Gold in magmatic hydrothermal solutions and the rapid formation of a giant ore deposit. Science 314, 288–91. doi:10.1126/science.1132866

Simmons, S.F., Brown, K.L., 2007. The flux of gold and related metals through a volcanic arc, Taupo Volcanic Zone, New Zealand. Geology 35, 1099. doi:10.1130/G24022A.1

Simmons, S.F., White, N., John, D., 2005. Geological characteristics of epithermal precious and base metal deposits. Econ. Geol. 100th Anni, 485–522.

Stefánsson, A., Seward, T.M., 2003a. The hydrolysis of gold(I) in aqueous solutions to 600°c and 1500 bar. Geochim. Cosmochim. Acta 67, 1677–1688. doi:10.1016/S0016-7037(02)01131-6

Stefánsson, A., Seward, T.M., 2003b. Stability of chloridogold(I) complexes in aqueous solutions from 300 to 600°C and from 500 to 1800 bar. Geochim. Cosmochim. Acta 67, 4559–4576. doi:10.1016/S0016-7037(03)00391-0

Stefánsson, A., Seward, T.M., 2004. Gold(I) complexing in aqueous sulphide solutions to 500°C at 500 bar. Geochim. Cosmochim. Acta 68, 4121–4143. doi:10.1016/j.gca.2004.04.006

Weatherley, D.K., Henley, R.W., 2013. Flash vaporization during earthquakes evidenced by gold deposits. Nat. Geosci. 6, 294–298. doi:10.1038/ngeo1759

Weis, P., Driesner, T., Heinrich, C.A., 2012. Porphyry-copper ore shells form at stable pressure-temperature fronts within dynamic fluid plumes. Science 338, 1613–6. doi:10.1126/science.1225009

Williams-Jones, A.E., Bowell, R.J., Migdisov, a. a., 2009. Gold in Solution. Elements 5, 281–287. doi:10.2113/gselements.5.5.281

Wiprut, D., Zoback, M.D., 2000. Fault reactivation and fluid flow along a previously dormant normal fault in the northern North Sea. Geology 28, 595. doi:10.1130/0091-7613(2000)28<595:FRAFFA>2.0.CO;2

Zang, A., Stephansson, O., Heidbach, O., Janouschkowetz, S., 2012. World Stress Map Database as a Resource for Rock Mechanics and Rock Engineering. Geotech. Geol. Eng. 30, 625–646. doi:10.1007/s10706-012-9505-6

Chapter 5. Conclusions

The results presented in this thesis provide new insights on the dynamic interplay between brittle deformation, fluid-rock interaction and mineralization in hydrothermal systems. In particular, this thesis contributes to our better understanding of the role of fault systems in the development of hydrothermal reservoirs, the impacts of hydrothermal alteration on brittle deformation, and the changes in the physicochemical conditions of dissolved species triggered by co-seismic fault rupture processes.

The study of the Villarrica-Chihuio area combined a regional-scale structural study with geochemical modeling of hot spring data to reveal that the interplay between tectonics and volcanism defines the nature and evolution of geothermal systems associated to the Liquiñe-Ofqui fault system (LOFS). This approach allowed the identification of two magmatic-tectonic-geothermal domains and suggests that the chemical evolution of hydrothermal fluids in the area is strongly dependent on structurally-controlled mechanisms of heat transfer.

Within this framework, conductive heat transfer dominates in geothermal systems hosted in crystalline rocks such as Liquiñe and Chihuio hot springs. This is the case for geothermal areas along the master and subsidiary faults of the LOFS that are favorably orientated for shear and extension, respectively. Fault–fracture networks related to the damage zone of the deep-seated NNE-striking master fault increase vertical permeability in the crystalline basement. These fracture networks promote the development of thin and deep (<3 km) convection cells and enhance heat–fluid–rock interaction after the infiltration of meteoric water. The heat–fluid–rock interaction and the lack of direct magmatic contribution imprint a chemical signature depleted in magmatically-derived components (e.g., B, As) and alkaline fluids. In marked contrast, magmatically enhanced advective transport dominates heat flow in the geothermal occurrences hosted in volcanoclastic rocks and located on the flanks of volcanoes forming WNW-trending alignments. These alignments are ultimately related to the WNW-striking long-lived basement fault systems (ALFS), which are strongly disorientated with respect to the prevailing stress field, and provide suitable conditions for the development of magma reservoirs. These crustal magmatic reservoirs supply heat and mass to form high enthalpy geothermal systems.

The interpretation regarding the effects of crustal deformation on the development of geothermal systems might be applicable to the rest of the Southern Volcanic Zone, where the most prominent geothermal resources would be genetically related to WNW-

striking volcanic chains and the ALFS. Therefore, these observations provide a new understanding towards efficient exploration strategies of geothermal resources in the Southern Andes.

In Chapter 3 the effect of the interplay between heat-fluid-rock interaction and brittle deformation on the evolution of hydrothermal systems was investigated. The study case is the active Tolhuaca hydrothermal system in the northern termination of the LOFS that has been explored for geothermal resources. Drillhole data from deep drillings (~ 3 km depth) reavealed a high enthalpy, metal-rich hydrothermal system that is still not affected by geothermal production or re-injection. This system provided the opportunity to develop a novel approach which combined field observations and drillhole data with analytical determinations of present-day fluids and and paleofluids trapped in fluid inclusions, thermodynamic modeling of metal solubility, and numerical models of fluid evolution and rock failure conditions.

This approach allowed constraining the pressure-temperature-enthalpy-composition (*P-T-H-X*) evolution of fluids at Tolhuaca. Mineralogical data and failure criteria revealed that hydrothermal alteration compartmentalized the system from a structural and hydrological perspective by developing a low-permeability and low-cohesion clay-rich zone on top the reservoir. Thus, in the clay-rich region the creation or reactivation of highly permeable extension fractures is inhibited, while the critical fluid pressure required to (re)activate shear faults is reduced. Contrastingly, at reservoir conditions precipitation of stronger minerals (i.e. epidote, quartz) retain dilatant behavior during slip and contributes in sustaining permeability. Such structural and hydrological configuration naturally develops by a combination of high permeability and a sustained heat source. Moreover, numerical models indicate that the lifespan and thermal structure of the hydrothermal system can be strongly affected by mineralogical changes. The numerical simulation of a Tolhuaca-like system indicates that the presence of a low permeability clay-cap may increase by a factor of three the duration of persistent boiling conditions in hydrothermal systems with a high relief on top (e.g., volcanic edifice). This may significantly enhances the development and sustainability of geothermal resources, and thus may also increase the efficiency of metal precipitation in the epithermal environment.

A fundamental question in economic geology deals with the impact of seismicity on the formation of gold-quartz veins and epithermal gold deposits. It is widely accepted that such deposits result from the combination of a sustained flux of gold-rich fluids and an efficient precipitation mechanism. Earthquakes may trigger precipitation but its efficiency and time-integrated contribution is poorly quantified. In Chapter 4, a novel model was developed, which integrated mechanical processes affecting the rock, changes in the thermodynamic conditions and gold solubility of ore-forming fluids during a seismic event.

We used the P-T-H fluid conditions at Tolhuaca combined with gold and silica solubility calculations to show that hydrothermal systems naturally approach the optimal conditions that maximize earthquake-induced gold precipitation. Such optimal conditions are characterized by liquid-saturated conditions with a saturated liquid pressure (P_{sat}) less than 100 bar (T_{sat} eq.<310°C), where subtle adiabatic pressure drops (~50 bar) cause the efficient precipitation of the dissolved gold carried by the hydrothermal fluid. It is worth highlighting that such optimal conditions are consistent with the documented ore precipitation conditions reported for epithermal gold deposits around the world. Additionally, estimations of the time-integrated contribution of earthquake-triggered precipitation to overall precipitation rates in epithermal systems indicate that the long-term and continuous effect of low magnitude earthquakes (Mw<2) may be key factor that makes epithermal gold deposits to increase their metal endowment.